Enhanced Multicarrier Techniques for Professional Ad hoc and Cell-Based Communications

(EMPhAtiC)

Document Number D7.1

Evaluation of relaying strategies

Contractual date of delivery to the CEC:	28/02/2014
Actual date of delivery to the CEC:	18/03/2014
Project Number and Acronym:	318362 EMPhAtiC
Editor:	Antonio Cipriano (THALES)
Authors:	Yao Cheng (ITU), Peng Li (ITU), Jianshu Zhang (ITU), Ahmad Nimr (ITU), Martin Haardt (ITU), Antonio Cipriano (THALES), Yahia Medjahdi (UCL), Jerome Louveaux (UCL), Slobodan Nedic (UNS), Vladimir Stanivuk (UNS), David Gregoratti (CTTC), Xavier Mestre (CTTC)
Participants:	CTTC, UCL, ITU, UNS, THALES
Workpackage:	WP7
Security:	Public (PU)
Nature:	Report
Version:	1.1
Total Number of Pages:	106

Abstract:

This deliverable collects part of the work performed in WP7 “Relay and coverage extension” and in particular under T7.1 “Range extension by using cooperative MIMO” and T7.2 “Design of relaying strategies” of the EMPhAtiC project. It deals with relaying applied to FBMC, OFDM and SC-FDMA waveforms and specifically on range extension using cooperative MIMO as well as the design and evaluation of relay strategies. The work ranges from theoretical investigation of the performance of the two relaying scheme via the characterization of the achievable rate region of a two-way DF relaying strategy, to more applied work like practical channel estimation schemes for two-way relaying.

Keywords: Relaying, coverage extension, two-way relaying, FBMC, OFDM

Document Revision History

Version	Date	Author	Summary of main changes
0.1	10.02.2014	From all involved partners	Contribution from all partners merged
0.2	18.02.2014	CTTC, TCS	Final contribution from TCS and CTTC
0.3	28.02.2014	UCL, ITU, UNS	Final contribution from ITU, UCL and UNS
0.4	07.03.2014	UCL, ITU, CTTC, TCS	Further refinements, especially in edition. Conclusion, introduction and extended abstract added.
1.0	07.03.2014	UCL, TCS	Final version with integration of final updates from UNS
1.1	13.02.2015	TCS	Re-insertion of material extracted from v1.0

Executive Summary

This deliverable collects part of the work performed in WP7 “Relay and coverage extension” and in particular under T7.1 “Range extension by using cooperative MIMO” and T7.2 “Design of relaying strategies” of the EMPhAtiC project. It is organized in two main sections, section 2 and section 3 dealing with work of T7.1 and T7.2 respectively.

Relaying is an important building block of Private Mobile Radio (PMR) systems, since it allows to increase coverage and/or to increase communication reliability. This document deals with relaying applied to FilterBank Multi Carrier (FBMC), Orthogonal Frequency Division Multiplexing (OFDM) and Single-Carrier Frequency Division Multiple Access (SC-FDMA) waveforms and specifically on range extension using cooperative MIMO as well as the design and evaluation of relay strategies. The work ranges from theoretical investigation of the performance of the two relaying scheme via the characterization of the achievable rate region of a two-way DF relaying strategy, to more applied work like practical channel estimation schemes for two-way relaying.

Section 2 presents a technique which can be used in the context of coverage extension by using multiple relaying. This is particularly interesting in Private Mobile Radio (PMR) systems with limited coverage, where Direct Mode Operation (DMO) is necessary. A Multiple Input Multiple Output (MIMO) FilterBank Multi Carrier (FBMC) multi-hop relaying scheme using precoding is presented and compared to a Cyclic-Prefix Orthogonal Frequency Division Multiplexing (CP-OFDM) one.

Section 3 contains several techniques related to relaying strategies, with a focus on two-way Decode-and-Forward (DF) relaying. Concerning two-way relaying, this technique has been studied over different angles, ranging from channel estimation for the multiple access phase (see section 3.1), to an investigation of its fundamental limits in terms of achievable rates (see section 3.2), to conclude with an implementation with advanced receiver based on interference cancellation (see section 3.3). Other relaying strategies have been studied too. Section 3.4 analyses the signal-to-noise-plus-distortion ratio (SNDR) of Amplify-and-Forward (AF) relays, which are simple and economic devices that can be deployed in both cellular and ad hoc scenarios of PMR systems. Finally, section 3.5 is devoted to the study of three different multiple access relaying strategies with FBMC, where the relaying operates as a facilitator of the reception at the Base Station (BS) when multiple signals arrive at the same time. This scenario is of interest in the case of PMR networks since it allows not decreasing too much the spectral efficiency of the system.

Section 4 draws the main conclusions of the deliverable.

Table of Contents

1 Introduction

This deliverable collects part of the work performed in WP7 “Relay and coverage extension” and in particular under T7.1 “Range extension by using cooperative MIMO” and T7.2 “Design of relaying strategies” of the EMPhAtiC project. It is organized in two main sections, section 2 and section 3 dealing with work of T7.1 and T7.2 respectively.

Section 2 presents a technique which can be used in the context of coverage extension by using multiple relaying. This is particularly interesting in Private Mobile Radio (PMR) systems with limited coverage, where Direct Mode Operation (DMO) is necessary. A Multiple Input Multiple Output (MIMO) FilterBank Multi Carrier (FBMC) multi-hop relaying scheme using precoding is presented and compared to a Cyclic-Prefix Orthogonal Frequency Division Multiplexing (OFDM) one. The particularity of the FBMC scheme with respect to the OFDM one is the presence of residual interference which limits performance of FBMC in the high Signal-to-Noise Ratio (SNR) regime, in particular in presence of frequency-selective channels. The solution presented in this section proposes a joint design (hop-by-hop) of a spatial precoding and decoding matrix which helps to deal with the interference in the case of multi-tap channels and to alleviate the problem of matrix dimensionality which turns out when multiple hops are required.

Section 3 contains several techniques related to relaying strategies. Its first three sub-sections are dedicated to two-way relaying, whose studies range from investigation of its fundamental limits in terms of achievable rates to channel estimation and performance with advanced receivers. The remaining two sections are dedicated to Amplify-and-Forward (AF) and Decode-and-Forward (DF) relaying in FBMC and to a more complex setting where relaying is also combined to multiple access.

Two-way relaying is studied in section 3.1 in the context of a Single Carrier Frequency Division Multiple Access (SC-FDMA) PHYsical (PHY) layer. The focus is on channel estimation of the multiple access phase, which is one of the critical point of a two-way DF protocol. The goal is to provide practical channel estimation algorithms which perform better than the standard very-low complexity Least Squares (LS) algorithm. The candidate algorithms are compared and a choice of their parameters is proposed in order to have a good performance over the whole range of frequency-selectivity conditions that can be found in PMR channels.

Section 3.2 studies the achievable rate region of an FBMC two-way DF relay strategy, in case of nodes equipped with a single antenna. This work helps understanding the fundamental limits of the two-way DF relaying techniques that can be useful in the PMR application for both in cell-based and ad hoc scenarios. The achievable rate region is compared to the one of CP-OFDM. In the case of FBMC, the dependence of the performance on the length of the equalizers or pre-equalizers is stressed, since it gives a measure of the additional complexity required with respect to and OFDM scheme.

Finally, a FBMC two-way relaying AF protocol is also studied in section 3.3, where its performance is studied in presence of a Successive Interference Cancellation (SIC) receiver.

The remaining two sections analyse and compare relaying strategies when using FBMC, including multiple access relaying schemes. Specifically, section 3.4 studies AF relays which are simple and economic devices that can be deployed in both cellular and ad hoc scenarios of PMR systems. This work analyses the signal-to-noise-plus-distortion ratio (SNDR) of an AF

relay strategy when a FBMC/OQAM modulation with a parallel multistage demodulator/equalizer is used over a highly frequency selective channel. The analysis shows the cumulated effects of (a) an imperfect equalization, (b) the noise of the source–relay channel and (c) the noise of the relay–destination channel. The SNDR is then used to compute the spectral efficiency of the relay link, which is compared to the spectral efficiency of the direct link and of two DF strategies.

Finally, section 3.5 presents a Compute-and-Forward (CoF) protocol for FBMC in the framework of Multiple Access Relay Channel (MARC). This strategy can be applied in a PMR cell-based scenario, in which say, two PMR users are helped in the UL transmission by a relay. This scheme is interesting in systems in which the Base Station (BS) may be limited in terms of number of receive antennas, as it can be the case for PMR systems, especially at low frequency carriers. As it is shown in this section, the relay can help the BS in receiving at the same time the transmissions of two users even in case of one receive antenna at the BS. The proposed scheme is compared to other multiple-access relaying schemes based on AF and DF strategies in terms of complexity, performance and suitability to the PMR case.

Section 4 draws the main conclusions of the deliverable.

2 Range extension using cooperative MIMO

In recent years, there has been increasing interest in exploring different architectures based on multi-hop relaying model for further wireless networks such as PMR and cellular networks. In this section, we investigate the range extension potentials of multi-hop relaying using cooperative Multiple Input Multiple Output (MIMO) Filter-Bank Multi Carrier (FBMC) and Cyclic Prefix-Orthogonal Frequency Division Multiplexing (CP-OFDM) techniques.

2.1 Investigation of FBMC in multi-hop relaying networks

2.1.1 Description and motivation

In this section we consider the range extension in Filter-Bank Multi Carrier/Offset Quadrature Amplitude Modulation (FBMC/OQAM) based multi-hop relaying networks. We first investigate different transmission schemes for point-to-point multiple stream MIMO FBMC/OQAM systems, which can be employed in each link of the multi-hop relaying network. Then, we explore possible relaying strategies at the relay nodes by taking into account the existence of the intrinsic interference inherited from the FBMC/OQAM modulation. Numerical results with respect to the range extension by using multi-hop relays in Private Mobile Radio (PMR) TErrestrial Trunked RAdio (TETRA) networks are presented. By introducing multiple relay nodes between source and destination node, in a PMR TETRA network, significant Bit Error Rate (BER) performance gains are observed.

In standard TETRA systems, the mobile terminals may support two transmission modes, namely Direct Mode Operation (DMO) and Trunked Mode Operation (TMO). In the DMO mode, the TETRA mobiles may communicate with each other directly instead of using up/down links between mobiles and TETRA base stations in the region where infrastructure network coverage is not available. Furthermore, the DMO mode is able to provide the support of using one or more TETRA mobile terminals as signal relays (repeaters) in emergency situations. A mobile terminal with connection to the network may relay the signal transmitted from other nearby mobiles that are out of range of the network coverage which provide rapid development for disaster relief and temporary increment in capacity.

2.1.2 Relaying schemes for multi-hop relaying network

In some publications (e.g., [51], [52]) on multi-hop relaying networks, Amplify-and-Forward (AF) is considered as the relaying strategy. The AF scheme is relatively simple and does not lead to heavy computational load at the relaying nodes. Nevertheless, in case of FBMC/OQAM-based multi-hop relaying networks, the overall interference term observed at the destination that results from the intrinsic interference induced in all hops of the transmissions is a challenge. Therefore, the employment of the intrinsic interference mitigation at each relay node is a straightforward solution. In the following text, we consider multi-hop relaying scheme which is combined with the aforementioned multicarrier MIMO precoding techniques in the simulations and compare its performance with the existing Zero Forcing (ZF) based precoder in both OFDM and FBMC scenarios.

This section deals with TETRA systems in the DMO mode with a one-dimensional linear multi-hop relay network, we consider a linear relay model where the TETRA relays are placed on a straight line between the base station and the mobile terminal. The effect of

frequency selective fading is considered among the base station, relay nodes and the mobile terminal. In the linear relay model given in [53], we first assume that a link between the base station and the mobile terminal is connected by R_{relays} relays and creating $R_{\text{relays}} + 1$ links between the base station and the destination mobile terminal. The model further assumes that the R_{relays} relays are uniformly placed between the base station and the mobile terminal.

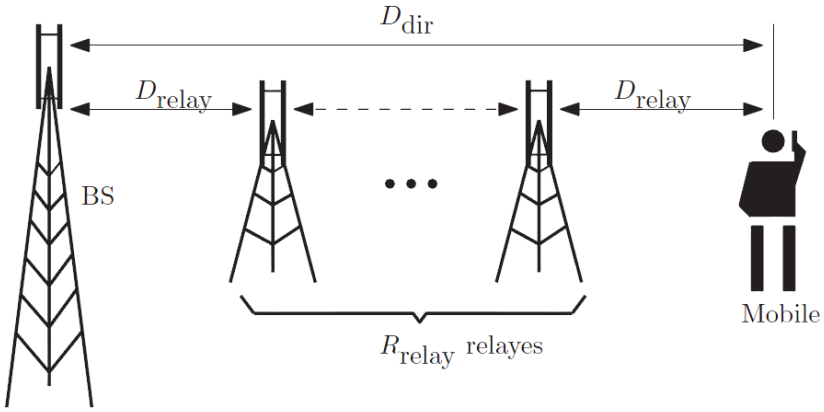

Figure 2-1: Linear Relay Model

This model can be easily extended to 2-D with more complicated relaying case. However, we believe that a simple linear relay model based on path-loss analysis is sufficient to provide considerable insight into the potential of multi-hop relays in a wireless relaying network.

Assuming that all relays have the same transmit power as the base station, the receiver Signal to Noise Ratio (SNR) in a relay model can be written as [53]:

$$SNR_{\text{relay}} = SNR_{\text{direct}} \left(\frac{D_{\text{direct}}}{D_{\text{relay}}} \right)^{\zeta} = SNR_{\text{direct}} \left(R_{\text{relay}} + 1 \right)^{\zeta} \qquad (2.1.1)$$

where the value ζ is the path-loss exponent and ζ = 2 for free space and 3.5 for typical cellular configurations. It can be seen that the SNR_{relay} increases as exponent ζ with increasing number of relays R_{relay} between base station and mobile terminal. From above SNR equation we can see that at mobile terminals, the SNR_{relay} rises with an increasing number of R_{relay}. Moreover, the increase in SNR_{relay} is more pronounced when a larger ζ is considered which usually represents a more realistic propagation path-loss scenario.

It is also worth to mention that for high SNR values, the wireless link capacity increases logarithmically with a growing SNR, this can be verified by considering the Shannon capacity expression of a wireless channels [51]. This analysis represents the potential in terms of improved receiver SNR with the use of multi-hop relays, the receiver SNR at the destination terminal can be increased dramatically, and therefore huge potential in terms of capacity is also expected. It is also worth to mention that if AF scheme is introduced for relaying, the noise terms are also amplified which limits the performance of a multi-hop relaying system.

2.1.3 MIMO techniques at the nodes of the FBMC/OQAM-based multi-hop relaying network

We assume that all nodes in the multicarrier multi-hop relaying network are equipped with multiple antennas. For each hop of the transmission, from the source to the destination, multicarrier MIMO techniques that have been designed for a point-to-point system are employed.

In FBMC/OQAM systems, the real and imaginary parts of each complex-valued data symbol are staggered by half of the symbol period [38], [39] such that the desired signal and the intrinsic interference are separated in the real domain and in the pure imaginary domain, respectively. In [40] and [41] where receive processing techniques have been developed for MIMO FBMC/OQAM systems, it is assumed that the channel frequency responses of adjacent subcarriers do not vary. Consequently, the intrinsic interference is cancelled by taking the real part of the resulting signal after the equalization. To alleviate the constraint on the frequency selectivity of the channel, a zero forcing (ZF) based approach has been proposed in [42] for multi-stream transmissions in a MIMO FBMC/OQAM system where the channel is not restricted to flat fading. More details of the performance analysis of this algorithm have been presented in [43]. However, the work in [42] and [43] is limited to the case where the number of receive antennas does not exceed the number of transmit antennas. In addition, the authors have shown numerically and have also pointed out that their proposed approach only provides a satisfactory performance in an asymmetric configuration, i.e., when the number of transmit antennas is larger than the number of receive antennas. In the context of the multi-user MIMO downlink with space division multiple access (SDMA), coordinated beamforming techniques [45], [44] have been proposed to cope with the dimension constraint imposed on block diagonalization based precoding algorithms [46]. Inspired by these works, we have designed a coordinated beamforming algorithm for MIMO FBMC/OQAM systems without restricting the number of transmit antennas and the number of receive antennas. Assuming perfect channel state information at the transmitter, the precoding matrix and the decoding matrix are calculated jointly in an iterative procedure for each subcarrier. Different choices of the decoding matrix in the initialization step are recommended for different scenarios. For a point-to-point MIMO FBMC/OQAM system, the performance superiority of the proposed approach over the state of the art has been demonstrated via numerical results. It should be noted that in case of highly frequency selective channels, equalization techniques have been proposed as in [48], [49] for FBMC/OQAM-based systems with single-antenna nodes and in [50] for MIMO FBMC/OQAM systems. In this work, we assume that the channel is mildly frequency selective, i.e., the channel on each subcarrier can be treated as flat fading [40], [41]. The cases where the coherence bandwidth of the channel is very small and more sophisticated equalization techniques are required are beyond our scope.

In the following, we first review the data model of a point-to-point MIMO FBMC/OQAM system and then briefly describe the aforementioned transmission strategies.

2.1.3.1 Data model of a point-to-point MIMO FBMC/OQAM system

Let us consider a point-to-point MIMO FBMC/OQAM system where the channel on each subcarrier can be treated as flat fading [40], [41]. The number of transmit antennas and the number of receive antennas are denoted by $\mathrm{M_T}$ and $\mathrm{M_R}$, respectively. The received signal on the kth subcarrier and at the nth time instant is written as follows

$$\boldsymbol{y}_k[n] = \boldsymbol{H}_k[n]\boldsymbol{F}_k[n]\boldsymbol{d}_k[n] + \sum_{i=n-3}^{n+3}\sum_{\ell=k-1}^{k+1} \boldsymbol{H}_\ell\,[i]\boldsymbol{F}_\ell[i]c_{i\ell}\boldsymbol{d}_\ell[i] + \boldsymbol{n}_k[n], \quad (\ell,i) \neq (k,n), \tag{2.1.2}$$

where $\boldsymbol{d}_k[n] \in \mathbb{R}^d$ is the desired signal on the kth subcarrier and at the nth time instant when $(k+n)$ is even[1], and d denotes the number of spatial streams. The terms $c_{i\ell}\boldsymbol{d}_\ell[i]$ contribute to the intrinsic interference and are pure imaginary, where $\ell = k-1, k, k+1$, $i = n-3, \ldots, n+3$, and $(\ell, i) \neq (k, n)$. The coefficients $c_{i\ell}$ represent the system impulse response determined by the synthesis and analysis filters. The PHYDYAS prototype filter [47] is used, and the overlapping factor is chosen to be $K = 4$. For more details about FBMC/OQAM systems, the reader is referred to [39]. Here $\boldsymbol{H}_k[n] \in \mathbb{C}^{M_\mathrm{R}\times M_\mathrm{T}}$ contains the frequency responses of the channels between each transmit antenna and each receive antenna, and $\boldsymbol{n}_k[n]$ denotes the additive white Gaussian noise vector with variance σ_n^2. In addition, $\boldsymbol{F}_k[n] \in \mathbb{C}^{M_\mathrm{T}\times d}$ represents the precoding matrix that maps the spatial streams to the transmit antennas.

2.1.3.2 Straightforward extension of the transmission strategy as in case of CP-OFDM

In several publications on MIMO FBMC/OQAM systems, such as [40] and [41], it is assumed that the channels on adjacent subcarriers are almost the same. The received signal on the kth subcarrier and at the nth time instant can be accordingly written as

$$\boldsymbol{y}_k[n] = \boldsymbol{H}_k[n]\boldsymbol{F}_k[n]\widetilde{\boldsymbol{d}}_k[n] + \boldsymbol{n}_k[n], \tag{2.1.3}$$

where $\widetilde{\boldsymbol{d}}_k[n]$ contains the real-valued desired signal and the pure imaginary interference

$$\widetilde{\boldsymbol{d}}_k[n] = \boldsymbol{d}_k[n] + \sum_{i=n-3}^{n+3}\sum_{\ell=k-1}^{k+1} c_{i\ell}\,\boldsymbol{d}_\ell[i], \quad (\ell,i) \neq (k,n). \tag{2.1.4}$$

Considering $\widetilde{\boldsymbol{d}}_k[n]$ as an equivalent transmitted signal, (2.1.3) resembles the data model of a MIMO CP-OFDM system. Consequently, transmission strategies that have been developed for MIMO CP-OFDM systems can be straightforwardly extended to MIMO FBMC/OQAM systems where only one additional step is required, i.e., taking the real part of the resulting signal after the multiplication by the decoding matrix

$$\widehat{\boldsymbol{d}}_k[n] = \mathrm{Re}\{\boldsymbol{D}_k^\mathrm{H}[n]\boldsymbol{y}_k[n]\}, \tag{2.1.5}$$

where $\boldsymbol{D}_k[n] \in \mathbb{C}^{M_\mathrm{R}\times d}$ is the decoding matrix on the kth subcarrier and at the nth time instant. Here $\mathrm{Re}\{\cdot\}$ symbolizes the real part of the input argument, while $\mathrm{Im}\{\cdot\}$ is used in the following text to represent the imaginary part.

[1]For the case where $(k+n)$ is odd, the desired signal on the kth subcarrier and at the nth time instant is pure imaginary, while intrinsic interference is real. As the two cases are essentially equivalent to each other, we only take the case where $(k+n)$ is even to describe the proposed algorithm in this paper.

2.1.3.3 Zero forcing based approach

In [42] and [43], the precoding matrix is designed such that the intrinsic interference (corresponding to the second term on the right hand side of (2.1.2)) can be cancelled by taking the real part of the received signal. Let us expand the real part of the received signal on the kth subcarrier and at the nth time instant

$$\mathrm{Re}\{\boldsymbol{y}_k[n]\} = \mathrm{Re}\{\boldsymbol{H}_k[n]\boldsymbol{F}_k[n]\}\boldsymbol{d}_k[n] + (-1)\cdot\sum_{i=n-3}^{n+3}\sum_{\ell=k-1}^{k+1}\mathrm{Im}\{\boldsymbol{H}_\ell[i]\boldsymbol{F}_\ell[i]\}\mathrm{Re}\{c_{i\ell}\boldsymbol{d}_\ell[i]\} + \mathrm{Re}\{\boldsymbol{n}_k[n]\}, \quad (\ell,i)\neq(k,n). \tag{2.1.6}$$

The precoding matrix $\boldsymbol{F}$ for each subcarrier and each time instant is calculated such that

$$\mathrm{Im}\{\boldsymbol{H}\boldsymbol{F}\} = \boldsymbol{0},$$

where $\boldsymbol{H}$ represents the channel matrix on the same subcarrier and at the same certain time instant, and the time as well as the subcarrier indices are ignored, as the precoding concept is on a per-subcarrier basis. Define a matrix $\breve{\boldsymbol{H}}$ as

$$\breve{\boldsymbol{H}} = [\mathrm{Im}\{\boldsymbol{H}\} \quad \mathrm{Re}\{\boldsymbol{H}\}] \in \mathbb{R}^{M_\mathrm{R}\times 2M_\mathrm{T}}. \tag{2.1.7}$$

The stacked version of the real part and the imaginary part of the precoding matrix $\boldsymbol{F}$, i.e., $[\mathrm{Re}\{\boldsymbol{F}\}^\mathrm{T} \quad \mathrm{Im}\{\boldsymbol{F}\}^\mathrm{T}]^\mathrm{T}$, should lie in the null space of $\breve{\boldsymbol{H}}$. However, this approach is designed only for scenarios where $\mathrm{M_T} \geq \mathrm{M_R}$. In addition, it is observed in the numerical results presented in [43] and is also pointed out in [42] that in a symmetric case where $\mathrm{M_T} = \mathrm{M_R}$, this scheme does not lead to a good performance.

2.1.3.4 Coordinated beamforming

We propose to jointly and iteratively update the precoding matrix and the decoding matrix to alleviate the dimension constraint on the precoding algorithm in [42], i.e., scenarios where $M_\mathrm{T} \leq M_\mathrm{R}$ will be dealt with. First, an equivalent channel matrix $\boldsymbol{H}_\mathrm{eq}$ is defined as [55]

$$\boldsymbol{H}_\mathrm{eq} = \boldsymbol{D}^\mathrm{T}\boldsymbol{H} \in \mathbb{C}^{d\times M_\mathrm{T}}, \tag{2.1.8}$$

where $\boldsymbol{D} \in \mathbb{R}^{M_\mathrm{R}\times d}$ is the real-valued decoding matrix. In addition, we decouple the precoding matrix into two parts, i.e.,

$$\boldsymbol{F} = \boldsymbol{F}_1\boldsymbol{F}_2 \in \mathbb{C}^{M_\mathrm{T}\times d}, \tag{2.1.9}$$

where $\boldsymbol{F}_1 \in \mathbb{C}^{M_\mathrm{T}\times M_x}$ and $\boldsymbol{F}_2 \in \mathbb{R}^{M_x\times d}$. The proposed coordinated beamforming algorithm is summarized as follows [55]:

- **Step 1**: Initialize the decoding matrix $\boldsymbol{D}^{(0)} \in \mathbb{R}^{M_\mathrm{R}\times d}$, set the iteration index p to zero, and set a threshold ϵ for the stopping criterion. The decoding matrix is generated randomly if the current subcarrier is the first one; otherwise set the decoding matrix as the one calculated for the previous subcarrier [44].

- **Step 2**: Set $p = p + 1$ and calculate the equivalent channel matrix $\boldsymbol{H}_{\mathrm{eq}}^{(p)}$ in the pth iteration as

$$\boldsymbol{H}_{\mathrm{eq}}^{(p)} = \boldsymbol{D}^{(p-1)^{\mathrm{T}}}\boldsymbol{H} \in \mathbb{C}^{d\times M_{\mathrm{T}}}. \tag{2.1.10}$$

  Define a matrix $\breve{\boldsymbol{H}}_{\mathrm{eq}}^{(p)} = \left[\mathrm{Im}\left\{\boldsymbol{H}_{\mathrm{eq}}^{(p)}\right\} \quad \mathrm{Re}\left\{\boldsymbol{H}_{\mathrm{eq}}^{(p)}\right\}\right] \in \mathbb{R}^{d\times 2M_{\mathrm{T}}}$.

- **Step 3**: Calculate the precoding matrix $\boldsymbol{F}^{(p)} = \boldsymbol{F}_1^{(p)}\boldsymbol{F}_2^{(p)}$ for the pth iteration. First, we perform the singular value decomposition (SVD) of $\breve{\boldsymbol{H}}_{\mathrm{eq}}^{(p)}$ as

$$\breve{\boldsymbol{H}}_{\mathrm{eq}}^{(p)} = \boldsymbol{U}_1^{(p)}\boldsymbol{\Sigma}_1^{(p)}\boldsymbol{V}_1^{(p)^{\mathrm{T}}}. \tag{2.1.11}$$

  Denoting the rank of $\breve{\boldsymbol{H}}_{\mathrm{eq}}^{(p)}$ as $r^{(p)}$, we define $\boldsymbol{V}_{1,0}^{(p)} \in \mathbb{R}^{2M_{\mathrm{T}}\times M_x}$ as containing the last $M_x = 2M_{\mathrm{T}} - r^{(p)}$ right singular vectors that form an orthonormal basis for the null space of $\breve{\boldsymbol{H}}_{\mathrm{eq}}^{(p)}$. Hence, the first part of the precoding matrix for the pth iteration $\boldsymbol{F}_1^{(p)}$ can be obtained via

$$\boldsymbol{V}_{1,0}^{(p)} = \begin{bmatrix}\mathrm{Re}\left\{\boldsymbol{F}_1^{(p)}\right\}\\ \mathrm{Im}\left\{\boldsymbol{F}_1^{(p)}\right\}\end{bmatrix} \in \mathbb{R}^{2M_{\mathrm{T}}\times M_x}. \tag{2.1.12}$$

  To further calculate the second part of the precoding matrix in the pth iteration $\boldsymbol{F}_2^{(p)}$, the following equivalent channel matrix after the cancellation of the intrinsic interference for the pth iteration is defined as

$$\widetilde{\boldsymbol{H}}_{\mathrm{eq}}^{(p)} = \mathrm{Re}\left\{\boldsymbol{H}_{\mathrm{eq}}^{(p)}\boldsymbol{F}_1^{(p)}\right\} \in \mathbb{R}^{d\times M_x}. \tag{2.1.13}$$

  Further calculate the SVD of $\widetilde{\boldsymbol{H}}_{\mathrm{eq}}^{(p)}$, and define $\boldsymbol{V}_{2,1}^{(p)} \in \mathbb{R}^{M_x\times d}$ as containing the first d right singular vectors. Thereby, $\boldsymbol{F}_2^{(p)}$ is obtained as $\boldsymbol{F}_2^{(p)} = \boldsymbol{V}_{2,1}^{(p)}$.

- **Step 4**: Update the decoding matrix based on the equivalent channel matrix after the cancellation of the intrinsic interference where only the processing at the transmitter is considered

$$\widetilde{\boldsymbol{H}}_{\mathrm{eq,tx}}^{(p)} = \mathrm{Re}\left\{\boldsymbol{H}\boldsymbol{F}^{(p)}\right\} \in \mathbb{R}^{M_{\mathrm{R}}\times d}. \tag{2.1.14}$$

  When the MMSE receiver[2] is used, the decoding matrix has the following form

$$\boldsymbol{D}^{(p)} = \widetilde{\boldsymbol{H}}_{\mathrm{eq,tx}}^{(p)}\left(\widetilde{\boldsymbol{H}}_{\mathrm{eq,tx}}^{(p)^{\mathrm{T}}}\widetilde{\boldsymbol{H}}_{\mathrm{eq,tx}}^{(p)} + \sigma_n^2\boldsymbol{I}_d\right)^{-1}. \tag{2.1.15}$$

- **Step 5**: Calculate the term $\Delta(\boldsymbol{F})$ defined as

[2]Other receivers, such as zero forcing or maximum ratio combining, can also be employed in this coordinated beamforming algorithm.

$$\Delta(\boldsymbol{F}) = \left\|\boldsymbol{F}^{(p+1)} - \boldsymbol{F}^{(p)}\right\|_{\mathrm{F}}^{2}, \tag{2.1.16}$$

which measures the change of the precoding matrix $\boldsymbol{F}$. If $\Delta(\boldsymbol{F}) < \epsilon$, the convergence is achieved, and the iterative procedure terminates. Otherwise go back to **Step 2**.

It is important to note that in the special case where $M_{\mathrm{T}} = M_{\mathrm{R}} = d + 1$, we propose to compute the decoding matrix in the initialization step as follows such that the coordinated beamforming technique only needs two iterations to converge. First, calculate the SVD of $\breve{\boldsymbol{H}} \in \mathbb{R}^{M_{\mathrm{R}} \times 2M_{\mathrm{T}}}$ as defined in (2.1.7), and let $\boldsymbol{V}_{1,0}^{(0)}$ contain the last $(2M_{\mathrm{T}} - M_{\mathrm{R}})$ right singular vectors. Defining $\boldsymbol{F}_{1}^{(0)}$ via

$$\boldsymbol{V}_{1,0}^{(0)} = \begin{bmatrix} \mathrm{Re}\left\{\boldsymbol{F}_{1}^{(0)}\right\} \\ \mathrm{Im}\left\{\boldsymbol{F}_{1}^{(0)}\right\} \end{bmatrix}, \tag{2.1.17}$$

we compute $\boldsymbol{U}_{2,1}^{(0)} \in \mathbb{R}^{M_{\mathrm{R}} \times d}$ from the SVD of $\mathrm{Re}\left\{\boldsymbol{H}\boldsymbol{F}_{1}^{(0)}\right\}$ such that it contains the first d left singular vectors. Then the decoding matrix for the initialization step is chosen as

$$\boldsymbol{D}^{(0)} = \boldsymbol{U}_{2,1}^{(0)}. \tag{2.1.18}$$

2.1.4 Relaying schemes for the FBMC-based multi-hop network

We consider FBMC/OQAM and CP-OFDM range extension systems with $R_{\mathrm{relays}} + 1$ hops and R_{relays} relay nodes where the channel on each subcarrier is treated as flat fading [42], [43]. For each relay nodes, the number of transmit antennas and the number of receive antennas are denoted by M_{T} and M_{R}, respectively. The received signal on the kth subcarrier and at the nth time instant for the τth hop is written as follows

$$\begin{aligned} \boldsymbol{y}_{k}^{(\tau)}[n] = \boldsymbol{H}_{k}^{(\tau)}[n]\boldsymbol{F}_{k}^{(\tau)}[n]\widehat{\boldsymbol{d}}_{k}^{(\tau-1)}[n] \\ + \sum_{i=n-3}^{n+3} \sum_{\ell=k-1}^{k+1} \boldsymbol{H}_{\ell}^{(\tau)}[i]\boldsymbol{F}_{\ell}^{(\tau)}[i] c_{i\ell} \hat{d}_{\ell}^{(\tau-1)}[i] \\ + \boldsymbol{n}_{k}^{(\tau)}[n], \quad (\ell, i) \neq (k, n), \end{aligned} \tag{2.1.19}$$

where vector $\widehat{\boldsymbol{d}}_{k}^{(\tau-1)}[n]$ denotes the signal estimate obtained from the previous hop. The terms $\boldsymbol{H}_{k}^{(\tau)}[n]$ and $\boldsymbol{F}_{k}^{(\tau)}[n]$ denote the channel state information and its corresponding precoding matrix for the τ th transmission hop, respectively.

2.1.4.1 Zero Forcing based relay nodes

For each relay, the received signal is retransmitted without decoding by using the AF scheme. Recall that AF requires much less delay and much less computing power as no decoding or quantizing operation is performed at each relay.

Thanks to the ZF precoding operations, for each relay node, the intrinsic interference terms are removed by taking the real part of the received signal as mentioned in previous sections, the signal is obtained as

$$\widehat{\boldsymbol{d}}_k^{(\tau)}[n] = \mathrm{Re}\left\{\boldsymbol{y}_k^{(\tau)}[n]\right\} \tag{2.1.20}$$

The estimated signal $\widehat{\boldsymbol{d}}_k^{(\tau)}[n]$ obtained in each relay node is then ready to be forward to the next relay (e.g. the $(\tau+1)$th hop). The signal from source node is forwarded R_{relays} times until it reaches the destination terminal. Here $\mathrm{Re}\{\cdot\}$ symbolizes the real part of the input argument, while $\mathrm{Im}\{\cdot\}$ is used in the following text to represent the imaginary part. Although precoding is performed before forwarding the signal to the next relay node, this scheme has an important similarity with the AF scheme that can be observed in $\widehat{\boldsymbol{d}}_k^{(\tau)}[n]$. In the noiseless case, it has the following form

$$\begin{aligned}\widehat{\boldsymbol{d}}_k^{(\tau)}[n] = \mathrm{Re}\left\{\boldsymbol{H}_k^{(\tau)}[n]\boldsymbol{F}_k^{(\tau)}[n]\right\}\cdot \\ \mathrm{Re}\left\{\boldsymbol{H}_k^{(\tau-1)}[n]\boldsymbol{F}_k^{(\tau-1)}[n]\right\}\cdots\ \mathrm{Re}\left\{\boldsymbol{H}_k^{(1)}[n]\boldsymbol{F}_k^{(1)}[n]\right\}\boldsymbol{d}_k[n].\end{aligned} \tag{2.1.21}$$

The channel effect of each hop is accumulated throughout the whole multi-hop transmission. This observation justifies that this relaying scheme is classified into the category of AF.

As already pointed out in Section 2.1.3.4, if the number of transmit antennas of each hop is not greater than the number of receive antennas, this scheme fails to provide a satisfactory performance.

2.1.4.2 Coordinated beamforming

By employing the coordinated transmit beamforming algorithm at each hop as introduced in section 2.1.3.4, the dimension constraint and the strict requirement for flat fading channels can be alleviated. Let us name this relaying scheme as Filter and Forward (FF). At the transmitter side of each hop, the calculation of the precoding matrix and the decoding matrix is carried out jointly in an iterative manner. At the receiver side, we take the real part of the resulting signal after the multiplication by the decoding matrix and obtain the signal estimates at relay τ as

$$\widehat{\boldsymbol{d}}_k^{(\tau)}[n] = \mathrm{Re}\left\{\boldsymbol{D}_k^{\mathrm{H}}[n]\boldsymbol{y}_k^{(\tau)}[n]\right\}, \tag{2.1.22}$$

where $\boldsymbol{D}_k[n] \in \mathbb{C}^{M_{\mathrm{R}}\times d}$ is the decoding matrix on the kth subcarrier and at the nth time instant. The estimation $\widehat{\boldsymbol{d}}_k[n]$ is then forwarded R_{relays} times until it reaches the destination. Unlike the AF scheme where the ZF-based precoding is employed, multiplying the decoding matrix leads to the elimination of the channel effect at each hop. Nevertheless, if the channel exhibits frequency selectivity such that the channel frequency responses across adjacent subcarrier vary severely, there is still residual intrinsic interference at each hop.

By introducing multiple relying stations for range extension, significant increase in receiver SNR can be observed, which results in an enhanced BER performance.

2.1.5 Simulation settings

The bit error rate performance for the direct link and the relay link transmission is demonstrated in this section, where the free space path-loss exponent ζ = 3.5 is given for

typical cellular configurations. For all simulation examples, there are 1024 subcarriers used, and the total available bandwidth is 10 MHz for all nodes. In case of CP-OFDM, the length of the CP is set to ¼ of the symbol period. The ITU Ped-A and Veh-A channel model is adopted [54] and antenna correlation is not considered. In terms of FBMC prototype filters, we employ a PHYDYAS defined pulse shaping filter [47] with an overlapping factor of K = 4. The data symbols are drawn from a 16-QAM constellation. By using the linear relay model given in [51], we assume that a link between the base station and the mobile is connected by $\mathrm{R}_{\mathrm{relay}}$ amplifier forward relays creating $(\mathrm{R}_{\mathrm{relay}}+1)$ links between the base station and the destination mobile terminal. In the model, $\mathrm{R}_{\mathrm{relay}}$ relay stations are uniformly placed between the base station and the mobile terminal.

Frame structure	
Bandwidth	10 MHz
Subcarriers number	1024 subcarriers OFDM CP length: ¼ Symbol period
Subcarrier spacing	10 kHz
Reference signals	LTE-like
FBMC filter	OFDM/OQAM PHYDYAS
Overlapping factor	4
Modulation and coding schemes	16-QAM, uncoded
Transmitter/Receiver	
Noise power spectral density	Various
MS/RS number of antenna	Symmetric 3x3
Transmission scheme	MIMO with 2 spatial data streams
HH antenna model	Isotropic
Propagation	
Path-loss model	Free-space with path-loss exponent $\zeta = 3.5$
Fast fading channel models	ITU Ped-A, ITU Veh-A
Channel estimation	Ideal

Table 2-1: Simulation settings and scenarios

2.1.6 Simulation results

In this section, a symmetric MIMO downlink relaying setting is considered, where the base station, relays and destination mobile terminals are equipped with 3 transmit and receive antennas, respectively, and the number of spatial streams from node to node is set to 2. For the relaying case, we vary the number of relay nodes but fix the distance between the source node and the destination terminal.

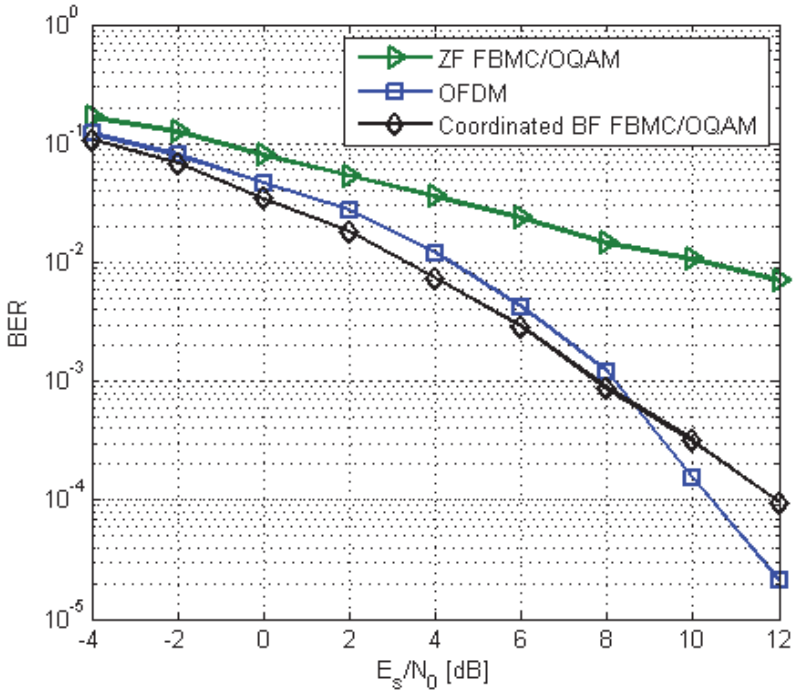

Figure 2-2: BER vs. SNR with one AF relay node (2 hops) between the base station and the destination terminal, ITU Ped-A channel is used for simulation

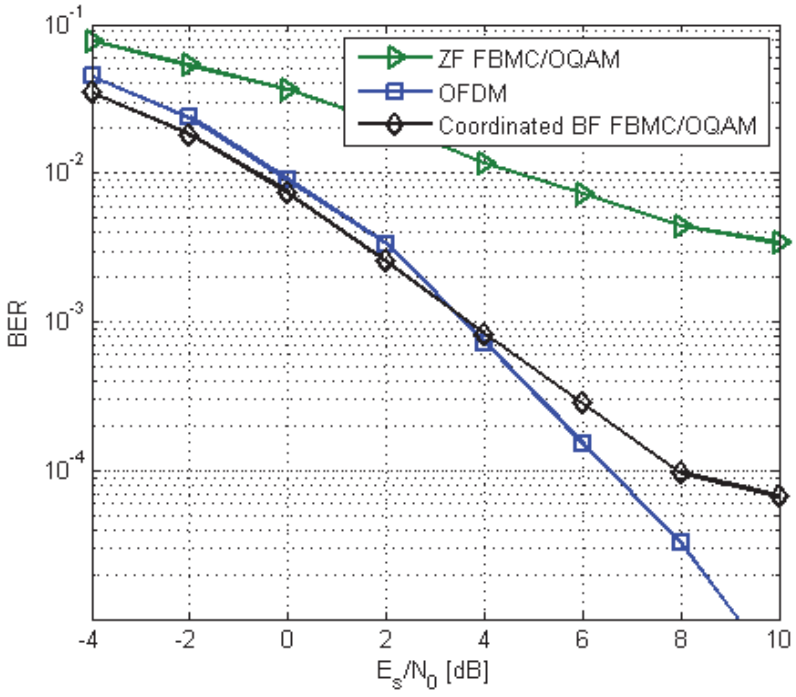

Figure 2-3: BER vs. SNR with 2 AF relay nodes (3 hops) between the base station and the destination, ITU Ped-A channel is used for simulation

The BER performances of different precoding schemes for FBMC/OQAM based systems are presented and also compared to that of a CP-OFDM based system in Figure 2-2**,** Figure 2-3 for ITU Ped-A channel and Figure 2-4**,** Figure 2-5 for ITU Veh-A channel. The transmission

scheme that is a straightforward extension of ZF [46] for CP-OFDM is described in [55]. The plots show that in the symmetric scenario, the proposed coordinated beamforming technique (CBF) significantly outperforms the ZF based FBMC/OQAM precoding schemes as well as its CP-OFDM counterpart in lower SNR regions. It is worth to mention that the CBF algorithm in each relay node takes only two iterations to converge. The transmission scheme that is a straightforward extension of ZF for the CP-OFDM case relies on the assumption that the channel frequency responses remain the same across adjacent subcarriers. As the ITU channel exhibits frequency selectivity and such an assumption is therefore violated, the performance of this scheme degrades especially in the high SNR regime. This Inter-Symbol Interference (ISI) can be partially removed by using multi-tap equalizers for each subcarrier with extra computational effort.

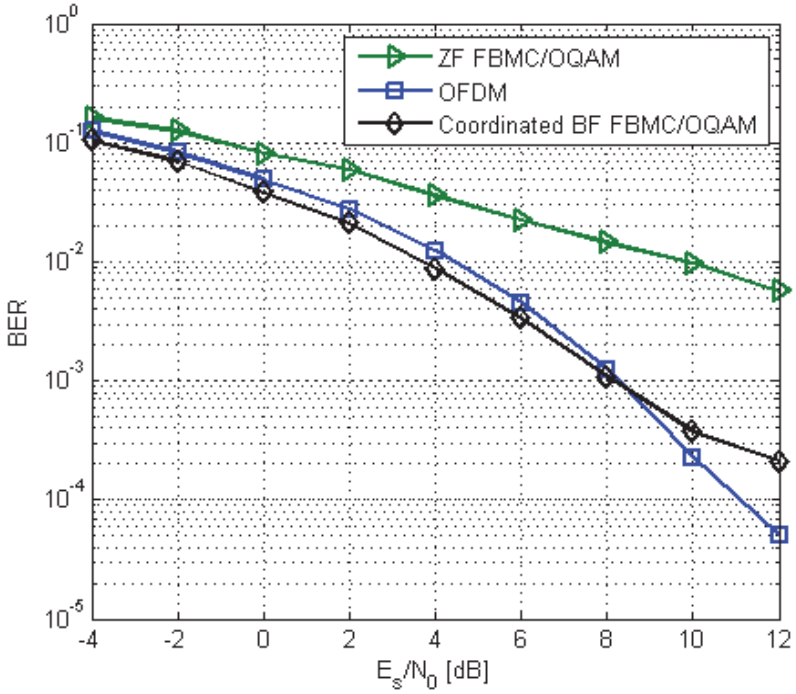

Figure 2-4: BER vs. SNR with one AF relay node (2 hops) between the base station and the destination, ITU Veh-A channel is used for simulation

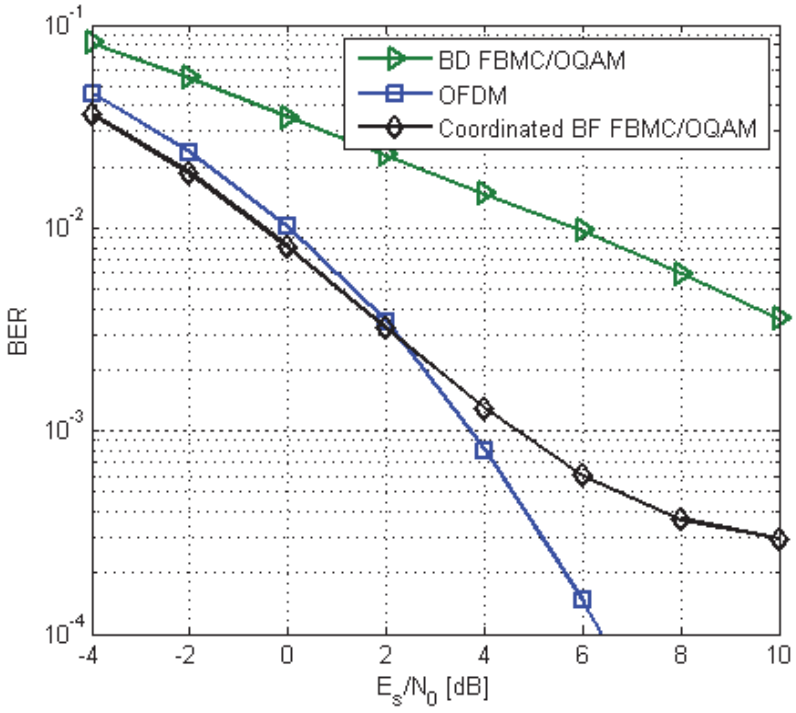

Figure 2-5: BER vs. SNR with 2 AF relay nodes (3 hops) between the base station and the destination, ITU Veh-A channel is used for simulation

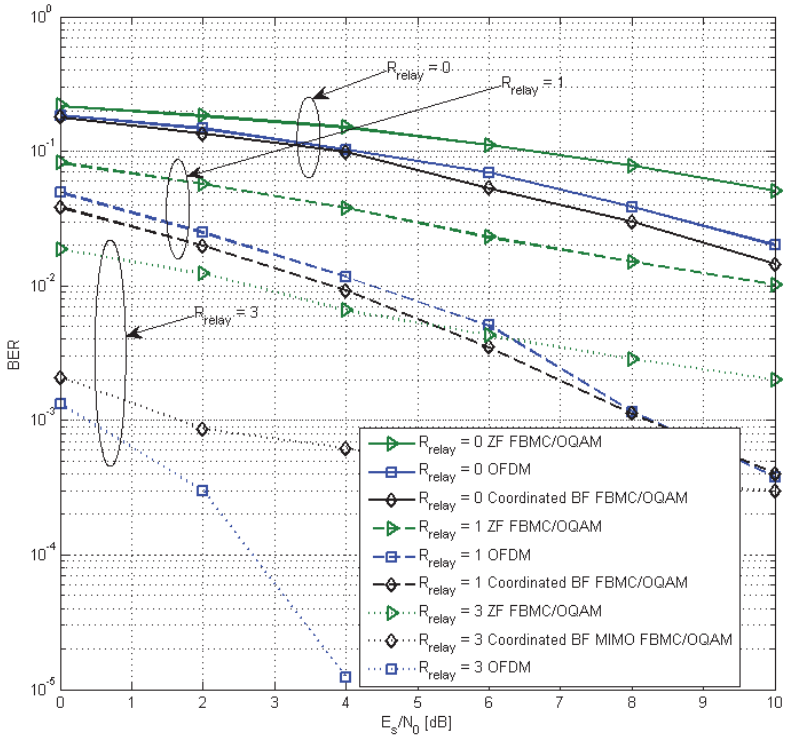

Figure 2-6: Comparison of the BER performance of different schemes in a MIMO relaying system, there are 3 antennas for each node with 2 data streams. The ITU Veh-A channel is considered here. By increasing the number of relays between the source and destination, a lower BER performance is observed.

In Figure 2-6 and Figure 2-7 we compare the BER performances against the increasing number of relay nodes between the base station and the destination terminal. By increasing the number of relays, the receiver SNR of each hop is increased dramatically, and therefore, a much lower BER performance is obtained. However, when multiple relay nodes are cooperated, the FBMC system performance is limited by residual intrinsic interference instead of the noise, which is evident by the observation of the decreasing slopes of the BER curves where more relays are introduced.

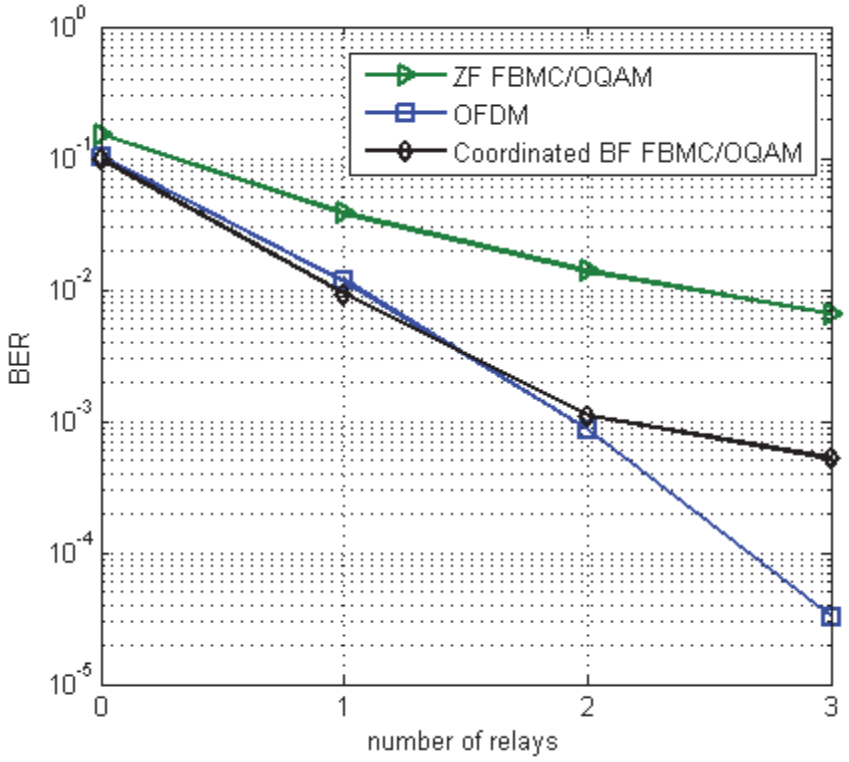

Figure 2-7: Comparison of the BER performance against number of AF relaying nodes for different transmission schemes, there are 3 antennas for each node with 2 data streams. The SNR for each link is 4 dB. The ITU Veh-A channel is considered here

2.1.7 Final remarks

This section deals with TETRA systems in the DMO mode with a multi-hop relay network, we first investigate different transmission schemes for point-to-point multiple stream MIMO FBMC/OQAM systems. We then review a simple one-dimensional linear relay model in section 2.1.4 where the TETRA relays are placed on a straight line between the base station and the mobile terminal. The effect of frequency selective fading is also considered among the transmission links of each node pairs. With this model, we conclude that by using multiple relay nodes, the receiver SNR_{relay} rises with an increasing number of relays. Section 2.1.4.1 and section 2.1.4.2 explore possible relaying strategies at the relay nodes by taking into account the existence of the intrinsic interference inherited from the FBMC/OQAM modulation. Numerical results with respect to the range extension by using multi-hop relays in PMR TETRA networks are presented in the section 2.1.6.

3 Design of relay strategies

3.1 Channel estimation for two-way relaying

3.1.1 Description and motivation

Two-way relaying recently emerged as an interesting candidate for relaying communications in order to lower latency and improve spectral efficiency of bi-directional communications via a relay. The technique assumes that there is a bi-directional information flow from a node A to a node B and vice versa, going through a relay node. Typically such a communication requires 4 resource slots (in time, frequency, code or other) but many recent works proposed strategies that reduced the resource occupation to 3 or 2 slots. Before going through a brief review of the technique, let us introduce the interest of the technique for EMPhAtiC. This section will be mainly devoted to standard CP-OFDM techniques, so 3GPP Long Term Evolution (LTE) technology will be taken as the baseline.

As it will be clearer in the following section, here we present a standard two-way relaying strategy by using a Multi-User (MU) MIMO technique applied to the multiple access phase, combined with a DF strategy and XOR of the received messages. However, the focus here will be just on channel estimation, in particular in the multiple access phase (corresponding to an UpLink (UL) in a cellular scenario), since it is a critical point for understanding the feasibility of the technique and for estimating the loss with respect to ideal performance.

3.1.1.1 Connection with PMR scenarios

In the context of the EMPhAtiC project, two-way relaying protocols may apply to the following scenarios:

- Cell-based communications: in a crisis situation or simply when an important event happens in a given location, many operators will converge in a cell. It is reasonable that a non-negligible part of the voice traffic will happen between users inside that cell. In this case, by exploiting features in part already present in 3GPP LTE, the Base Station (BS), called eNodeB in 3GPP LTE, can use a two-way relaying protocol in order to spare Resource Blocks (RB), independently of the PHY layer used. This situation is schematically represented in Figure 3-1.
- DMO operation in ad hoc mode: a group of PMR users are outside the coverage of the cellular network, for instance in case of bad coverage (parkings, tunnels, shadowing of big buildings) or network/BS fault. A node (either vehicular –preferred choice– or handheld) is elected cluster-head for managing the resources among the nodes in coverage. In some sense, a small cell is created around the Cluster-Head (CH). If bi-directional traffic (e.g. voice) must be exchanged between two nodes in the cluster which are not under mutual coverage, then the CH may use a two-way relaying protocol to improve the efficiency and latency of the communications. This situation is schematically represented in Figure 3-1.

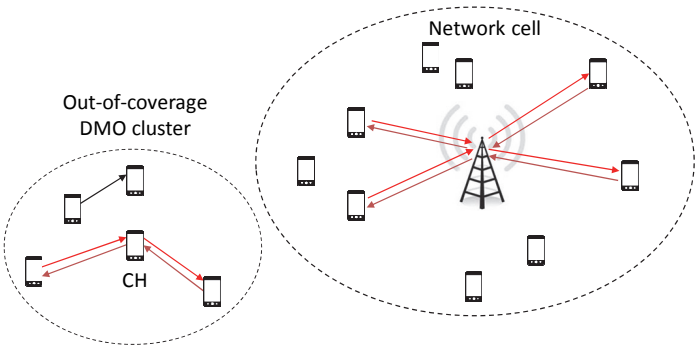

Figure 3-1: Network cell scenario and out-of-coverage DMO scenario with two-way relaying

- Clusterized ad hoc network: in a crisis situation, when the standard cellular network is not available or is down due to some human of natural event (damaged, destroyed network), a wireless ad hoc network can be quickly deployed. The network creates different clusters (cells) which are interconnected by a wireless back-bone. Some bridging nodes are in charge of exchanging traffic among two clusters. In this situation it is seems reasonable to have also some bi-directional traffic. Two-way relaying may be used by the bridging nodes in this context to lower latency and improve efficiency. This situation is schematically represented in Figure 3-2.

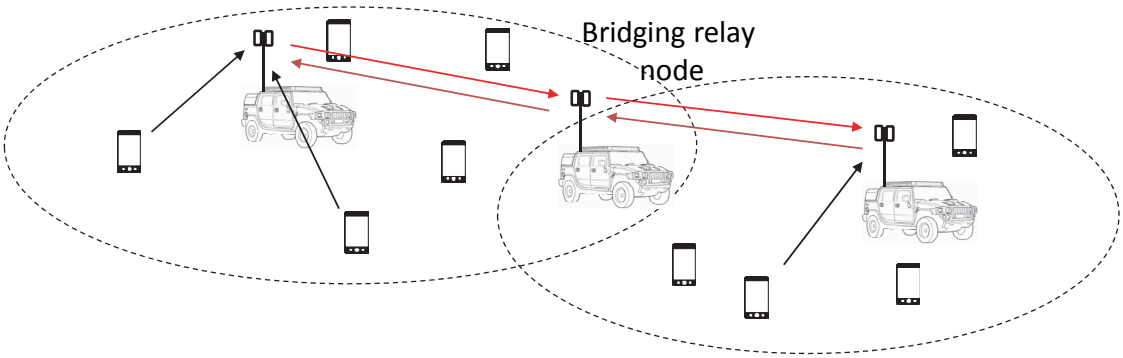

Figure 3-2: Clustered wireless ad hoc network with bridging relay

3.1.1.2 State of the art

Two-way relaying

A good tutorial on two-way relaying is presented in [30]. A large variety of techniques exist for both multiple access and broadcast phase. In order to have the maximum spectral efficiency and minimum latency, the multiple access phase from the sources to the relay should be made ideally at the same time, so that the signals are superimposed over the same resources. In the broadcast phase, a technique must be found so that users may recover from the same signal the information which is of interest to them.

In [19] the achievable rate region for a MIMO two-way relaying protocol with Channel State Information (CSI) at the transmitter was established. The channel here is frequency flat for all links, and there is no CSI at the transmitter in the multiple access phase (OFDM case). In the broadcast phase two strategies are proposed, but the relays always decode the two

signals, hence a DF strategy is used. The first one is a superposition coding in which the relay creates two sent signals which are precoded by assuming perfect CSI at the transmitter and then summed up before modulation. The second strategy consists in XOR precoding of the messages received in the multiple access phase. When a MIMO precoder is used, the authors show that the XOR strategy performs better than the superposition coding one even when there is no CSI at the relay. For 2 transmit antennas at the nodes and 2 or 3 antennas at the relay, all strategies with or without CSI gives substantially equal performance in terms of average sum rate. Differences in the sum rate with or without CSI are more important only with a higher number of antennas at the relay. Comparisons with the one-way relaying strategy (4 slots for communication) confirm that two-way relaying even without CSI almost doubles the sum rate.

The optimal relaying strategy depends of course on the constraints and knowledge of the channels. For example [37] presents recent results on the achievable rate region of a two-way relaying channel when the two users have different channel qualities and do not need to receive the same amount of information.

When applying DF, the decoding can include the channel code (higher complexity) or not (more limited complexity). In this case [25] makes an overview of proposals based on the so-called DeNoise-and-Forward (DNF) strategy. Different strategies for the detection of the received symbols at the relay and remapping are proposed. This work is focussed on flat channels.

[12] investigates two-way relaying in the framework of a direct-sequence Code Division Multiple Access (CDMA) system in which a common spreading code is applied to each couple of communicating nodes and the signal are synchronized at reception and are received with the same power (power control is active). An AF technique is investigated as well as a joint demodulate-and-XOR forward technique based on linear MMSE filtering. Flat fading channel is investigated and a comparison between the techniques is done.

The flat MIMO channel case is investigated, for instance, in [16], [17]. Here node pairs in the multiple access phase are separated thanks to multiple antennas. In the broadcast phase, they are separated spatially by a ZF precoder (under hypothesis of channel reciprocity), while the interference inside each pair is cancelled by the standard XOR precoding of the decoded signal. An algorithm is provided in order to maximize the sum-rate of all the pairs.

Issues related to resource allocation are investigated for instance in [32], which proposes to guarantee data rate fairness in a two-way relay channel with optimal power control at all nodes, for both AF and DF protocols. Data rate fairness means that two transmitting nodes are constrained to use the same data rate, and power allocation is adapted with respect to fading (supposed Single Input Single Output (SISO) flat and constant during the protocol). Gaussian codebook is assumed as well as perfect CSI at the relay and at the nodes in order to calculate the optimal powers.

Resource allocation plus buffering at the relay side can be used in order to increase the spectral efficiency of the relaying protocol, when channel state information is available and the traffic is not strictly latency constrained. [26] proposed a two-way relay protocol in three Time Division Multiple Access (TDMA) steps (transmission of A, then B, then network coding and common broadcast phase), plus a resource allocation algorithm for this case. The relay inserts the received packets in a buffer and waits for a good channel realization for transmission.

Concerning the evaluation of practical two-way relaying in realistic systems [22] provides some results on two-way relaying applied to LTE for a link eNodeB – Relay Node – User Equipment (UE). The investigation is over a simple two-way relay protocol in three steps with network combining of the packets at MAC level; in fact Transport Blocks (TB) are combined. Different versions of the protocol, also using Subcarrier Division Duplexing, in which part of the subcarriers of a, say, DownLink (DL) channel can be assigned to the UL. Results demonstrate an interest of two-way relaying even in a realistic scenario, and a robustness of the algorithm with respect to many changing parameters.

Finally, two-way relaying in for multi-user MIMO Single-Carrier Frequency Domain Equalization (SC-FDE) systems is investigated in [14]. In this reference however, transmit beamforming is used by the sources and relays. Moreover, a sort of AF protocol is used by the relay which linearly processes the received signals before re-transmission. This scheme however requires the knowledge of the beamforming matrices of all users.

Channel estimation

As it will be explained in the following subsection, the study will focus on two-way relaying in the context of future broadband PMR which will be based on 3GPP LTE. The proposed two-way relaying strategy uses two slots, one for multiple access and the other for broadcast. In the multiple access phase virtual MU-MIMO is used to multiplex the users. It is clear, as also reported in the literature, that multiple access is the most delicate phase, since there will be Multi User Interference (MUI) or multi-antenna interference, if the users are seen as virtual antennas. Hence it is important to understand if the channel estimation functionality introduces some limitations in terms of quality estimate and number of users supported by the technique. The rest of this section is devoted to the state of the art on channel estimation related to LTE and to MU-MIMO.

3GPP LTE UL uses Single-Carrier Frequency Division Multiple Access (SC-FDMA), for an introduction of this modulation and multiplexing technique please refer for instance to [34], [28], [27] and references therein. Reference signals for channel estimation in LTE are described in the document [35], also for virtual MU-MIMO in the UL. A more straightforward and clear explanation can be found in textbooks on LTE/LTE-A, like [34]. Concerning LTE UL, channel estimation is based on reference signal which are Constant Amplitude Zero Auto-Correlation (CAZAC) sequences, in particular on Zhadoff-Chu sequences [33], [18], [11]. The case of MU-MIMO implies the capability of discriminating multiple channels for each receive antenna. That is achieved by assigning to the UEs the same base sequence but cyclically shifted of a certain value called cyclic shift. By reposing on the zero-autocorrelation property of the CAZAC sequences, when the signals are synchronized at the receiver, the impulse responses of the channels will appear with a delay corresponding to the cyclic shift of the respective reference signal. Hence, as long as their delay spread is shorter than the minimum cyclic shift, separation of the channel impulse responses is possible.

LTE design for MIMO responds in some sense to the study in [29], where optimal training sequences for MIMO frequency selective fading channels are found to be orthogonal. Training sequences in the paper are not the LTE CAZAC sequences; however, CAZAC sequences achieve an approximate orthogonality thanks to the zero-autocorrelation properties, under the hypotheses of synchronization of the received signals and channel delay spread less than the minimum cyclic shift.

[20] deals with practical channel estimation exactly in the UL MU-MIMO case, inserting also considerations on Orthogonal Cover Codes (OCC) for giving additional possibilities of channel estimation in the Single User (SU) MIMO case in UL, a transmission mode introduced in LTE-Advanced (LTE-A). The authors exploit the properties of shifted CAZAC sequences explained before for channel estimation. However, they notice that, due to subcarrier mapping in SC-FDMA, the channel impulse responses are convolved in time with a periodic sinc function (depending on the number of allocated RBs), which produces an energy leakage of the channel impulse responses. As observed by the authors, the smaller the number of RB, the higher the leakage. This effect destroys perfect time separation of the channel impulse responses, even if the channel delay spread is less than the cyclic shift. Notice that this effect does not occur in standard SC-FDE transmissions, in which all the subcarriers are used for estimation, while it always occurs in LTE, since there are always some guard subcarriers even when all the RBs are allocated to one user. Nevertheless, the authors propose some optimization of the algorithm in order to improve the performance.

A standard reference in OFDM channel estimation, which can be applied also with some modification for SC-FDMA, is [9]. The authors here propose Least Squares (LS) channel estimation, which is in fact more complex than the algorithm in [20], but has still acceptable complexity. As it happens in SC-FDMA, the LS estimator [9] is based on an ill-conditioned matrix, hence the authors propose a regularized LS channel estimator and a down-sampled impulse response channel estimator, two ways of resolving the ill-conditioning of the original LS estimator. Comparisons with MMSE channel estimation and a variety of simplified MMSE estimators are presented in [31]. Interestingly, the regularized LS channel estimator has almost identical performance of a mismatched MMSE channel estimator in which the channel correlation matrix is the identity and only the noise variance is used in the MMSE estimator. The work is derived in the context of channel interpolation for OFDM in LTE.

Other linear MMSE estimators with reduced complexity for OFDM systems are presented (in the context of OFDM) in [15]; the authors present different versions of the algorithm based on the SVD of the channel correlation matrix in the frequency domain. What it is not stated in the article is that, for the most simple estimator based on the assumption of a uniform power delay profile, the number of significant singular values, which leads the complexity figure, depends also on the ratio between the FFT size of the system and the Cyclic Prefix (CP) length. In the article a ratio of FFT size over CP equal to 16 is taken, which gives 8 significant singular values. However in PMR based on extended CP, the previous ratio is 4, which gives about 20 significant singular values, thus reducing the interest of the technique.

Another approach is taken by [13], where the authors introduce a model for the estimation problem and derive an Maximum Likelihood (ML) estimator with respect to the model. Of course, the estimator is sensitive to the model, but, for channels inside the model it works slightly better than the SVD linear MMSE estimator of [15] and with smaller complexity, especially when ratio of FFT size over CP is low as in the PMR case.

In [21] a standard LS algorithm is combined with a sliding window in the frequency domain. This approach, when correctly tuned, allows to approach MMSE estimator performance. The authors propose a dynamic tuning of the parameters of the algorithm. Its complexity in comparison to the others algorithms is not clear but it depends on the width of the window. This technique is specifically presented for SC-FDMA.

A simple LS channel estimator and a two-steps estimation procedure is presented in [23]. The first step is a regularized LS algorithm and the second one is a refinement obtained by adding some decided data (hard decision after equalization) to the pilots.

[36] is a recent reference on optimization of some parameters of the reference signals and performance evaluation of channel estimation for MU-MIMO in the DL of LTE-A.

MU-MIMO is an environment rich of interference, as far as channel estimation in concerned. Even if this work if focused on the DL, section 3.2 in [10] in interesting since it is developed in the context of co-channel interference in heterogeneous networks. The authors propose that UE performs interference cancellation in synchronized co-channel heterogeneous networks, by taking into account the strongest interfering signal. In particular the soft interference cancellation is done over the LTE DL Common Reference Signals (CRS), i.e. pilots, in order to improve the channel and noise estimates of the desired signal. This kind of processing is used to improve detection of Physical DL Control Channels in LTE, which is affected by the CRS interference of the interfering eNodeB even in case of application of the almost-blank subframe technique. In this technique data is not transmitted but CRS are sent anyway. However, this kind of cancellation techniques will not be taken into account in this study.

3.1.1.3 Description of the technique

A practical two-way relaying strategy is proposed here based on MU-MIMO techniques in the access phase, and on network coding at TB level (in the Medium Access Control (MAC) layer) for packet combining, and then on simple broadcast in the broadcast phase. For simplicity and robustness with respect to variable channel condition, on open loop MU-MIMO is implemented in the access phase.

Our aim here is to understand if there are blocking points to the feasibility of such a simple two-way relaying protocol. The most delicate phase is surely the multiple access one. In particular, putting the study in the framework of the future PMR based on LTE in a cellular network or in a clusterized ad hoc network, standard assumptions of LTE system will be done, i.e. the system is supposed to be synchronized in frequency and in time: all the signals arrive at the same moment to the receiver, thanks to a timing-advance procedure. In this framework, the other critical point is channel estimation in the access phase, in which multiple signals are multiplexed together on the same RBs. In this section, channel estimation performance in the multiple access case will be studied. A simple linear receiver for MU-MIMO in SC-FDMA is depicted in Figure 3-3.

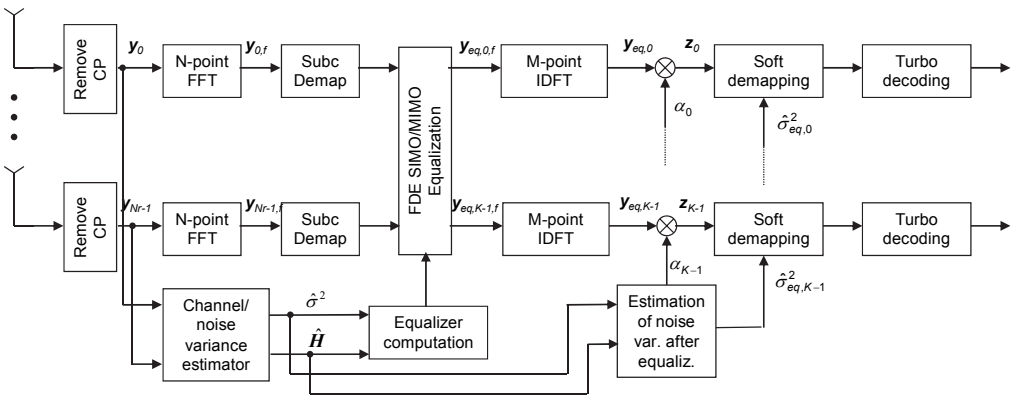

Figure 3-3: Simple linear receiver for SC-FDMA UL MIMO

Under the previously discussed assumptions (synchronization of the received signals), by supposing that all the transmitters have 1 transmit antennas and the receiver has N_r receive antennas, the received signal after the N-point FFT can be written as

$$\mathbf{r} = \mathbf{H}(\mathbf{I}_K \otimes \mathbf{F}_M)\mathbf{s} + \mathbf{w} = \mathbf{H}\mathbf{s}_f + \mathbf{w} \tag{3.1.1}$$

where $\otimes$ is the Kronecker product $\mathbf{F}_M$ is the normalized FFT matrix, M is the number of subcarriers allocated to the users (multiple of 12 in LTE), $\mathbf{s}^T = [\mathbf{s}_0^T \ldots \mathbf{s}_{K-1}^T]$ is the vector stacking the signal sent by the K users, in our case the CAZAC sequences. Notice that $\mathbf{s}_f$ is the column vector collecting the FFTs of the corresponding signals in time (user by user). The noise vector $\mathbf{w}$ has independent identically distributed (iid) entries which are complex symmetric Gaussian variables $\mathcal{CN}(0, \sigma^2)$. $\mathbf{H}$ is a MN_r x MK the block-diagonal matrix (blocks of size M) containing the channel frequencies responses extracted at the allocated subcarriers (the same for all users):

$$\mathbf{H} = (\mathbf{I}_{N_R} \otimes \mathbf{A}^H)(\mathbf{I}_{N_R} \otimes \mathbf{F}_N)\mathcal{H}(\mathbf{I}_K \otimes \mathbf{F}_N^H)(\mathbf{I}_K \otimes \mathbf{A})$$

With:

- $\mathbf{A}$ the subcarrier allocation matrix of size N x M, N is the Inverse Fast Fourier Transform (IFFT) size at the transmitter and the matrix has just one 1 per column at the position of the allocated subcarrier. The matrix is in common to all users, because they are superimposed.
- $\mathbf{F}_N$ the Fourier transform matrix of size N x N
- $\mathcal{H}$ is a block circulant channel matrix of size NN_R x NK.

After CP extraction and under the hypothesis that the channel is static and its length is shorter than the CP, the channel matrix is:

$$\mathcal{H} = \begin{bmatrix} circ(\mathbf{h}_{0,0}) & \cdots & circ(\mathbf{h}_{0,K-1}) \\ \vdots & \ddots & \vdots \\ circ(\mathbf{h}_{N_R-1,0}) & \cdots & circ(\mathbf{h}_{N_R-1,K-1}) \end{bmatrix}$$

where $circ(\mathbf{h}_{n,k})$ is the circulant matrix with the first column equal to $\mathbf{h}_{n,k}$, the vector containing the impulse response of the channel from transmitter k to receiver antenna n, in the time domain at the sampling time of the FFT of size N. Vector $\mathbf{h}_{n,k}$ has length N.
Notice that by setting

$$\mathbf{H}_N = (\mathbf{I}_{N_R} \otimes \mathbf{F}_N)\mathcal{H}(\mathbf{I}_K \otimes \mathbf{F}_N^H) = \begin{bmatrix} diag(\mathbf{h}_{0,0,f}) & \cdots & diag(\mathbf{h}_{0,K-1,f}) \\ \vdots & \ddots & \vdots \\ diag(\mathbf{h}_{N_R-1,0,f}) & \cdots & diag(\mathbf{h}_{N_R-1,K-1,f}) \end{bmatrix}; \quad \mathbf{h}_{n,k,f} = \sqrt{N}\mathbf{F}_N\mathbf{h}_{n,k}.$$

then

$$\mathbf{H} = (\mathbf{I}_{N_R} \otimes \mathbf{A}^H)\mathbf{H}_N(\mathbf{I}_K \otimes \mathbf{A}) = \begin{bmatrix} diag(\mathbf{h}_{0,0,f}^{(M)}) & \cdots & diag(\mathbf{h}_{0,K-1,f}^{(M)}) \\ \vdots & \ddots & \vdots \\ diag(\mathbf{h}_{N_R-1,0,f}^{(M)}) & \cdots & diag(\mathbf{h}_{N_R-1,K-1,f}^{(M)}) \end{bmatrix}$$

With

$$\mathbf{h}_{n,k,f}^{(M)} = \begin{cases} \sqrt{M}\mathbf{F}_M \mathbf{h}_{n,k}^{(M)} \\ \mathbf{A}^H \mathbf{h}_{n,k,f} = \sqrt{N}\mathbf{A}^H \mathbf{F}_N \mathbf{h}_{n,k} \end{cases} \tag{3.1.2}$$

The previous formula shows that we can work either at the symbol period, top formula (input of the Discrete Fourier Transform (DFT) precoding at the transmitter), or at the sample period, bottom formula (after the IFFT at the transmitter).

In the definition of the Reference Signals (RS), the LTE philosophy was followed but not exactly the letter of the specification. Without loss of generality, the RS of user 0 in the frequency domain was set to

$$\mathbf{s}_{0,f}(m) = \exp\left(j\pi \frac{m^2}{M} \right), \qquad m = 0,\ldots,M-1 \tag{3.1.3}$$

If there are *K* users superimposed on the same RBs, then the sequence of user *k* is

$$\mathbf{s}_{k,f}(m) = \exp(-j\alpha_k m)\mathbf{s}_{0,f}(m), \qquad \alpha_k = \frac{2\pi}{K}k, \qquad m = 0,\ldots,M-1, \qquad k = 0,\ldots,K-1,$$

which can be written also in matrix form

$$\mathbf{s}_{k,f} = diag(\mathbf{a}_k)\mathbf{s}_{0,f}.$$

In the time domain this operation corresponds to a cyclic time shift of *kM*/*K* symbols, while in the time domain at symbol period, it roughly corresponds to a shift of *kN*/*K* samples.

Without loss of generality, let us now focus on the channel estimation on the first antenna. It comes to consider a system with multiple users and just one antenna at the receiver. By letting the antenna index fall

$$\mathbf{r} = \mathbf{H}\mathbf{s}_f + \mathbf{w} = \left[\sum_{k=0}^{K-1} diag(\mathbf{a}_k \bullet \mathbf{h}_{k,f}^{(M)}) \right] \mathbf{s}_{0,f} + \mathbf{w} = diag(\mathbf{h}_{eq,f}^{(M)})\mathbf{s}_{0,f} + \mathbf{w} = diag(\mathbf{s}_{0,f})\mathbf{h}_{eq,f}^{(M)} + \mathbf{w} \tag{3.1.4}$$

where the symbol • stands for entry by entry product. In (3.1.4) it is put in evidence the fact that the channel is not known. The previous problem is a linear estimation problem corrupted by Gaussian noise.

Standard LS channel estimation

The selected baseline channel estimation is the one in [20], in which however, the windowing step was skipped in order to keep the complexity very low. This LS algorithm will be called "standard algorithm" in the following, and it has been optimized with respect to the typical channels model and LTE configuration of broadband PMR. We quickly derive the estimator here based on the LS theory (see Chapter 8 in [24]). The least square estimator applied to (3.1.4) is

$$\mathbf{G}_{LS} = \left[diag(\mathbf{s}_{0,f}^*) diag(\mathbf{s}_{0,f}) \right]^{-1} diag(\mathbf{s}_{0,f}^*) = \left[diag(\mathbf{s}_{0,f}^* \bullet \mathbf{s}_{0,f}) \right]^{-1} diag(\mathbf{s}_{0,f}^*) = diag(\mathbf{s}_{0,f}^*)$$

where we used the property of constant modulus of the CAZAC sequence. Hence, the LS estimate of the equivalent channel is

$$\tilde{\mathbf{h}}_{eq,f}^{(M)} = \mathbf{G}_{LS}\mathbf{r} = \mathbf{h}_{eq,f}^{(M)} + diag(\mathbf{s}_{0,f}^*)\mathbf{w} = \mathbf{h}_{eq,f}^{(M)} + \mathbf{w}_s \tag{3.1.5}$$

where the noise $\mathbf{w}_s$ has still iid entries belonging to $\mathcal{CN}(0, \sigma^2)$ thanks to the properties of the CAZAC sequence. Notice that in the time domain at symbol period, the equivalent channel is

$$\mathbf{h}_{eq}^{(M)} = \sum_{k=0}^{K-1} \mathbf{h}_k^{(M)}(-kM/K)$$

where the minus is intended as a cyclic shift inside the vector of the channel of each user. If the maximum channel spread is less than M/K symbol periods, then it is possible to separate the users' channels by extracting chunks of M/K symbols. The previous equation is true if and only if K divides M, otherwise things get more complicated. Unfortunately, the windowing operation in the time domain which consists in the subcarrier mapping, produces a convolution by a periodic sinc function in time, spreading the contribution of the channels. The choice of [20] is still to separate temporally the estimates of the channel impulse responses, but adding a temporal shift s in order to reduce the effect of the energy leakage. The estimation algorithm proceeds as follows: first, by using (3.1.2), the equivalent channel impulse response estimate is calculated via an Inverse Discrete Fourier Transform (IDFT) of size M:

$$\tilde{\mathbf{h}}_{eq}^{(M)} = \frac{1}{\sqrt{M}} \mathbf{F}_M^H \tilde{\mathbf{h}}_{eq,f}^{(M)} = \sum_{k=0}^{K-1} \mathbf{h}_k^{(M)}(-kM/K) + \mathbf{w}_t \tag{3.1.6}$$

The entries of $\mathbf{w}_t$ are iid random variables belonging to $\mathcal{CN}(0, \sigma^2/M)$. The estimates of the channel impulse response of user k is

$$\tilde{\mathbf{h}}_k^{(M)}(m) = \begin{cases} \tilde{\mathbf{h}}_{eq}^{(M)}(m - s + kM/K), & m = 0,\ldots,(M/K)-1 \\ 0 \qquad\qquad\qquad\quad , & m = 0,\ldots,M-1 \end{cases} \tag{3.1.7}$$

The operations inside the entries are sums and subtractions modulo M, s is a shift parameter to be optimized. Of course, the estimate of the channel frequency response, which is used by the equalizer in the frequency domain, is just

$$\tilde{\mathbf{h}}_{k,f}^{(M)} = \sqrt{M}\mathbf{F}_M \tilde{\mathbf{h}}_k^{(M)}.$$

Noise variance estimate before equalization

Noise variance estimate before equalization is obtained in a simple way under the hypothesis that the channel does not change over the RS affected to the same subcarriers. Notice also that the channel variance at one antenna is independent of the number of users (and channels) ad their attenuations. Hence, the equivalent channel at each antenna (3.1.5) will be used, since less distortion is introduced in its estimate. First the average channel estimate is calculated by averaging over the N_{RS} RS in the slot:

$$\tilde{\mathbf{h}}_{eq,f,av}^{(M)} = \frac{1}{N_{RS}} \sum_{p=0}^{N_{RS}-1} \tilde{\mathbf{h}}_{eq,f,p}^{(M)}.$$

This algorithm is suboptimum for calculating the channel estimate in time-varying channel, but it is still acceptable when the channel estimate is used for estimating the noise variance.

The noise variance estimate is then calculated as

$$\hat{\sigma}^2 = \frac{1}{(N_{RS}-1)M} \left| \sum_{p=0}^{N_{RS}-1} \sum_{m=0}^{M-1} \left(\left| \tilde{\mathbf{h}}_{eq,f,p}^{(M)}(m) \right|^2 - N_{RS} \left| \tilde{\mathbf{h}}_{eq,f,av}^{(M)}(m) \right|^2 \right) \right|. \tag{3.1.8}$$

The absolute value outside the summations is used in case of negative value, which can occur at low SNR and with a small number of RSs.

The previous expression gives an estimate of the noise variance per receive antenna. If all the antennas and receiver chains have substantially the same noise factor and amplifier, then a finer estimate can be obtained by averaging also over the number of receive antennas.

ML channel estimation

Here we extend the ML channel estimator proposed in [13] to the case of multi-user channel estimation. The main idea is to state the problem in the time domain at the sampling time in order to try to lower the number of variables of the problem and at the same time to try to recover a better orthogonality of the shifted channels. However, before stating the model, it is better to understand how the channel impulse responses look like after CP removal at the receiver. Let us focus on one receive antenna and one user *k*. At the transmitter side, after subcarrier mapping and IFFT, the RS sequence of user 0 (not-shifted) corresponds to the RS sequence in the time domain (at the symbol period) oversampled by an interpolator filter. The interpolator filter is the IFFT of the window corresponding to the subcarrier mapping. Let us call this base CAZAC sequence $\mathbf{s}_0^{(N)} = \mathbf{F}_N^H \mathbf{A}\mathbf{s}_{0,f}$. The sequence can be written also in signal format $s_0^{(N)}(nT) = \mathbf{s}_0^{(N)}(n)$, n = 0, …, N-1, T is the sampling time. Its Fourier transform is $s_{0,f}^{(N)}(nF) = (\mathbf{A}\mathbf{s}_{0,f})(n)$, F = 1/(NT) is the sampling frequency and TF = 1/N. Now, consider the basic rule of the Fourier transform of delayed signals

$$s_0^{(N)}(nT - n_0T) \xleftarrow{Fourier} s_{0,f}^{(N)}(nF)e^{-j2\pi nFn_0T} = s_{0,f}^{(N)}(nF)e^{-j2\pi nn_0/N}$$

The previous formula is valid only if n_0 is an integer number, otherwise it cannot be seen as a time shift in the sampling time domain. Consider the RS signal of user *k* in the interpolated frequency domain after subcarrier mapping. It can be written

$$s_{k,f}^{(N)}(nF) = \begin{cases} \mathbf{s}_{0,f}(m)e^{-j2\pi km/K}, & n = n_g + m, \quad m = 0,\ldots,M-1 \\ 0 \qquad\qquad\quad , & n \neq n_g + m, \quad m = 0,\ldots,M-1 \end{cases} \tag{3.1.9}$$

where n_g is the index of the first non-zero subcarrier. Let suppose that $n_k = Nk/K$ is an *integer*. In this case it can be shown[3] that the RS sequence of user *k* (k = 0, …, K-1) in the sampling time domain can be written as

$$s_k^{(N)}(nT) = s_0^{(N)}(nT - n_kT)e^{j2\pi n_k n_g/N} = s_0^{(N)}(nT - kNT/K)e^{j2\pi kn_g/K} = s_0^{(N)}(nT - n_kT)e^{j\varphi_k}$$

i.e. the RS sequence can be seen as a time-shifted version of the RS sequence of user 0, multiplied just by a scalar (phase). Here "time-shift" means the circular time shift modulo *N*. The received signal at the antenna, after CP removal, is

$$y(nT) = \sum_{k=0}^{K-1} h_k * s_k^{(N)}(nT) = \sum_{k=0}^{K-1} e^{j\varphi_k} h_k * s_0^{(N)}(nT - n_kT) = \underbrace{\left[\sum_{k=0}^{K-1} e^{j\varphi_k} h_k(nT - n_kT)\right]}_{h_{eq}(nT)} * s_0^{(N)}(nT)$$

where n = 0, …, N-1, $*$ is the circular convolution and we applied the properties of the convolution. Notice that the equivalent channel impulse response can be seen as the sum of

[3] The proof consists in the direct computation of the RS in the frequency domain and checking that it corresponds to the expression above, when calculated for $n = n_g + m$.

the time-shifted impulse responses of the single channels multiplied by a phase constant. If the maximum channel spread L (in the sampling time domain) is less than N/K, then the supports of the impulses responses do not intersect and they can be separated. Since in LTE specifications there is no shaping filter we suppose that the channel impulses responses h_k are not spread by any other additional filter (otherwise h_k must include the convolution with the shaping filter or others). As proposed in [13], we set the following model: the impulse response taps with delay greater than L are set to zero. If $L < N/K$, the equivalent channel, in vector form, can hence be restated as follows

$$\mathbf{h}_{eq} = \mathbf{I}_{L,N}\mathbf{h}_{eq}^{(L)}; \quad \mathbf{h}_{eq}^{(L)} = \begin{bmatrix} h_0(0) & \cdots & h_0(L-1) & h_1(0) & \cdots & h_{K-1}(L-1) \end{bmatrix}^T \tag{3.1.10}$$

$\mathbf{h}_{eq}^{(L)}$ gathers the non-zero taps of the impulses responses of all users and is long LK samples. $\mathbf{I}_{L,N}$ is a N x KL matrix whose $l+Lk$ column is zero except for the entry corresponding to the index of $h_k(l)$ inside $\mathbf{h}_{eq}$, which is set to 1. This set of indexes is [0, …, $L-1$, N/K, …, $N/K + L - 1$, …, $(K-1)\,N/K + L - 1$].

Hence at the receiver side, in the frequency domain after subcarrier de-allocation, by using the previous derivations, the estimation model in (3.1.4) can be restated as

$$\mathbf{r} = \sqrt{N}diag(\mathbf{s}_{0,f})\mathbf{A}^H\mathbf{F}_N\mathbf{h}_{eq} + \mathbf{w} = \sqrt{N}diag(\mathbf{s}_{0,f})\mathbf{A}^H\mathbf{F}_N\mathbf{I}_{L,N}\mathbf{h}_{eq}^{(L)} + \mathbf{w} = \mathbf{B}\mathbf{h}_{eq}^{(L)} + \mathbf{w} \tag{3.1.11}$$

which has the advantage of using less variables, LK instead of NK.

Things get more involved when $n_k = Nk/K$ is *not* an integer. Since the IFFT size N is usually a power of 2, for instance when the users are $K = 3$, n_1 and n_2 are not integers. In this case the property of the Fourier transform of a translated signal cannot be applied because the delay does not fall into the time domain. Let us set a description of n_k in terms of its integer part and the remaining real part:

$$n_k = k\frac{N}{K} = \bar{n}_k + \varepsilon_k; \qquad \bar{n}_k = \left\lfloor k\frac{N}{K} \right\rfloor; \qquad \varepsilon_k = n_k - \bar{n}_k; \qquad k = 0,\ldots,K-1$$

Let us define the following filter

$$a_k^{(N)}(nT) = \frac{1}{N}e^{j\pi(n-\varepsilon_k)(N-1)/N}\frac{\sin(\pi(n-\varepsilon_k))}{\sin(\pi(n-\varepsilon_k)/N)}; \quad n = 0,\ldots,N-1$$

which has the frequency response in the interpolated frequency domain equal to $a_{k,f}^{(N)}(nT) = e^{-j2\pi\varepsilon_k n/N}$. It can be shown (just by calculating the signal in the frequency and checking it against (3.1.9)), that

$$s_k^{(N)}(nT) = a_k^{(N)} * s_0^{(N)}(nT - \bar{n}_k T)e^{j\varphi_k}; \quad \varphi_k = 2\pi kn_g/K = 2\pi n_k n_g/N$$

i.e. the RS sequence can be seen as a time-shifted version of the RS sequence of user 0, multiplied just by a scalar (phase) and filtered through a filter $a_{k,f}^{(N)}(nT)$ which looks like a spread impulse (it is a perfect Dirac function when $\varepsilon_k = 0$). The received signal at the antenna, after CP removal, is

$$y(nT) = \sum_{k=0}^{K-1} e^{j\varphi_k}h_k * a_k^{(N)} * s_0^{(N)}(nT - \bar{n}_k T) = \underbrace{\left[\sum_{k=0}^{K-1} e^{j\varphi_k}a_k^{(N)} * h_k(nT - \bar{n}_k T)\right]}_{h_{eq}(nT)} * s_0^{(N)}(nT)$$

The equivalent channel is composed by the time-shifted original impulses responses multiplied by a phase factor and convolved with a filter which depends on the user. Unfortunately this filter spreads the channel impulse responses; such that even if the original delay spread was less than *N*/*K*, the convolved channel has a longer time-support and cross interference shows up, like for the LS algorithm in the symbol period time domain.

In order to keep the complexity low, model (3.1.11) is selected. For *Nk*/*K* not integer, the model will be mismatched since it considers that $a_{k,f}^{(N)}(nT)$ is not present. This simplification will introduce degradations in the estimate. A suboptimum estimator will then be introduced later on, in order to mitigate this effect.

The ML estimator, applied to model (3.1.11) is (see Chapter 15 in [24])

$$\hat{\mathbf{h}}_{eq}^{(L)} = \mathbf{G}_{ML}\mathbf{r}; \qquad \mathbf{G}_{ML} = (\mathbf{B}^H\mathbf{C}_{\mathbf{w}}^{-1}\mathbf{B})^{-1}\mathbf{B}^H\mathbf{C}_{\mathbf{w}}^{-1} = (\mathbf{B}^H\mathbf{B})^{-1}\mathbf{B}^H$$

where the simplification comes from the fact that the Gaussian noise vector **w** has iid circularly symmetric entries. Matrix **B** is *M* x *LK*. In practical cases related to PMR the number of variables *LK* > *M*, because *M* is equal to the number of used RB x 12. In fact, in PMR the available bands are small, and PMR voice services will probably require few (even 1) RBs. When *LK* > *M*, matrix $\mathbf{B}^H\mathbf{B}$ is not invertible. The proposal is to regularize the bad-conditioned matrix, as done in [9]

$$\mathbf{G}_{ML,r} = (\mathbf{B}^H\mathbf{B} + \sigma_r^2\mathbf{I}_{LK})^{-1}\mathbf{B}^H$$

where matrix $\mathbf{B}^H\mathbf{B}$ can be simplified thanks to the property of CAZAC sequences:

$$\mathbf{B}^H\mathbf{B} = N\mathbf{I}_{L,N}^H\mathbf{F}_N^H\mathbf{A}diag(\mathbf{s}_{0,f}^*)diag(\mathbf{s}_{0,f})\mathbf{A}^H\mathbf{F}_N\mathbf{I}_{L,N} = N\mathbf{I}_{L,N}^H\mathbf{F}_N^H\mathbf{A}\mathbf{A}^H\mathbf{F}_N\mathbf{I}_{L,N}$$

and σ_r^2 is a regularization factor to be optimized.

Notice also that when all subcarriers are used, i.e. in a pure SC-FDE system (in LTE it never happens since there are always guard sub-carriers), matrix **A** is the identity, **B** is *N* x *LK*, $\mathbf{B}^H\mathbf{B}$ is the identity and the ML estimator boils down to $\mathbf{G}_{ML} = \mathbf{B}^H$.

The estimator matrix takes the form

$$\mathbf{G}_{ML,r} = (N\mathbf{I}_{L,N}^H\mathbf{F}_N^H\mathbf{A}\mathbf{A}^H\mathbf{F}_N\mathbf{I}_{L,N} + \sigma_r^2\mathbf{I}_{LK})^{-1}\sqrt{N}\mathbf{I}_{L,N}^H\mathbf{F}_N^H\mathbf{A}diag(\mathbf{s}_{0,f}^*)$$

The receiver is interested to the estimate of the channel of each user in the frequency domain and only on the subcarriers of interest. This estimate can be obtained as follows. First the samples related to the channel of user *k* are extracted, translated back in time by $\bar{n}_k$ and the estimate in the sampling time domain is rebuilt; in vector form:

$$\hat{\mathbf{h}}_k = \mathbf{R}_k\hat{\mathbf{h}}_{eq}^{(L)}; \qquad \mathbf{R}_k = \begin{bmatrix} \mathbf{0}_{L\times\bar{n}_k} & \mathbf{I}_L & \mathbf{0}_{LK\times(LK-\bar{n}_k-L)} \\ & & \mathbf{0}_{(N-L)\times LK} \end{bmatrix}$$

Then the estimate is transformed in the frequency domain (corresponding to the sampling frequency) and the phase and the residual phase offset are corrected, if present. Finally the estimated frequency response is selected over the subcarrier of interest via the allocation matrix. In vector form

$$\hat{\mathbf{h}}_{k,f}^{(M)} = e^{-j\varphi_k}\sqrt{N}\mathbf{A}^H diag((\mathbf{a}_{k,f}^{(N)})^*)\mathbf{F}_N\hat{\mathbf{h}}_k = e^{-j\varphi_k}\sqrt{N}\mathbf{A}^H diag((\mathbf{a}_{k,f}^{(N)})^*)\mathbf{F}_N\mathbf{R}_k\hat{\mathbf{h}}_{eq}^{(L)};$$

Notice that when Nk/K is integer, than $\overline{n}_k$ coincides with n_k, $\varepsilon_k = 0$, $diag((\mathbf{a}_{k,f}^{(N)})^*)$ becomes the identity and the previous estimator becomes exact, as far as the channel matches the model. Otherwise, when $\overline{n}_k$ is different n_k, ε_k is not 0, then the estimator is suboptimal because the correction $diag((\mathbf{a}_{k,f}^{(N)})^*)$ is done after the windowing function implemented by matrix $\mathbf{R}_k$, which has inevitably cut part of the spread channel response.

Finally, the total estimator to be applied to the received signal $\mathbf{r}$ is

$$\mathbf{G}_{ML,tot} = e^{-j\varphi_k}\sqrt{N}\mathbf{A}^H diag((\mathbf{a}_{k,f}^{(N)})^*)\mathbf{F}_N\mathbf{R}_k(N\mathbf{I}_{L,N}^H\mathbf{F}_N^H\mathbf{A}\mathbf{A}^H\mathbf{F}_N\mathbf{I}_{L,N} + \sigma_r^2\mathbf{I}_{LK})^{-1}\sqrt{N}\mathbf{I}_{L,N}^H\mathbf{F}_N^H\mathbf{A}diag(\mathbf{s}_{0,f}^*);$$

In case of non-integer Nk/K the set of indexes characterizing $\mathbf{I}_{L,N}$ is [0, …, $L-1$, $\overline{n}_1$, …, $\overline{n}_1 + L - 1$, …, $\overline{n}_{K-1} + L - 1$].

Efficient implementations can be found via FFT. The inverse matrix is constant for a given number of users and IFFT size N, so it can be pre-calculated and stored. The $diag((\mathbf{a}_{k,f}^{(N)})^*)$ can also be made after the subcarrier extraction in order to lower the number multiplications from N to M.

The calculation of the variance of the noise estimate is a little bit involved and will not be presented here. It follows the general rules of a linear Gaussian model.

ML channel and noise estimation

A final algorithm is proposed, inspired by the ML algorithm described before, in which the noise variance before equalization is estimated jointly with the channel.

The rationale of this algorithm is the following one. Consider the equivalent channel estimate in the sampling time domain (after the IFFT at the transmitter side). If the users' channels have limited delay, then the remaining channel taps will contain only noise. The algorithm consists in estimating the channel on a larger number of taps, the ones exceeding the channel delay will be used to estimate the channel variance just by calculating the average of the mean amplitude of the channel taps. At this aim the matrix $\mathbf{I}_{L,N}$ in (3.1.10) must be redefined according to an enlarged set of taps [0, …, $L-1$, n_{ns}, …, n_{ne}, $\overline{n}_1$, …, $\overline{n}_1 + L - 1$, $\overline{n}_1 + n_{ns}$, …, $\overline{n}_1 + n_{ne}$, …, $\overline{n}_{K-1} + L - 1$, $\overline{n}_{K-1} + n_{ns}$, …, $\overline{n}_{K-1} + n_{ne}$], with

$$L - 1 < n_{ns}, n_{ne} < \overline{n}_k$$

Let's call this matrix $\mathbf{I}_{Ln,N}$ is a N x KL_n with $L_n = L + n_e - n_s + 1$.

$$\mathbf{G}_{ML,tot} = e^{-j\varphi_k}\sqrt{N}\mathbf{A}^H diag((\mathbf{a}_{k,f}^{(N)})^*)\mathbf{F}_N\mathbf{R}_k(N\mathbf{I}_{L,N}^H\mathbf{F}_N^H\mathbf{A}\mathbf{A}^H\mathbf{F}_N\mathbf{I}_{L,N} + \sigma_r^2\mathbf{I}_{LK})^{-1}\sqrt{N}\mathbf{I}_{L_n,N}^H\mathbf{F}_N^H\mathbf{A}diag(\mathbf{s}_{0,f}^*);$$

and matrix $\mathbf{R}_k$ is now defined in order to extract only the channel taps and not the ones of noise which are used for noise variance estimate. Notice that when Nk/K is not integer, the noise estimation will be in any case degraded, since the suboptimal estimator is not able to suppress all the convolution effects from the channel estimate and this will influence the noise variance estimate too. Moreover, the regularization will be harder since the number of variables to be estimated is larger than the ones in the ML algorithm. This will be detailed further in the simulation section.

3.1.2 Simulation settings

The investigation of channel estimation for two-way relaying is carried out under SC-FDMA. 3GPP LTE specifications have been followed as far as possible in the simulator, but we do

not strictly follow them, even if the results are representative of what can be obtained in 3GPP LTE.

Main simulation parameters are reported in Table 3-1. The study consists in a comparison of the performance of different channel estimation techniques and on the optimization of their parameters. Details on the variation of these parameters will be given or recalled in the subsection with simulation results.

Frame structure	
Bandwidth	1.4 MHz
Subcarriers number	128 subcarriers, 72 useful
Frame length in time	10 ms
Subframe length (granularity in time)	1 ms (2 slots)
Subcarrier spacing	15 kHz
Number of symbols per subframe	12, corresponding to extended CP
Allocation unity	1 Resource Block (RB)
RB spacing	180 kHz, 1 ms
Number of subcarriers per RB	12
Total number of resource elements per RB	12x12 = 144
Control channel overhead	NA
Total number of pilots per RB, Pilot channel overhead	2 Reference Signals (RS) consisting of 1 OFDM symbol each (over the allocated subcarrier) per subframe
Total symbols for time synchronization per frame	NA (UL only is studied here)
Reference signals	LTE-like: CAZAC sequences of the length of allocated RBs
FBMC filter	NA (SC-FDMA with CP)
Overlapping factor	NA
Modulation and coding schemes	Uncoded QPSK (only channel estimation is studied here)
Transmitter/Receiver	
BS number of antenna	From 1 to 4
HH number of antenna	1
Transmission scheme	Virtual-MIMO (up to 4x4)
BS antenna pattern	isotropic
HH antenna model	Isotropic

Propagation	
Fast fading channel models	Extended Typical Urban (ETU), Extended Pedestrian-A (EPA), Hilly Terrain 1 (HT1)
Channel estimation	Standard (LS), ML and ML + no

Table 3-1: Simulation parameters for channel estimation for two-way relaying

For every point in the simulation at least 10000 subframes have been simulated. For definition of fast fading channel models, please refer to [6]. It is supposed that all users are synchronized and timing advance is working so that signals arrive all at the same time at the receiver. Simulations were done by sampling the signal (and the channel realization) at the sampling frequency Fs = 15 * 128 = 1.92 MHz. An extended CP of 16.67 μs has been used in order to have maximum robustness in very spread channels like the HT1. The extended CP is equal to 32, which is 1/4 of 128 and corresponds to the CP overhead. Since the channel user are multiplexed by time shifts of the CAZAC sequences, a maximum of 4 users can be multiplexed without renouncing to cover the maximum delay spread of 16.67 μs.

Since channel estimation is more challenging when the number of pilot symbols is small, a configuration with 2 and 4 RB has been studied, i.e. respectively 24 and 48 subcarriers, meaning that the CAZAC sequences have length equal to 24 and 28 respectively. Notice that a small number of RB matches well with the voice application in PMR, which does not require a lot of band.

The CAZAC sequences used here are not exactly the ones specified in 3GPP LTE. As a matter of fact, RSs in LTE are specified starting from CAZAC sequences of length equal to the largest prime number smaller than the target RS length, which are cyclically extended to match the RS length. This generation procedure has been inserted in the standard in order to have a large number of available RSs of the same length. However, the RS sequences generated with the previous procedure lose their perfect zero-correlation property. This fact introduces a degradation of the channel estimation performance. In order to avoid these effects, which are not the focus of this study, CAZAC sequences matched exactly to the RS length have been used (even if from their family has smaller cardinality). The expression of these CAZAC sequences, in the frequency domain, is given in (3.1.3).

The metric used to characterize the performance of the estimation algorithms are:

- The BER before decoding called also uncoded BER. Quadrature Phase Shift Keying (QPSK) is used in all simulations.
- The Normalized Truncated Mean Squared Error (NTMSE) of the channel estimate, which measures the error of estimate just over the sub-band of interest, normalized over the channel power

$$TNMSE = \frac{E\left[\left\|\hat{\mathbf{h}}_{k,f}^{(M)} - \mathbf{h}_{k,f}^{(M)}\right\|^2\right]}{E\left[\left\|\mathbf{h}_{k,f}^{(M)}\right\|^2\right]}$$

- The Mean Squared Error (MSE) of the noise variance estimate calculated as

$$MSE_{\text{var}} = E\left[\left|\hat{\sigma}^2 - \sigma^2\right|^2\right]$$

Notice that the NTMSE of the channel estimate depends on the user and the antenna identity, $\hat{\mathbf{h}}_{k,f}^{(M)}$ is the estimate of the channel frequency response over the *M* subcarrier of interests from user *k* and antenna 1 (without loss of generality), while $\mathbf{h}_{k,f}^{(M)}$ is the ideal channel. NTMSE is currently stated in the frequency domain but it can be equivalently calculated in the time domain. In this case, the impulse response must be calculated at the symbol time. The definition coincides with the one in [31].

3.1.3 Simulation results

In the figures of this subsection, "standard" or "stand." refers to the LS equalizer (3.1.5). Extensive simulations were done in Extended Typical Urban (ETU), Extended Pedestrian-A (EPA), and Hilly Terrain 1 (HT1) channels as said in section 3.1.2. However, in order to not have tens of figures in the deliverable, only a selection of results and the main conclusions are presented here. EPA, ETU and HT1 have been chosen because their different degrees of frequency selectivity, low for EPA, medium for ETU and high for HT1 which has also taps with delays higher than the CP length.

3.1.3.1 Single user case

The proposed channel estimation algorithms are first validated in the single user scenario. Results on the ETU channel are presented since it is a representative channel in urban environment which is important to PMR application. The results are provided for an allocation of 2 RBs, i.e. 24 subcarriers.

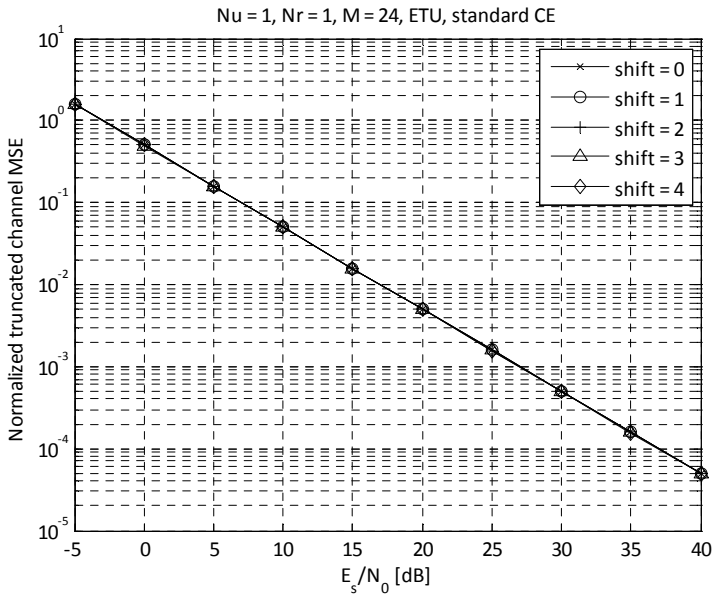

Figure 3-4: NTMSE of channel estimate for ETU channel, 1 user and 1 rx antenna, 2 RB, LS estimation

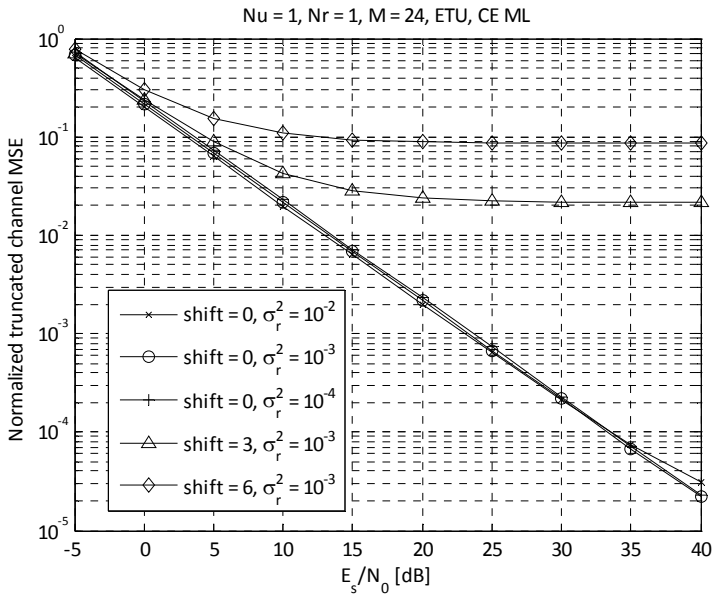

Figure 3-5: NTMSE of channel estimate for ETU channel, 1 user and 1 rx antenna, 2 RB, ML estimation

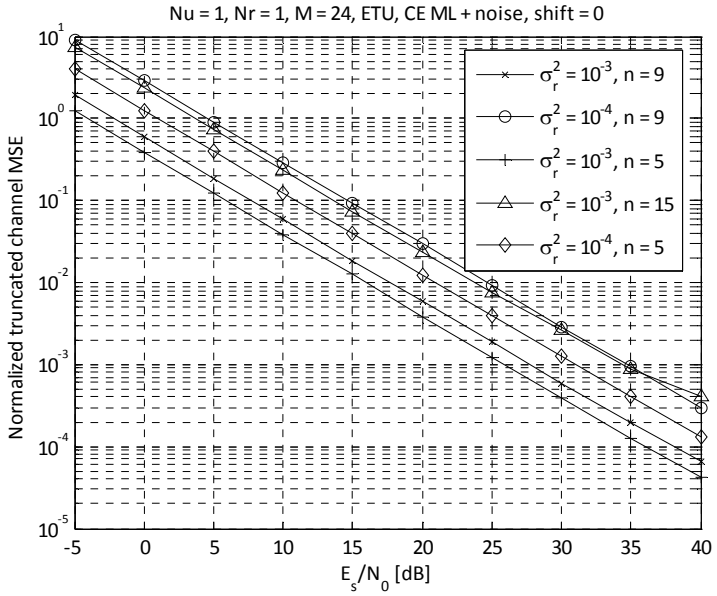

Figure 3-6: NTMSE of channel estimate for ETU channel, 1 user and 1 rx antenna, 2 RB, ML + noise variance estimation

Figure 3-4, Figure 3-5, Figure 3-6 present the NTMSE of the studied channel estimation algorithms with one user and 1 receiver antenna. In this simple case, the shift parameter *s* of the LS algorithms given in (3.1.7) has no impact since there is no channel impulse response truncation for separating users (see Figure 3-4). For the ML algorithm the effect of the shift is counterproductive, while the regularization factor σ_r^2 has negligible impact (see Figure 3-5). It has to be selected according implementation issues (e.g. good conditioning of matrixes). For the ML estimation algorithm plus noise variance, the shift was directly set to 0, and the performance of the estimation was studied with respect to the regularization factor and the number of samples per user dedicated to the noise variance estimate (*n* in

Figure 3-6). The optimum value of σ_r^2 is 10^{-3}, while 5 samples for estimating the noise. This number is directly linked to the fact that increasing the number of samples for the noise variance estimate worsens the matrix conditioning of the algorithm.

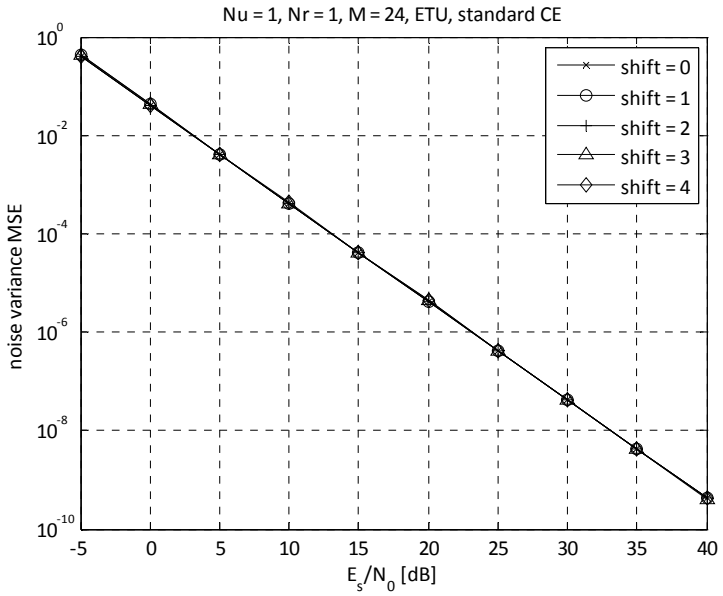

Figure 3-7: MSE of noise variance estimate for ETU channel, 1 user and 1 rx antenna, 2 RB, LS and ML estimation

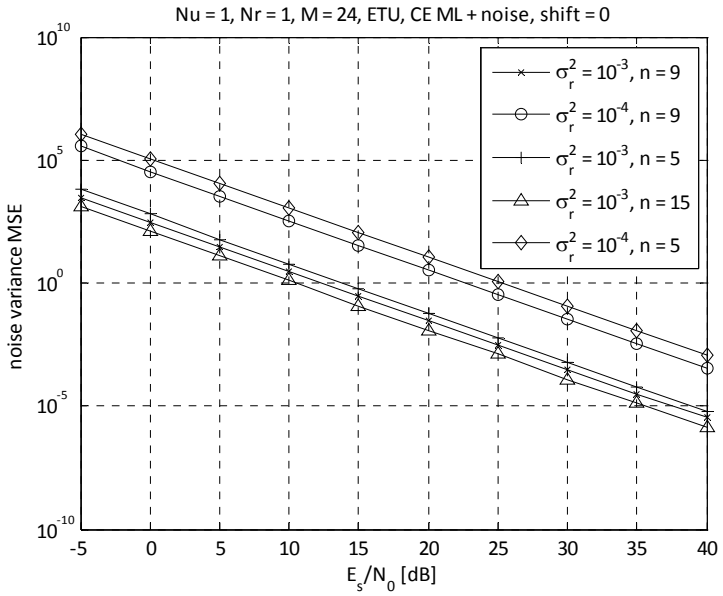

Figure 3-8: MSE of noise variance estimate for ETU channel, 1 user and 1 rx antenna, 2 RB, LS and ML estimation

Noise variance estimate (3.1.8) has been used for both LS and ML algorithms, results are in Figure 3-7. Figure 3-8 shows the noise variance MSE for the ML + noise algorithm but the performance is deceiving with respect the simple algorithm in (3.1.8). Better performance is obtained by increasing the number of samples dedicated to noise estimate, but this way cannot be followed because of problems of bad matrix conditioning in the channel estimate as explained before.

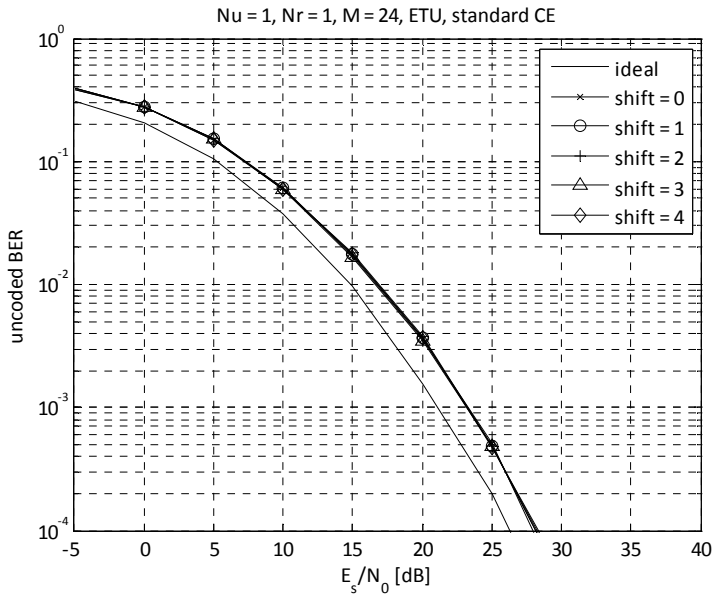

Figure 3-9: BER for ETU channel, 1 user and 1 rx antenna, 2 RB, LS estimation

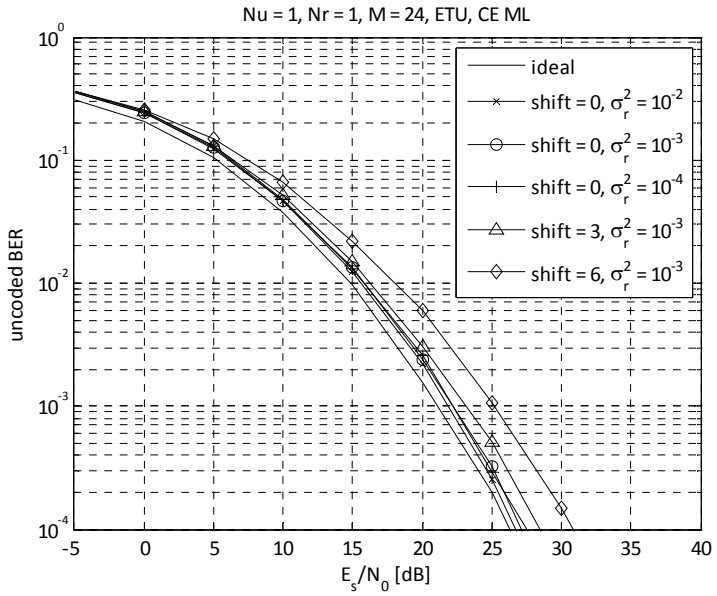

Figure 3-10: BER for ETU channel, 1 user and 1 rx antenna, 2 RB, ML algorithm

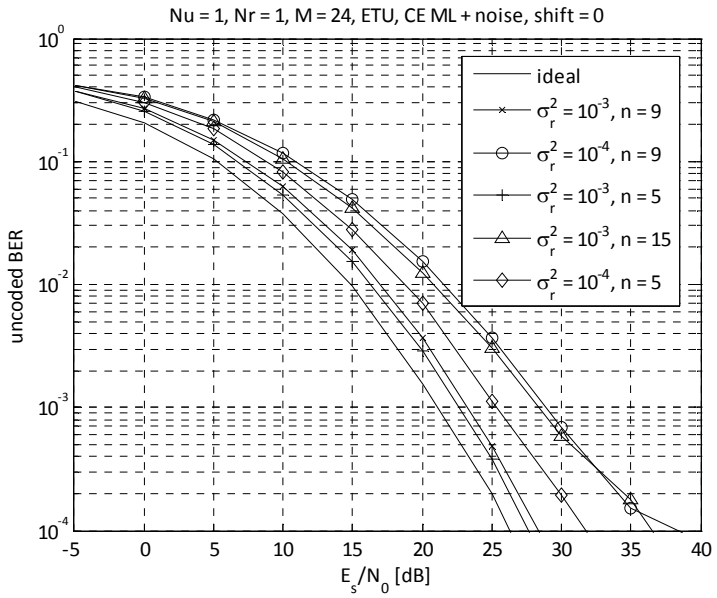

Figure 3-11: BER for ETU channel, 1 user and 1 rx antenna, 2 RB, ML + noise algorithm

Figure 3-9, Figure 3-10, Figure 3-11 present BER curves (over coded bits, without decoding) for the three algorithms. These curves give a measure of the degradation of performance when both channel and noise variance estimates are used. The LS standard algorithm loses roughly 2 dB, the ML one about 1 dB and the ML + noise one about 1.5 dB. For the ML + noise algorithm the best combination of parameters is $\sigma_r^2 = 10^{-3}$ and 5 samples for noise estimate.

It has been verified by simulation that the standard LS algorithm loses around 2 dB also for EPA and HT1 channel (for HT the measure point is at BER = 10^{-2}). The ML algorithm loses about 1 dB for EPA and HT1. The ML + noise algorithm loses about 1.3 dB in EPA channel and about 4 dB in HT1 channel.

Table 3-2 gives the optimal parameters for the different algorithms and channels selected by observing minimum degradation in BER. For the ML algorithm the choice of $\sigma_r^2 = 10^{-3}$ and s = 0 is done. Sensitivity to the regularization factor was observed, except in channel with extreme frequency selectivity.

Algorithm	**EPA**	**ETU**	**HT1**
LS (standard)	Independent of s	Independent of s	Independent of s
ML	s = 0, $\sigma_r^2 = 10^{-3}$	s = 0, $\sigma_r^2 = 10^{-2}$	s = 0, $\sigma_r^2 = 10^{-4}$
ML + noise	s = 0, $\sigma_r^2 = 10^{-3}$, n = 5	s = 0, $\sigma_r^2 = 10^{-3}$, n = 5	s = 0, $\sigma_r^2 = 10^{-3}$, n = 5

Table 3-2: Optimum parameters of the channel estimation algorithm in the single user case

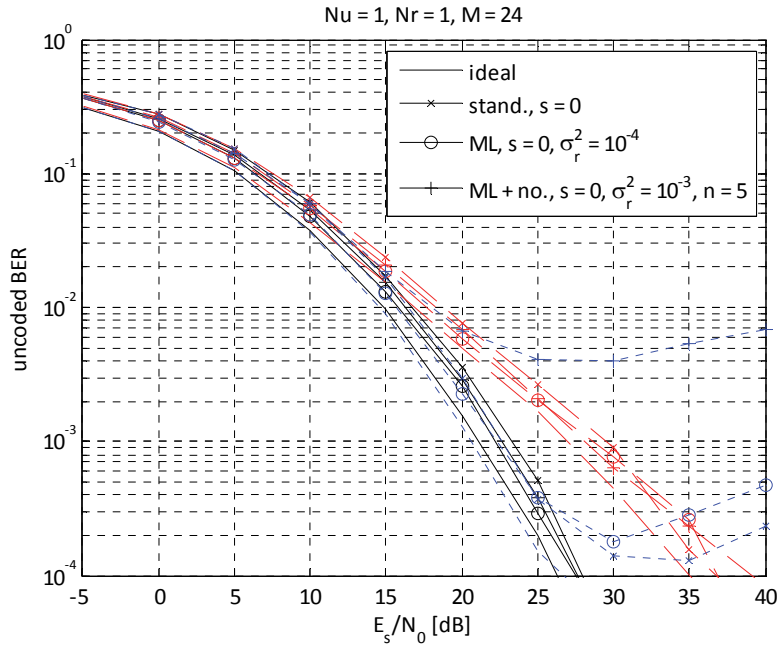

Figure 3-12: BER for QPSK in SU setting, 2 RB; black solid curves ETU, red dashed curves EPA, blue dotted curves HT1

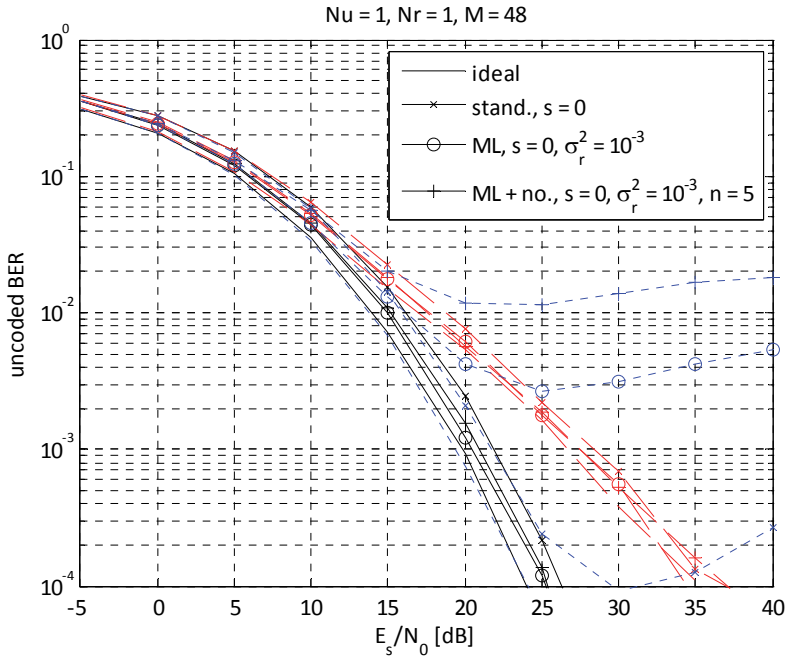

Figure 3-13: BER for QPSK in SU setting, 4 RB (right plot); black solid curves ETU, red dashed curves EPA, blue dotted curves HT1

A summary of the BER performance with the channel and noise variance estimation algorithms is given in Figure 3-12 and Figure 3-13, respectively for 2 and 4 RB.

Degradation is observed for $\sigma_r^2 = 10^{-3}$ with increasing number of RB for the ML algorithm, this is due to the fact that the channel becomes more frequency selective and hence a better approximation of the matrices is required.

The ML + noise algorithm is the worst performing one and hence will not be investigated in the multi-user case.

3.1.3.2 Multi user case

The MU case is of interest to the two-way relaying technique and more in general to any technique with superposed users, like virtual MIMO in UL.

In the MU case the standard LS algorithms shows its limitations, linked to the fact that for separating the channels, the impulse responses must be truncated. The truncation generates a loss of energy and a degradation of performance which is higher with increasing frequency selectivity of the channel. In EPA channel and 2 users, the LS algorithm behaves acceptably. However, in ETU and HT1 channel a strong degradation is present. Results on ETU are reported here in detail.

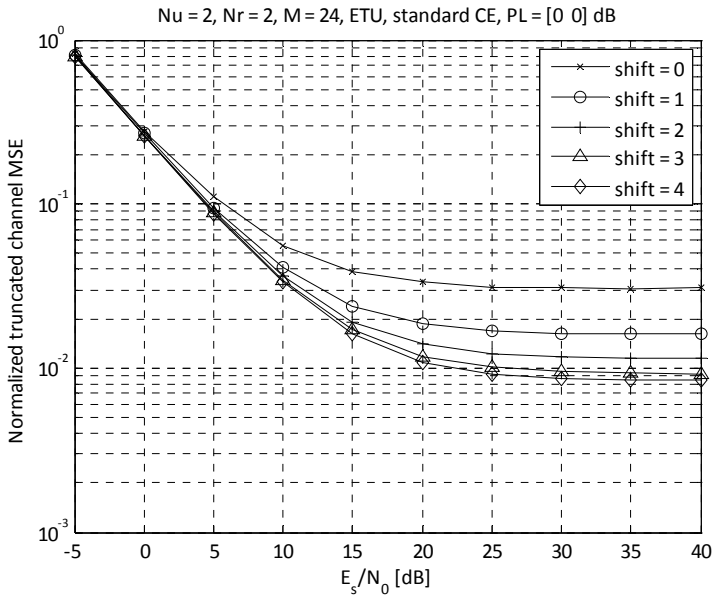

Figure 3-14: NTMSE of channel estimate for ETU channel, 2 users and 2 rx antennas, 2 RB, LS estimation

Figure 3-14 show the NTMSE of the LS algorithm for ETU channel with 2 users superposed over the same 2 RB. An error floor appears in the NTMSE due to truncation of channel power when separating the two channel estimates. This floor is minimized by selecting a shift *s* equal to 3 or 4. Figure 3-15, in the same case, the MSE of the noise variance estimate. The estimate is independent of the shift value and does not show any floor because it is derived by using the equivalent channel estimates (sum of all the delayed channels), which has not problems of truncation. No other figures of the MSE of the noise variance estimate will be shown below because its behaviour is always acceptable and it does not raise any issue. Figure 3-16 shows the BER performance. As for the NTMSE, the optimal shift *s* is equal to 3 or 4. An error floor appears due to the low quality of channel estimate.

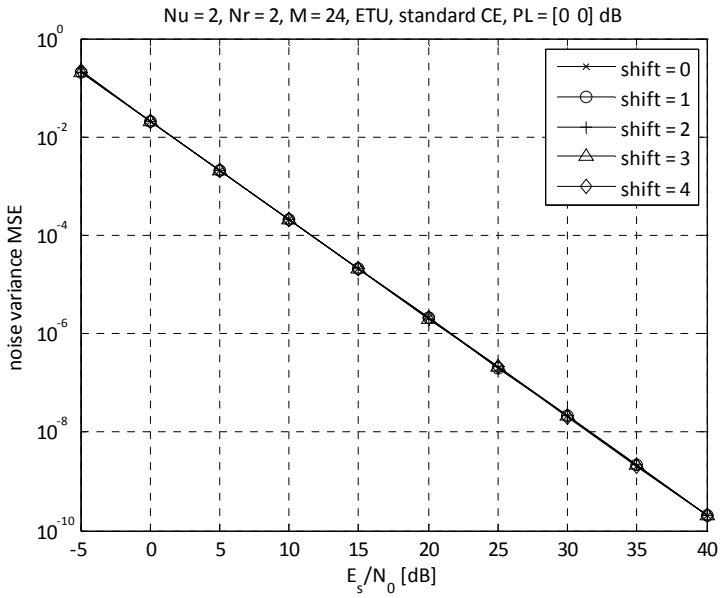

Figure 3-15: MSE of noise variance estimate for ETU channel, 2 users and 2 rx antennas, 2 RB, LS and ML estimation

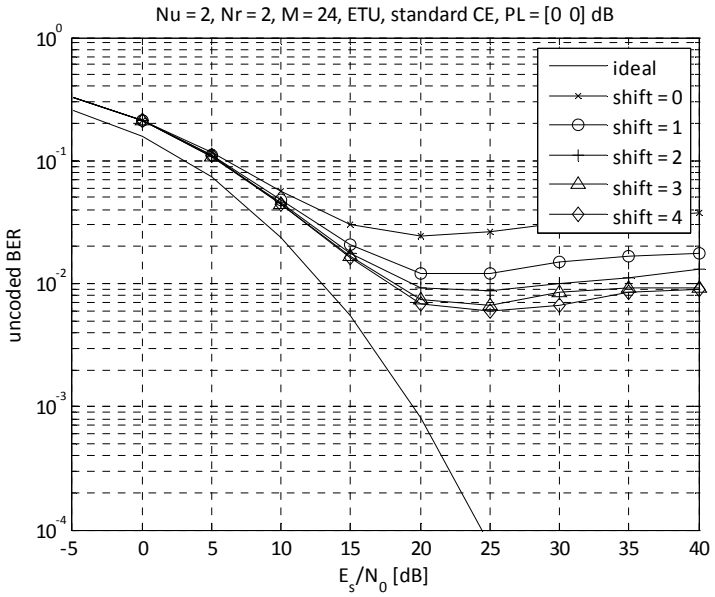

Figure 3-16: BER for ETU channel, 2 users and 2 rx antennas, 2 RB, LS estimation

Figure 3-17 presents the comparison of BER curves with 2 users and 2 receive antennas for the LS and ML algorithm. The ML algorithm uses the following indexes {0, 1, …, 31} for the first channel and {64, 65, …, 95} for the second channel. While in EPA channel the two algorithms have substantially the same performance (about 2 dB from the case with ideal channel information), performance of ML is radically better in ETU channel. In ETU at target BER = 10^{-2}, the ML estimation algorithms loses about 3 dB while the LS algorithms 5 dB and exhibits an error floor later on. In HT1 the two algorithms show a high error floor, which is smaller for the ML algorithm.

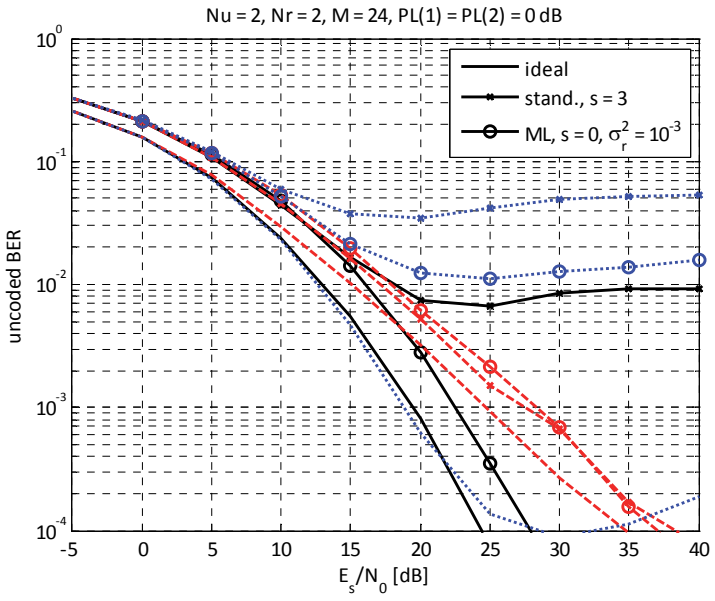

Figure 3-17: BER for QPSK, 2 users and 2 rx antennas, 2 RB; black solid curves ETU, red dashed curves EPA, blue dotted curves HT1

The estimation algorithm should work also in the case in which path-losses of the users are different. This fact is particularly important in ad hoc applications without a central receiver which manages the times of arrival and controls the power levels as in LTE. Different power loading factors were then allocated to the two users in order to simulate the impact of unequal path losses. The ratios between the powers range in between 0 dB and -30 dB.

Figure 3-18 and Figure 3-19 show the NTMSE in ETU channel for 2 users and different power ratios respectively for the LS (standard) and ML algorithms. Solid curves refer to the user with fixed power (0 dB) while dashed curves refer to the user with variable power. The E_s/N_0 is calculated for the user with fixed power. For the second user, its SNR at the receiver will be PL(2)E_s/N_0 where PL(2) is its power loading factor. It can be seen in the figures that the LS algorithm continues to have a NTMSE floor for all the power loading factors simulated here. The ML algorithm does not introduce such a floor, even for very unbalanced power loading factors. Similar results hold also for the other channels. The noise variance estimate (not shown here) has an MSE independent of the power loading factors applied to the users, since it is calculated over the total received channel which is agnostic of the power loading factors, only the total receive power matters.

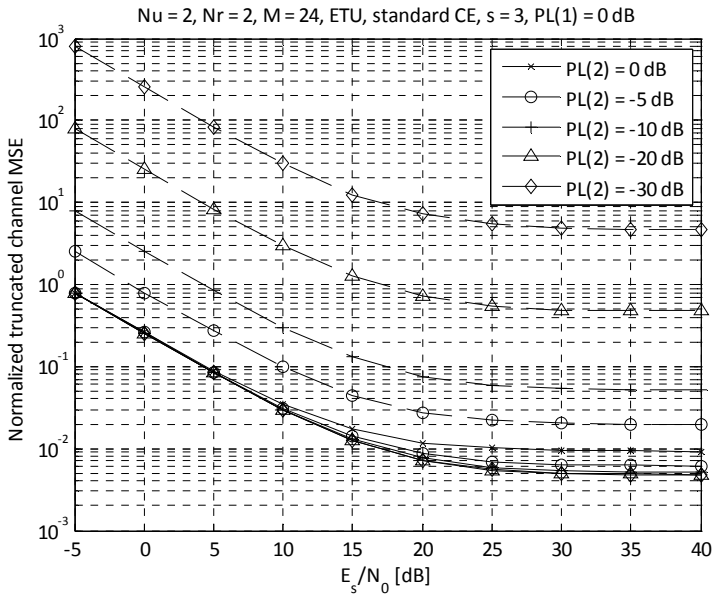

Figure 3-18: NTMSE of channel estimate for ETU channel for different power loadings, 2 users and 2 rx antennas, 2 RB, LS estimation; solid curves user with 0 dB power loading, dashed curves user with moving power loading

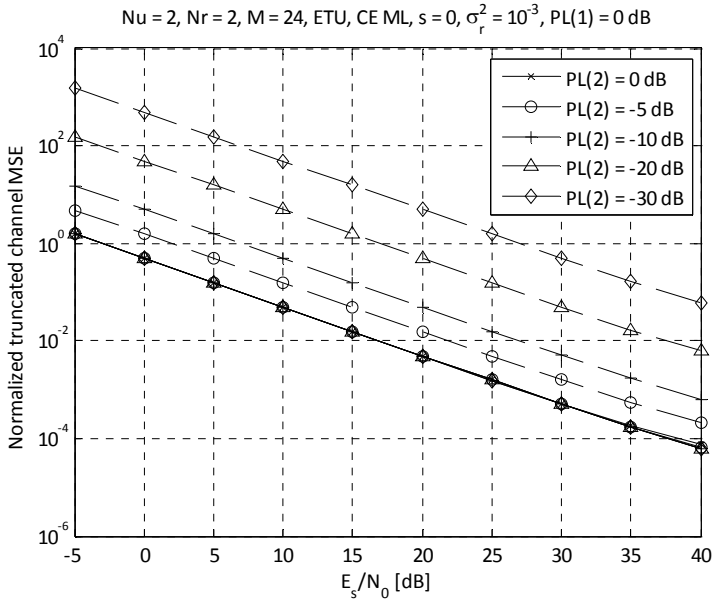

Figure 3-19: NTMSE of channel estimate for ETU channel for different power loadings, 2 users and 2 rx antennas, 2 RB, ML estimation; solid curves user with 0 dB power loading, dashed curves user with moving power loading

Figure 3-20 shows the BER curves for the case with users with equal powers (solid curves) and users with a difference of 10 dB in the received power (dashed curves) for the three channel models investigated here. As for the case with equal powers, the ML algorithm performs better than the LS algorithm for ETU and HT1 channel, while it is comparable for EPA channel.

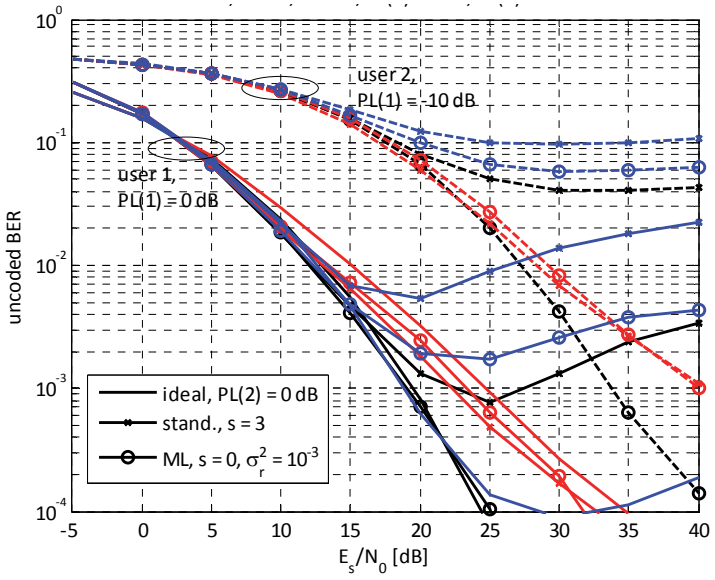

Figure 3-20: BER for ETU channel for 2 users having equal power loading (solid curves) or a difference of 10 dB (dashed curves), 2 rx antennas, 2 RB; black curves ETU, red curves EPA, blue curves HT1

Figure 3-21 show BER results for the case with 3 users, 3 receive antennas and equal power loadings. In this case, the model corresponding to the ML algorithm, which has been chosen for its low complexity, does not matches exactly the reality of the signal and thus it introduces degradation in the channel estimate. This degradation increases with the number of RB; hence, only the case with 4 RB is reported, where the effect is more evident. In these cases, the ML algorithm works worse than the standard LS one for EPA, it works comparably for HT1 and it works better for ETU but only starting from a certain SNR value.

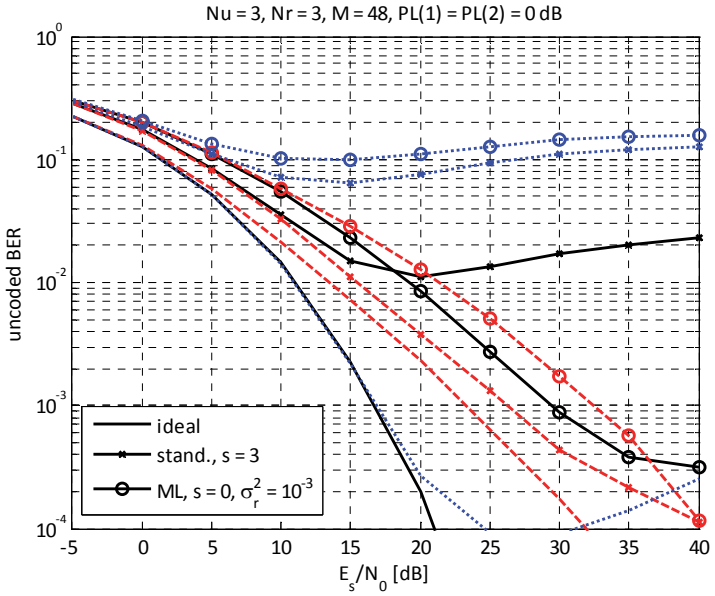

Figure 3-21: BER for QPSK, 3 users and 3 rx antennas, 4 RB; black solid curves ETU, red dashed curves EPA, blue dotted curves HT1

In case of 4 users with an extended CP, the LS and ML technique arrive at their maximum theoretical capability. In fact, for 4 users, the delay of the RS between two users is equal to

the CP length. Hence, increasing the number of users above 4 implies sacrificing the robustness to delay spread, or introducing additional interference in case of high delay spread. Moreover, inside the ML algorithm, matrix becomes more and more badly conditioned, which degrades the performance. Let L_{ce} be the number of channel tap estimates per user, then the maximum L_{ce} is equal to 32. The performance of the algorithm has been studied for different channels and number of RB. As an example, results in ETU are reported hereafter for the case of 4 RBs.

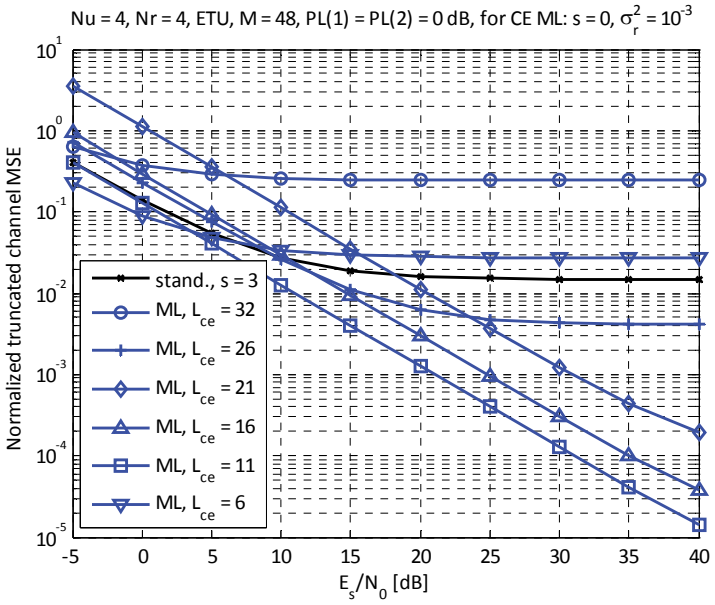

Figure 3-22: NTMSE of channel estimate for ETU channel, 4 users and 4 rx antennas, 4 RB, LS and ML estimation

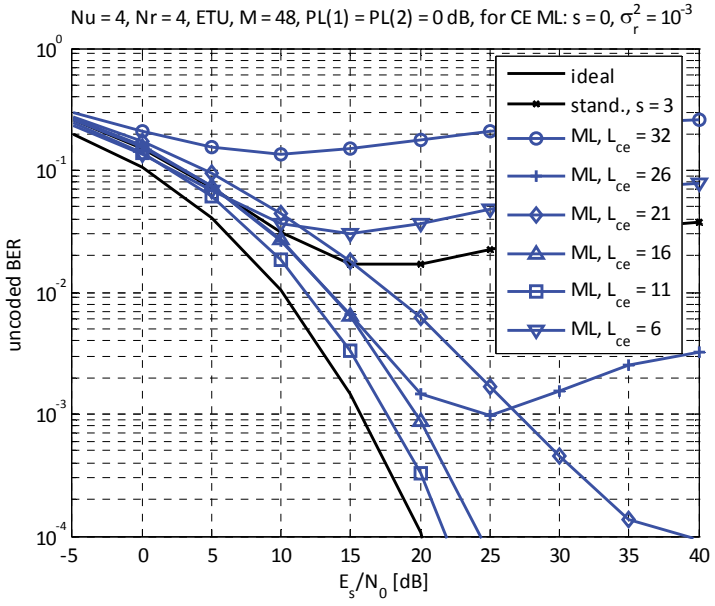

Figure 3-23: BER for QPSK for ETU channel, 4 users and 4 rx antennas, 4 RB, LS and ML estimation

The NTMSE of the channel estimate with 4 users 4 receive antennas for ETU channel is shown in Figure 3-22. The NTMSE presents a floor for high L_{ce} and for low L_{ce}, the optimal

value being L_{ce} = 11. High L_{ce} introduces degradation due to the bad conditioning of the matrices of the ML algorithm, even in presence of a regularization factor, fixed to 10^{-3}. Low L_{ce} introduces degradation due to model mismatch (too few taps considered in the channel). The BER view is given in Figure 3-23. The optimal L_{ce} yields a BER degradation of only 2 dB with respect to the ideal curve. The same result is found for the case with 2 RB, where the degradation is 3 dB.

For EPA channel, the optimal L_{ce} is 6 for both 2 and 4 RBs, with a degradation of 2 and 3 dB respectively. The standard LS algorithm loses 2 dB with respect to the case with ideal channel information for both 2 and 4 RBs.

For HT1 channel, performance is in any case degraded, even trying to tuning further the regularization factor. The best L_{ce} is 32 in this case.

Since the receiver is in general agnostic to the fast fading channel model, a unique L_{ce} for all channels must be fixed for the ML algorithm, which will introduce degradation in the performance. We choose to set L_{ce} to 21, since it will allow to deals channels with a delay spread up to 11 μs.

An overview of the BER results for variable number of users and receiver antennas for ETU channel is given in Figure 3-24 and Figure 3-25 respectively for 2 and 4 RBs. Black curves represent performance with ideal channel state information, blue curves are for ML algorithms and red curves for the LS algorithm. For the case of 4 users L_{ce} is equal to 21 while in the other cases it is equal to 32. In general the ML algorithm works better than the LS one for ETU even with the suboptimal choices of the algorithm for 4 users. Degradation for 3 users is due to the mismatch of the theoretical model of the ML algorithm, while for 4 users it is due to a mismatch in the choice of L_{ce}. It has to be noticed that for 2 RBs, even if error floors appears, at the target BLER of 10^{-2}, the ML algorithm compares favorably to the LS one. Nevertheless the degradation with respect to the ideal CSI performance improves with the number of users, due to the higher number of variables in the estimation problem. In the case of 4 RB, at the target BLER of 10^{-2}, the ML algorithm suffers from higher degradation for 3 and 4 users, but nevertheless it compares favorably to the LS one in all cases.

In the EPA case, not shown here for reducing the deliverable length, the ML algorithm performs substantially equivalently to the LS algorithm for 2 RBs. In the case of 4 RBs, it suffers from BER degradation with respect to the LS algorithm for the case of 3 and 4 users, for the same reasons of the ETU channel.

In the HT1 channel and 2 RB, not shown here for reducing the deliverable length, the LS works better for 1 user, but the ML wins for 2 and 3 users, while they have the same performance for 4 users. In the 4 RB case, the LS works better for 1 user and the two algorithms have substantially the same performance for 2, 3 and 4 users.

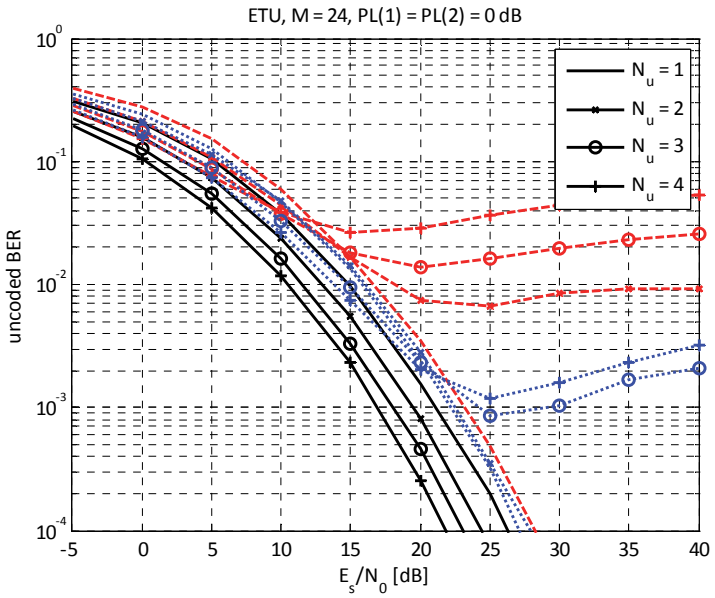

Figure 3-24: BER for QPSK and ETU channel 2 RB; black: ideal CSI, red: LS, blue: ML

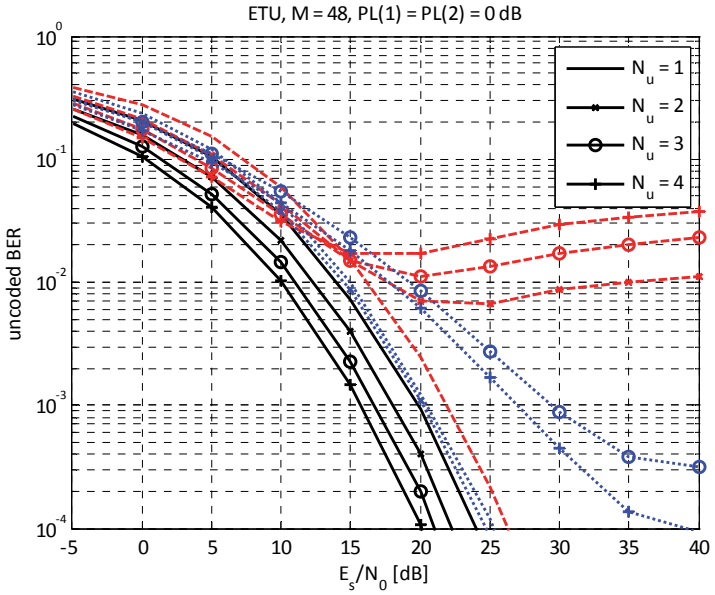

Figure 3-25: BER for QPSK and ETU channel 4 RB; black: ideal CSI, red: LS, blue: ML

3.1.4 Final remarks

In this subsection different channel estimation algorithms for two-way relaying with SC-FDMA were presented and compared. The standard LS algorithm suffers from performance degradation as long as more than 1 channel per antenna is estimated. The proposed ML algorithm is able to improve the estimate quality, especially for frequency selective channels, whose delay spread is lower than the CP length. A third algorithm estimating at the same time the channel and the noise was tested but it is not retained due to its inferior performance. The ML algorithm can be optimized according the number of users and fast fading channel model. A setting of parameters agnostic to the channel model was proposed,

which introduces performance degradation in certain cases. Even if the LS estimation algorithm has similar or slightly better performance than the ML one in channel with low frequency selectivity, the ML algorithm seems to be the best choice when the estimation algorithm must face channels with changing frequency selectivity. The conclusion is that there is no blocking point to the implementation of the two-way relaying technique as far as channel estimation is concerned and the number of users is less or equal to 4. Increasing the number of users above 4 is not recommended, especially in the PMR context, since important degradation of the channel estimates are expected. Increasing the number of users above 4 could be supported by using another base CAZAC sequence having low inter-correlation with respect to the first one. This option is not supported by LTE but could be a possibility if the channels of more than 4 users are to be estimated.

3.2 Achievable rate region for FBMC based two-way relaying systems

In this section we characterize the achievable rate region of FBMC based two-way Decode-and-Forward (DF) relaying channel.

3.2.1 Description and motivation

Orthogonal Frequency Division Multiplexing (OFDM) has been widely applied in modern broadband systems to provide high data rate service. However, the large frequency sidelobes of OFDM signal result in inter-band interference to the adjacent systems when synchronization is not guaranteed [57]. Moreover, the insertion of the Cyclic Prefix (CP) in each OFDM symbol decreases the system spectral efficiency. To overcome the limitations, the attention is drawn toward FBMC techniques. FBMC does not require any CP and has reduced sidelobes and thus less inter-band interference. Therefore, the FBMC system is more spectrally efficient and thus might be more suitable for critical communications such as public safety applications as shown in Section 3.1.1.1.

Relaying techniques have been invented to improve the coverage and throughput of wireless networks. Compared to one-way relaying schemes, two-way relaying schemes provide better spectral efficiency since two nodes exchange information simultaneously through an intermediate relay node in two time slots. In [56], OFDM based two-way DF relaying network has been investigated. A power allocation problem has been formulated to maximize exchange rate, which is defined as the maximal data rate can be simultaneously achieved in both directions.

In the following, we study the power allocation problem for a FBMC based two-way DF system in order to maximize the exchange rate. For our considered scenario, if the channel is frequency flat fading, the power allocation problem is convex and thus is solved in the same way as in [56]. However, the existence of frequency selective channels results in Inter-Symbol Interference (ISI) and Inter-Carrier Interference (ICI) and the resulting problem is a Difference of Convex functions (DC) problem, which is in general non-convex and NP-hard. Therefore, convex relaxation methods are required.

3.2.1.1 FBMC based two-way DF relaying channel

We consider a 3-node two-way DF relaying system in Figure 3-26, where two Hand-Held Terminals (HHTs) HHT_1 and HHT_2 exchange information via an intermediate relay node. Each node is equipped with a single antenna and operates in half-duplex mode. FBMC/OQAM is chosen as the multi-carrier technique and the available bandwidth is

divided into N subcarriers. Moreover, the channels are block fading and perfect synchronization is assumed. The transmission takes two phases. In the, Multiple Access (MA) phase all the HHTs transmit to the relay simultaneously. The HHTs use multi-tap pre-equalizers per subcarrier as in [57]. That is, the Signal to Leakage plus Noise Ratio (SLNR) is minimized. The relay decodes the received symbols using a real valued single-tap equalizer, i.e., only power allocation is considered at the relay. Afterwards, in the BroadCast (BC) phase, it re-encodes the data using network coding and via single-tap power adjustment. Then it re-transmits the encoded data to the HHTs [56]. Again, multi-tap equalizers are implemented at the HHTs. Moreover, the equalizer is designed such that the SLNRs at the receivers are maximized [57]. Finally, a complete received data model is given by

$$Y_{Rn} = \sqrt{P_{1n}} h_{1n}^{(e)} X_{1n} + \sqrt{P_{2n}} h_{2n}^{(e)} X_{2n} + Z_{Rn}, \tag{3.2.1}$$

$$Y_{1n} = \sqrt{P_{Rn}} \tilde{h}_{1n}^{(e)} X_{Rn} + Z_{1n}, \tag{3.2.2}$$

$$Y_{2n} = \sqrt{P_{Rn}} \tilde{h}_{2n}^{(e)} X_{Rn} + Z_{2n}, \tag{3.2.3}$$

where X_{1n} and X_{2n} are transmitted Pulse Amplitude Modulation (PAM) symbols on the n-th subcarrier in the MA by the terminals HHT_1 and HHT_2, respectively. X_{Rn} denotes the transmitted data by the relay T_R in the BC phase and P_{in}, i = 1, 2, R represent the powers allocated to terminal T_i on the n-th subcarrier. The interference terms and the noise terms are presented by $Z_{Rn} = I_{1n} + I_{2n} + W_{Rn}$, $Z_{1n} = \tilde{I}_{1n} + W_{1n}$, and $Z_{2n} = \tilde{I}_{2n} + W_{2n}$, where I_{in} represents the ICI in the MA phase and $\tilde{I}_{in}$ denotes the ICI in the BC phase. Furthermore, we have

$$\begin{aligned} E\left\{\left|W_{in}\right|^2\right\} &= \sigma_i^2, \quad i = 1,2,R \\ E\left\{\left|I_{in}\right|^2\right\} &= \Omega_{in,n-1} P_{in-1} + \Omega_{in,n} \Omega_{in,n+1} P_{in} + P_{in+1}, \quad i = 1,2 \\ E\left\{\left|\tilde{I}_{in}\right|^2\right\} &= \tilde{\Omega}_{in,n-1} P_{Rn} + \tilde{\Omega}_{in,n} P_{Rn-1} + \tilde{\Omega}_{in,n+1} P_{Rn+1}, \quad i = 1,2 \end{aligned} \tag{3.2.4}$$

The equivalent channel from HHT_i to relay is denoted by $h_{in}^{(e)}$ and $\tilde{h}_{in}^{(e)}$ represents the channel from the relay to HHT_i. The coefficients $\Omega_{in,n}$ and $\tilde{\Omega}_{in,n}$ are calculated as discussed before and their detailed description is the same as in [57]. It is worth mentioning that these parameters depend on the channel state information h_i between HHT_i and the relay and $\tilde{h}_i$ between the relay and HHT_i.

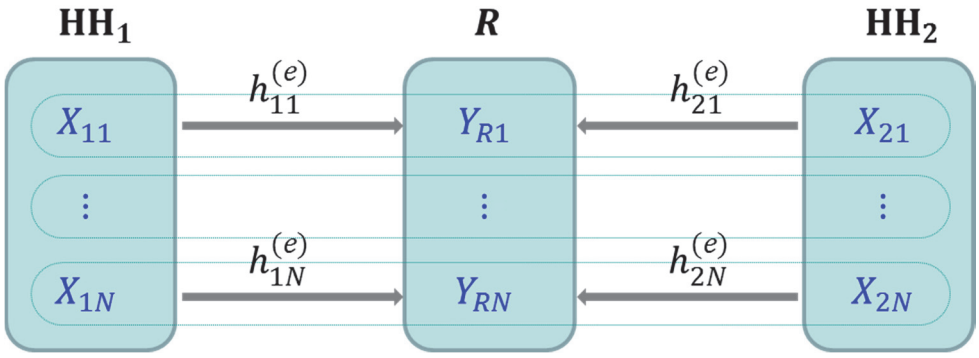

(a) Multiple Access (MA) phase

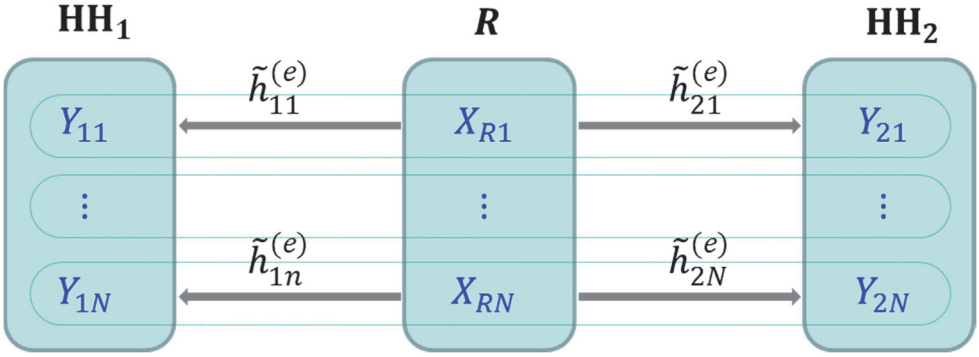

(b) Broadcast (BC) phase

Figure 3-26: Multiple access and broadcast phase in the proposed two-way DF protocol

3.2.1.2 Achievable rate region via optimal power allocation

Let R_{12} and R_{21} represent the rates from HHT_1 to HHT_2 and from HHT_2 and HHT_1, respectively. According to [56], they should satisfy

$$\begin{aligned} R_{12} &\le \min\{\mu I(X_1;Y_R|X_2),(1-\mu)I(X_R;Y_2)\} \\ R_{21} &\le \min\{\mu I(X_2;Y_R|X_1),(1-\mu)I(X_R;Y_1)\} \\ R_{12} = R_{21} &\le \min\{\mu I(X_1,X_2;Y_R)\}, \end{aligned} \tag{3.2.5}$$

where $\mu \in (0,1)$ denotes the fixed proportion of time slot allocated to the MA phase, $X_i = [X_{i1},\cdots,X_{iN}]^T$, i = 1, 2, R and $Y_i = [Y_{i1},\cdots,Y_{iN}]^T$, i = 1, 2, R. Following the proof in [56], each mutual information term corresponds to a parallel point-to-point channel. For example, $I(X_R;Y_2) = \sum_{n=1}^{N} I(X_{Rn};Y_{2n})$. In our FBMC model, if the PAM input symbols are independently Gaussian distributed with unit variance, the interference is also Gaussian distributed because it is the sum of Gaussian random independent variables. Therefore, we get the following inequalities

$$
\begin{aligned}
R_{12} &\le \mu \sum_{n=1}^{N} \log_2\left(1+\frac{|h_{1n}^{(e)}|^2 P_{1n}}{E\{|I_{1n}|^2\}+\sigma_{Rn}^2}\right),\\
R_{12} &\le (1-\mu) \sum_{n=1}^{N} \log_2\left(1+\frac{|\tilde{h}_{2n}^{(e)}|^2 P_{Rn}}{E\{|\tilde{I}_{2n}|^2\}+\sigma_{2n}^2}\right),\\
R_{21} &\le \mu \sum_{n=1}^{N} \log_2\left(1+\frac{|h_{2n}^{(e)}|^2 P_{2n}}{E\{|I_{2n}|^2\}+\sigma_{Rn}^2}\right),\\
R_{21} &\le (1-\mu) \sum_{n=1}^{N} \log_2\left(1+\frac{|\tilde{h}_{1n}^{(e)}|^2 P_{Rn}}{E\{|\tilde{I}_{1n}|^2\}+\sigma_{1n}^2}\right),\\
R_{12}+R_{21} &\le \mu \sum_{n=1}^{N} \log_2\left(1+\frac{|h_{1n}^{(e)}|^2 P_{1n}+|h_{2n}^{(e)}|^2 P_{2n}}{E\{|I_{1n}|^2\}+E\{|I_{2n}|^2\}+\sigma_{Rn}^2}\right),\\
&\sum_{n=1}^{N} P_{in} \le P_{i\max}, i=1,2,R,\\
&P_{in} \ge 0,\ i=1,2,R,\ \forall \in \mathcal{N},
\end{aligned}
\tag{3.2.6}
$$

where $\mathcal{N}=1,\cdots,N$. The terms inside the logarithmic function can be expanded as

$$
\begin{aligned}
1+\frac{|h_{in}^{(e)}|^2 P_{in}}{E\{|I_{in}|^2\}+\sigma_{Rn}^2}
&= 1 + \frac{|h_{in}^{(e)}|^2 P_{in}}{\Omega_{in,n-1}P_{in-1}+\Omega_{in,n}P_{in}+\Omega_{in,n+1}P_{in+1}+\sigma_{Rn}^2}\\
&= \frac{1+\frac{\Omega_{in,n-1}}{\sigma_{Rn}^2}P_{in-1}+\frac{\Omega_{in,n}+|h_{in}^{(e)}|^2}{\sigma_{Rn}^2}P_{in}+\frac{\Omega_{in,n+1}}{\sigma_{Rn}^2}P_{in+1}}{1+\frac{\Omega_{in,n-1}}{\sigma_{Rn}^2}P_{in-1}+\frac{\Omega_{in,n}}{\sigma_{Rn}^2}P_{in}+\frac{\Omega_{in,n+1}}{\sigma_{Rn}^2}P_{in+1}}\\
&= \frac{1+\boldsymbol{a}_{in}^T\boldsymbol{p}_i}{1+\boldsymbol{b}_{in}^T\boldsymbol{p}_i}, i=1,2,
\end{aligned}
\tag{3.2.7}
$$

where $\boldsymbol{p}_i$, $\boldsymbol{a}_{in}$ and $\boldsymbol{b}_{in}$ are column vectors $\in \mathbb{R}^N$. The elements of $\boldsymbol{a}_{in}$ and $\boldsymbol{b}_{in}$ are zeros except at the indexes $\{n-1,n,n+1\}$. These vectors can be expressed as

$$
\boldsymbol{p}_i = [P_{i1},\cdots,P_{iN}]^T, \tag{3.2.8}
$$

$$
\boldsymbol{a}_{in}([n-1,n,n+1]) = \frac{1}{\sigma_{Rn}^2}\left[\Omega_{in,n-1}, \Omega_{in,n}+|h_{in}^{(e)}|^2, \Omega_{in,n+1}\right]^T, \tag{3.2.9}
$$

$$
\boldsymbol{b}_{in}([n-1,n,n+1]) = \frac{1}{\sigma_{Rn}^2}\left[\Omega_{in,n-1}, \Omega_{in,n}, \Omega_{in,n+1}\right]^T. \tag{3.2.10}
$$

The indexes 0 and $N+1$ are discarded. Following the same calculation we get

$$1+\frac{|\tilde{h}_{in}^{(e)}|^2 P_R}{E\{|\tilde{I}_{in}|^2\}+\sigma_{in}^2}=\frac{1+\widetilde{\boldsymbol{a}}_{in}^T \boldsymbol{p}_R}{1+\widetilde{\boldsymbol{b}}_{in}^T \boldsymbol{p}_R}, i=1,2, \tag{3.2.11}$$

where

$$\boldsymbol{p}_R=[P_{R1},\cdots,P_{RN}]^T, \tag{3.2.12}$$

$$\widetilde{\boldsymbol{a}}_{in}([n-1,n,n+1])=\frac{1}{\sigma_{in}^2}\left[\widetilde{\Omega}_{in,n-1},\widetilde{\Omega}_{in,n}+|\tilde{h}_{in}^{(e)}|^2,\widetilde{\Omega}_{in,n+1}\right]^T, \tag{3.2.13}$$

$$\widetilde{\boldsymbol{b}}_{in}([n-1,n,n+1])=\frac{1}{\sigma_{in}^2}\left[\widetilde{\Omega}_{in,n-1},\widetilde{\Omega}_{in,n},\widetilde{\Omega}_{in,n+1}\right]^T. \tag{3.2.14}$$

Our objective is to maximize the exchange rate $R_X=\min(R_{12},R_{21})$. This optimization problem can be decomposed into finding the multiple access rate R_{MA}, which corresponds to finding P_{1n} and P_{2n} in the MA phase, and the broadcast rate R_{BC}, which aims at finding optimal P_{Rn} [56] in the BC phase.

In the MA phase, the terminals HHT_1 and HHT_2 can transmit total powers less or equal to $P_{1\max}$ and $P_{2\max}$ respectively. The optimization problem can be formulated as follows

$$\begin{aligned}
&\max_{P_{1n},P_{2n},R_{\mathrm{MA}},n\in\mathcal{N}} R_{\mathrm{MA}}\\
&s.t.\\
&R_{\mathrm{MA}}\le\mu\sum_{n=1}^{N}\log_2\left(\frac{1+\boldsymbol{a}_{1n}^T\boldsymbol{p}_1}{1+\boldsymbol{b}_{1n}^T\boldsymbol{p}_1}\right),\\
&R_{\mathrm{MA}}\le\mu\sum_{n=1}^{N}\log_2\left(\frac{1+\boldsymbol{a}_{2n}^T\boldsymbol{p}_2}{1+\boldsymbol{b}_{2n}^T\boldsymbol{p}_2}\right),\\
&R_{\mathrm{MA}}\le\frac{\mu}{2}\sum_{n=1}^{N}\log_2\left(\frac{1+\boldsymbol{a}_{1n}^T\boldsymbol{p}_1+\boldsymbol{a}_{2n}^T\boldsymbol{p}_2}{1+\boldsymbol{b}_{1n}^T\boldsymbol{p}_1+\boldsymbol{b}_{2n}^T\boldsymbol{p}_2}\right),\\
&\sum_{n=1}^{N}P_{1n}\le P_{1\max},\ \sum_{n=1}^{N}P_{2n}\le P_{2\max},\\
&P_{1n}\ge 0,\ P_{2n}\ge\mathbf{0},\ \forall n\in\mathcal{N}.
\end{aligned} \tag{3.2.15}$$

The first three constrains are differences of concave functions, i.e. $\log_2(1+\boldsymbol{a}^T\boldsymbol{x})-\log_2(1+\boldsymbol{b}^T\boldsymbol{x})$. The problem is known as DC programming problem which is in general non-convex. In order to solve this problem, we propose to extend the POTDC method introduced in [58].

Taking the first constraint as an example, we introduce an auxiliary variable t_1

$$R_{\mathrm{MA}} \leq \frac{\mu}{\log(2)} \sum_{n=1}^{N} \log\left(1 + \boldsymbol{a}_{1n}^{T} \boldsymbol{p}_1\right) - t_1, \tag{3.2.16}$$

$$\frac{\mu}{\log(2)} \sum_{n=1}^{N} \log\left(1 + \boldsymbol{b}_{1n}^{T} \boldsymbol{p}_1\right) \leq t_1. \tag{3.2.17}$$

The non-convex function is then replaced by its linear approximation around a starting value $\boldsymbol{p}_1^0$ such that P_{1n}^0 are positive and satisfy the maximum power constraint. The linear approximation of logarithmic function is given by

$$\log\left(1 + \boldsymbol{a}^T \boldsymbol{x}\right) \approx \log\left(1 + \boldsymbol{a}^T x^{\mathbf{0}}\right) + \frac{\boldsymbol{a}^T}{1 + \boldsymbol{a}^T \boldsymbol{x}^0} (\boldsymbol{x} - \boldsymbol{x}^0). \tag{3.2.18}$$

Then the non-convex constraints can be rewritten as

$$R_{\mathrm{MA}} \leq \frac{\mu}{\log(2)} \sum_{n=1}^{N} \log\left(1 + \boldsymbol{a}_{1n}^{T} \boldsymbol{p}_1\right) - t_1, \tag{3.2.19}$$

$$\frac{\mu}{\log(2)} \sum_{n=1}^{N} \left\{ \log\left(1 + \boldsymbol{b}_{1n}^{T} \boldsymbol{p}_1^0\right) + \frac{\boldsymbol{b}_{1n}^{T}}{1 + \boldsymbol{b}_{1n}^{T} \boldsymbol{p}_1^0} (\boldsymbol{p}_1 - \boldsymbol{p}_1^0) \right\} \leq t_1. \tag{3.2.20}$$

In the same way the second and third constraints are formulated. In the third constraint we have $\boldsymbol{b}_{1n}^{T} \boldsymbol{p}_1 + \boldsymbol{b}_{2n}^{T} \boldsymbol{p}_2 = [\boldsymbol{b}_{1n}^{T}, \boldsymbol{b}_{2n}^{T}][\boldsymbol{p}_{1n}^{T}, \boldsymbol{p}_{2n}^{T}]^T$. Finally, we obtain the following convex problem

$$\begin{gathered}
\max_{P_{1n},\, P_{2n},\, R_{\mathrm{MA}},\, n \in \mathcal{N}} R_{\mathrm{MA}} \\
s.t. \\
R_{\mathrm{MA}} \leq \frac{\mu}{\log(2)} \sum_{n=1}^{N} \log\left(1 + \boldsymbol{a}_{1n}^{T} \boldsymbol{p}_1\right) - t_1, \\
\frac{\mu}{log(2)} \sum_{n=1}^{N} \left\{ \log\left(1 + \boldsymbol{b}_{1n}^{T} \boldsymbol{p}_1^0\right) + \frac{\boldsymbol{b}_{1n}^{T}}{1 + \boldsymbol{b}_{1n}^{T} \boldsymbol{p}_1^0} (\boldsymbol{p}_1 - \boldsymbol{p}_1^0) \right\} \leq t_1, \\
R_{\mathrm{MA}} \leq \frac{\mu}{\log(2)} \sum_{n=1}^{N} \log\left(1 + \boldsymbol{a}_{2n}^{T} \boldsymbol{p}_2\right) - t_2, \\
\frac{\mu}{log(2)} \sum_{n=1}^{N} \left\{ \log\left(1 + \boldsymbol{b}_{2n}^{T} \boldsymbol{p}_2^0\right) + \frac{\boldsymbol{b}_{2n}^{T}}{1 + \boldsymbol{b}_{2n}^{T} \boldsymbol{p}_2^0} (\boldsymbol{p}_2 - \boldsymbol{p}_2^0) \right\} \leq t_2, \\
R_{\mathrm{MA}} \leq \frac{\mu}{\log(2)} \sum_{n=1}^{N} \log\left(1 + \boldsymbol{a}_{1n}^{T} \boldsymbol{p}_1 + \boldsymbol{a}_{2n}^{T} \boldsymbol{p}_2\right) - t_3,
\end{gathered} \tag{3.2.21}$$

$$\frac{\mu}{\log(2)}\sum_{n=1}^{N}\left\{\log\left(1+\boldsymbol{b}_{1n}^{T}\boldsymbol{p}_{1}^{0}+\boldsymbol{b}_{2n}^{T}\boldsymbol{p}_{2}^{0}\right)+\frac{\boldsymbol{b}_{1n}^{T}(\boldsymbol{p}_{1}-\boldsymbol{p}_{1}^{0})+\boldsymbol{b}_{2n}^{T}(\boldsymbol{p}_{2}-\boldsymbol{p}_{2}^{0})}{1+\boldsymbol{b}_{1n}^{T}\boldsymbol{p}_{1}^{0}+\boldsymbol{b}_{2n}^{T}\boldsymbol{p}_{2}^{0}}\right\}\leq t_{3},$$

$$\sum_{n=1}^{N}P_{1n}\leq P_{1\max},\ \sum_{n=1}^{N}P_{2n}\leq P_{2\max},$$

$$P_{1n}\geq 0,\ P_{2n}\geq \mathbf{0},\ \forall n\in\mathcal{N}.$$

After solving the problem in the first iteration, the optimum value is denoted as $R_{MA^{(1)}}$, the optimal solution are obtained as $\boldsymbol{p}_1^{(1)}$ and $\boldsymbol{p}_2^{(1)}$. In the second iteration, $\boldsymbol{p}_1^{(1)}$ and $\boldsymbol{p}_2^{(1)}$ are used in the linear approximation of the second iteration. This process continues so that in the k-th iteration, $\boldsymbol{p}_1^{(k-1)}$ and $\boldsymbol{p}_2^{(k-1)}$ are used. The iterations stops when the difference between the optimum values of two successive iterations is less or equal to a desired threshold, that is

$$|R_{MA}^{(k)}-R_{MA}^{(k-1)}|\leq\eta. \tag{3.2.22}$$

The similar approach can be applied obtain the achievable rate in the BC phase. Finally, the exchange rate is calculated as the minimum achievable rates in the MA phase and the BC phase.

3.2.2 Simulation settings

In all the Monte-Carlo simulations, the ITU-Vehicular A channel model is considered. Using sampling frequency $F_s = 15.36$ MHz leads to a channel with 40 taps, all are zeros except at the indexes $0, 5, 11, 17, 27, 39$ and the complex coefficients at these taps are i.i.d Rayleigh distributed random variables with power equal to the values given in the power delay profile. The frequency domain channel gains for OFDM are generated using M-point Fast Fourier Transform (FFT).

The maximum allowed power P_T is equal to 1 W for all nodes, and the noise variance is identical and equal to σ^2 at all nodes. The average sum rate for both nodes is calculated as

$$R=\frac{2R_X}{N_{sy}T_sW}\ (\text{bit/Hz/s}), \tag{3.2.23}$$

where $\mathrm{N_{sy}}$ denotes the number of samples per symbol, T_s the sampling frequency and W the bandwidth. In OFDM, a cyclic prefix (CP) of length C samples is added so that, the symbol length is $N + C$ samples, whereas in FBMC twice number of samples are generated but each sample represents a PAM symbol. To have a fair comparison between the OFDM/QAM system and the FBMC/OQAM system, the rate achieved in the FBMC system is divided by 2. And in both systems $T_sW = 1$, therefore

$$R_{\mathrm{OFDM}} = \frac{2R_X}{N+C} \text{ (bit/Hz/s)}, \tag{3.2.24}$$

$$R_{\mathrm{FBMC}} = \frac{2R_X}{N} \text{ (bit/Hz/s)}. \tag{3.2.25}$$

The cyclic prefix in OFDM system is assumed to be 6.67% and the average SNR is taken as $\frac{P_T/N}{\sigma^2}$. The equalizer (pre-equalizer) has $L_{a_1} = L_{a_2}$ $(L_{b_1} = L_{b_2})$ so its length is represented by L_a (L_b).

Frame structure	
Sampling frequency	15.36 MHz
Subcarriers number	64, 128, 512
OFDM CP	6.67% Symbol period
FBMC filter	OFDM/OQAM PHYDYAS
Overlapping factor	4
Transmitter/Receiver	
Noise power spectral density	Various
Equalizer length	1, 3, 5, 7
Pre-equalizer length	1, 3, 5, 7
Transmission scheme	SISO
Propagation	
Fast fading channel models	ITU-Vehicular A
Channel estimation	Ideal

Table 3-3: Simulation settings for FBMC based two-way relaying strategies

3.2.3 Simulation results

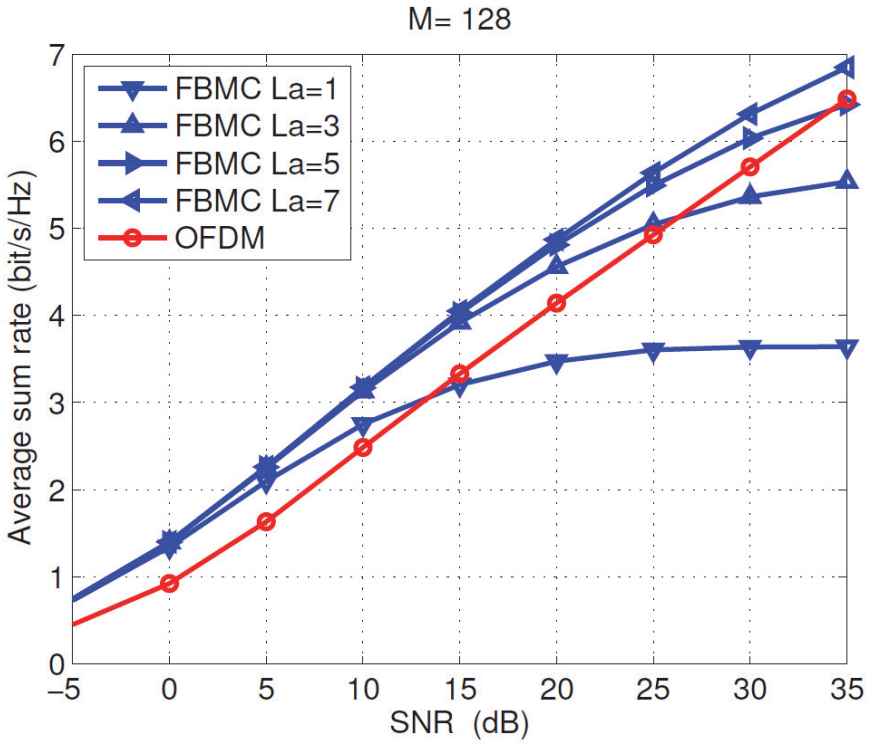

Figure 3-27: Sum rate vs SNR achieved by FBMC with different L_a and OFDM for $M = 128$

Figure 3-27 illustrates the achieved rate in a FBMC system using $\mathrm{M} = 128$ subcarriers and the same number of taps $L_a$for both the pre-equalizer and equalizer in MA and BC phases, respectively. It is shown that FBMC outperforms OFDM until specific SNR, namely $15, 25, 35$ dB for $L_a = 1, 3, 5$ respectively. The effect of the equalizer length is important in the high SNR regime. For example, $L_a = 3, 5, 7$ have the same performance at 15 dB. But if we increase the number of taps by 2 every 10 dB starting from $L_a = 2$, the achievable rate will keep increasing.

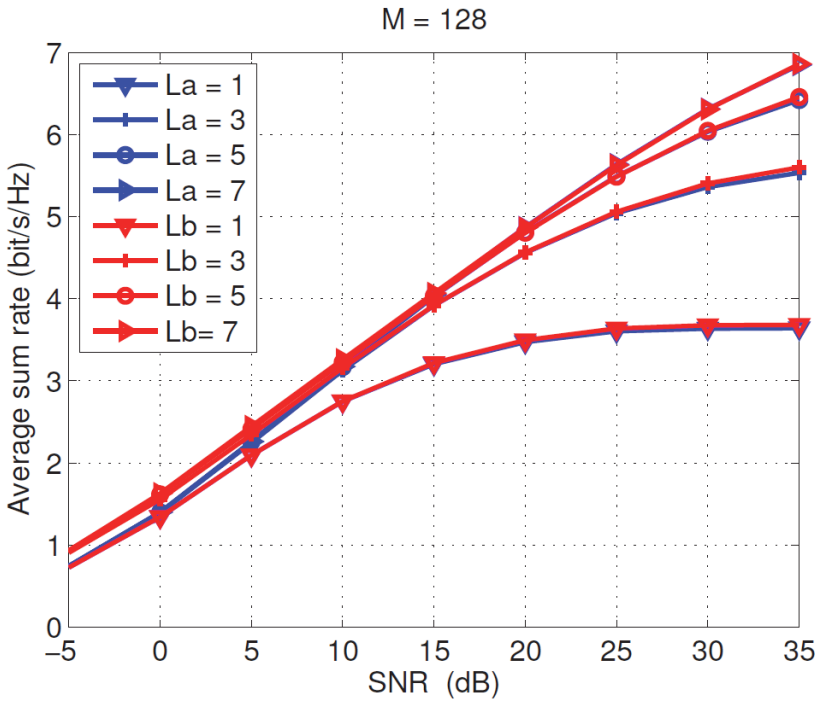

Figure 3-28: Data transfer rate for each hop achieved by FBMC two way relaying for $M = 128$ with different L_a and L_b

The comparison between implementing equalizer or pre-equalizer is drawn in Figure 3-28. It is seen that for the same length i.e., $L_a = L_b$, the same performance is achieved.

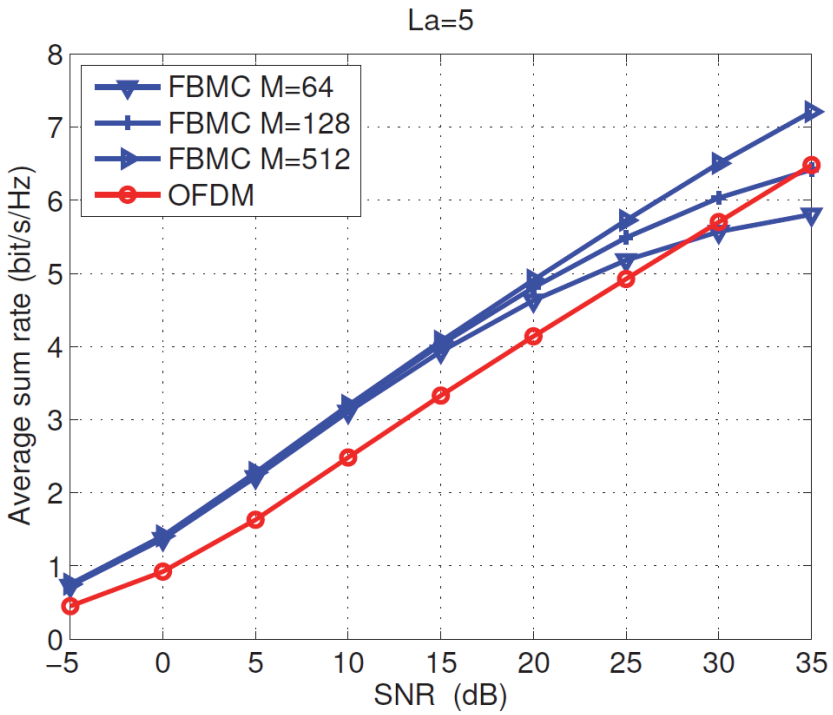

Figure 3-29: Sum rate vs SNR achieved by FBMC for different M and $L_a = L_b = 5$

In Figure 3-29 the effect of M is evaluated. As expected, higher number of subcarriers requires less number of taps for the equalizer to maintain the same performance.

3.2.4 Final remarks

We have evaluated the achievable exchange rates of OFDM and FBMC based two-way DF relaying systems. Simulation results show that the FBMC-based systems can provide a higher data rate than OFDM-based ones especially when multi-tap equalizer or pre-equalizer is applied at the terminals. The drawback of applying pre-equalizers and equalizers is the increased computational complexity compared to pure power allocation schemes. Nevertheless, the achieved gain is worth the complexity and the FBMC based systems can become a candidate for future broadband PMR systems.

3.3 Two-way AF relaying for FBMC with SIC

3.3.1 Description and motivation

Since the successive interference cancellation is currently available only for the SISO configuration, as elaborated in EMPhAtiC D3.2 [2], for the two-relaying application, only direct application of the SISO configuration is available at the moment. The real-domain processing, pertinent to the FBMC format is used, allowing for utilization of mutual independence of noise components on in-phase and quadrature components at the Analysis FilterBank (AFB) outputs to provide a form of (additional) diversity. At this stage the potentials of the embedded noise prediction and cancellation to be developed and presented in EMPhAtiC D3.2 [2] will not be evaluated.

The targeted application is ad hoc networking with insufficient coordination among transmit, and receive user terminals, in terms of time and frequency synchronization and channel estimation, and in cellular one, where is of interest to reduce the relaying overhead. Examples of these two scenarios are summarized in Figure 3-1, please refer to its description for the out-of coverage DMO cluster part for more details on the PMR scenario.

In SISO case, AF is considered here. Further elaboration and simulation results are provided in the sections below. Notice that DF can also be considered for the SISO case, but it is left for future work. Block diagrams of the considered SISO two-way relaying configuration is shown in Figure 3-30 for the two phases of transmission indicated by the respective a) and b) parts.

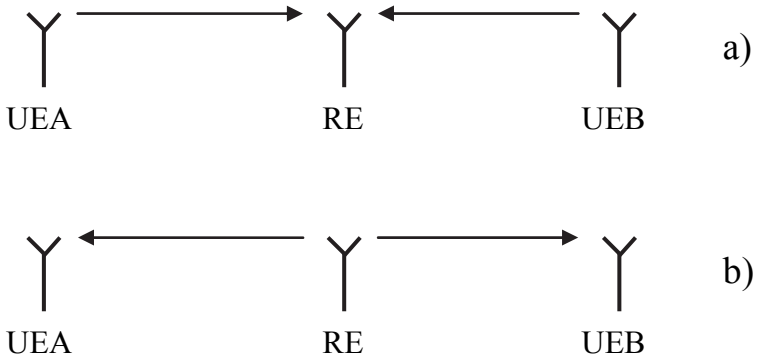

Figure 3-30: SISO two-way relaying: phase 1, a) and phase 2, b)

In line with the real-valued framework SISO model (EMPhAtiC D2.2 [4]) and its extension to the MISO, as introduced in EMPhAtiC D4.1 [1], the (*n,k*)-th received signal time-frequency bin in the second phase by each of the two user terminals is the sum of two signals and receiver noise, that is, in case of the terminal A

$$r_n^k(A) = \sum_{k"=-1}^{1} \sum_{n"=-2L_{g+\xi_\tau}}^{2L_{g+\xi_\tau}} d_{n-n"}^{k+k"}(A)\xi_{n"}^{k,k"}(A) + \sum_{k"=-1}^{1} \sum_{n"=-2L_{g+\xi_\tau}}^{2L_{g+\xi_\tau}} d_{n-n"}^{k+k"}(B)\xi_{n"}^{k,k"}(B) + \beta_n^k(A) \quad (3.3.1)$$

where $\xi_{n"}^{k,k"}$ are the real-domain three impulse responses of the global filters. $\xi_{n"}^{k,0}$ is the impulse response for the subchannel k, $\xi_{n"}^{k,1}$ represents the interferences from the upper sub carrier of index $k+1$ and $\xi_{n"}^{k,-1}$ interferences from the lower subchannel of index $k-1$.

As described in EMPhAtiC D3.2 [2], for SISO case, in absence of the second term in (3.3.1), and with availability of the equivalent subchannel impulse responses decoding of the (presumably unknown) data proceeds in an iterative – Successive Interference Cancellation (SIC) manner, illustrated in Figure 3-31.

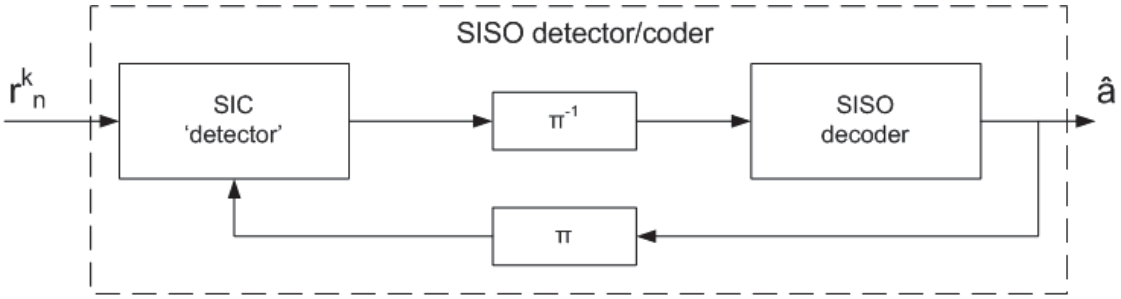

Figure 3-31: Block-scheme of the turbo-like iterative interference cancellation based data detection

3.3.1.1 SISO AF case

In this configuration, the single-antenna relaying terminal merely amplifies the signals received from the two communicating terminals, and retransmits the composite signal to them in the next time frame. This implies different channel transfer functions for the terminal's own signal and the signal that had been sent to the relay from the other terminal.

More detailed block-diagram, with simplified notations regarding the signals and transfer functions involved, is shown in Figure 3-32.

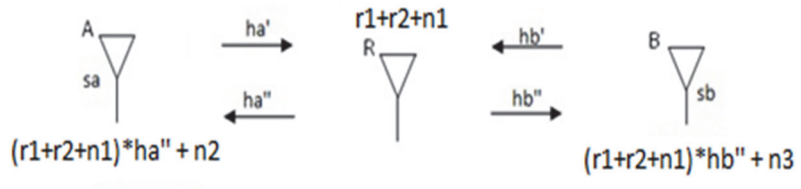

Figure 3-32: The relay system in the case of AF

Although in the transmission phase 1, there is no need for use of preamble signals regarding the channel estimation from the point of view of the reception by the repeater, its presence is needed for the second phase of transmission, when each of the two communicating terminals needs suitable organized training blocks to estimate the subchannel impulse responses pertaining to its (known) signal and the signal from the other terminal, in order to be able to subtract (the contribution to the composite signal) of its own signal and to subsequently detect/decode the signal that had been sent from the other one – UEA from UEB and vice-versa, UEB from UEA.

Since the channel pertaining to the UEA as seen from UEB is different form the channel between the repeating terminal, either a training signal with interlaced pilot, i.e. training symbols could be devised for the reduction of the training overhead, at least for the initial analysis it is assumed that the training interval is separated into two parts, for example the first half devoted to the signal transmitted from the UEA, and the first half for the signal transmitted from the UEB. (The preamble organization and channel estimation is to be performed in an efficient way regarding the introduced overhead, in particular pilot-based as in EMPhAtiC D3.1 [2]. For the presented simulation results, we did use relatively long preambles and estimated the subchannels impulse responses consecutively.) Considering only the User terminal A side, in the first step, the UEA firstly estimates the relevant (subchannel, direct and inter-bin cross-talk) impulse responses. In the second step, it reconstructs its signal sent in the phase 1. In the third step it estimates the relevant impulse responses pertaining to the signal sent from the UEB, and subsequently performs its transmit signal detection/decoding as in the standards SISO mode.

More specifically, taking the received signal into relay having the form:

$$r = r_1 + r_2 + n_1, \tag{3.3.2}$$

where r_1 represents the signal sent from antenna *A* after passing through channel h_a', r_2 is signal send from antenna *B* after passing through channel h_b' and n_1 is white Gaussian noise, it is sent to antennas *A* and *B* through channels h_a'' and h_b'', respectively.

The signal which is arrived into antenna *A* has form

$$u_1 = (s_a * h_a' + s_b * h_b')*h_a'' + n_2 \tag{3.3.3}$$

where s_a and s_b represents the symbols sent from antennas *A* and *B* to the relay, and n_2 is the repeater's retransmitted (receive) noise. If we denote $h_a'*h_a''$ as h_a and $h_b'*h_a''$ as h_b, (3.3.3) becomes:

$$u_1 = s_a * h_a + s_b * h_b. \tag{3.3.4}$$

The user terminal *A* knows its own symbols s_a, in order to decide on the symbols s_b sent from antenna *B*, what is needed is to estimate the impulse responses h_a and h_b.

First, training sequence is sent to relay by antenna *A* through channel h_a'. Then the relay sends the received training sequence to antenna *A* through channel h_a''. The received training sequence into antenna *A* is:

$$t_1 = s_a * h_a' * h_a'', \tag{3.3.5}$$

or if $h_a' * h_a''$ is denoted as h_a (3.3.5) can be rewritten as:

$$t_1 = s_a * h_a. \tag{3.3.6}$$

By using training signal from (3.3.6), based on known data, the impulse response h_a is determined. In the same way is determined the impulse response h_b, based on the training sequence having been sent in the phase 1 from the antenna *B*.

The symbols sent from antenna *B* can now be inferred from the signal that remains after subtracting the contribution of the known signal, as per the following equation*:*

$$r_{2n}^{k} + \beta_{1n}^{k} = r_{n}^{k} - \sum_{k'=-1}^{1} \sum_{n''=-2L_{g+h_\tau}}^{2L_{g+h_\tau}} s_{a\,n-n''}^{k+k'} \hat{h}_{a\,n'}^{k',k} \tag{3.3.7}$$

where the left over user terminal B signal model for the SIC-based detection of its data can be written as

$$r_{2n}^{k} = \sum_{k'=-1}^{1} \sum_{n''=-2L_{g+h_\tau}}^{2L_{g+h_\tau}} s_{b\,n-n''}^{k+k'} \hat{h}_{b\,n'}^{k',k} + \tilde{\beta}_{1n}^{k} \tag{3.3.8}$$

In the (3.3.8), the term $\tilde{\beta}_{1n}^{k}$ represents the sum of two noise samples, one on relay reception side and another one on antenna *A* reception side, denoted with n_1 and n_2 in Figure 3-32.

3.3.2 Simulation settings

For the simulation we use Rayleigh flat fading channel and multi-tap channel model and the 1000 independent fading realization are used to get reasonably good statistic.

Frame structure	
Subcarriers number	8 subcarriers / 6 useful
Subcarrier spacing	175 kHz
FBMC filter	Raised cosine
Overlapping factor	4
Modulation and coding schemes	4 QAM , convolutional code with rate 1/2
Propagation	
Static fading channel models	Rayleigh, flat Rayleigh, multi-tap channel (delay profile given in Table 3-9.
Channel estimation	Preamble-based Least-Squares method

Table 3-4: Summary of simulation parameters

Delay [ns]	**Power [dB]**
0	0
100	-5.4287
200	-2.5162
300	-5.8905
400	-9.1603
500	-12.5105
600	-15,6126
700	-18,7147
800	-21.8168

Table 3-5: Multi-tap channel delay profile

3.3.3 Simulation results

3.3.3.1 SISO AF case

Simulation results are shown in Figure 3-33 and Figure 3-34. In these pictures is shown the comparison between standard SISO scenario (blue curves) and the described AF scenario (green curves). The "*BER raw"* and "*BER coding"* represent un-coded and coded (convolutional code of constraint length 7 and coding rate 0.5) curves respectively. The green curves represent the BER for the unknown data on the e.g. side *A,* see Figure 3-30, when the known data is subtracted from the arrived*,* as shown in (3.3.7). It can be seen that there is a mismatch of several dB which is expected because when we use AF relaying strategy, we have two noise components, one on the relay side and another on receive-terminal antenna side, which is denoted with n_2 and n_1 in Figure 3-30 respectively. The noise prediction and cancellation methodology, to be presented in EMPhAtiC D3.2 [3] can be used to partly compensate for the reduced SNR due to the AF relaying mechanism.

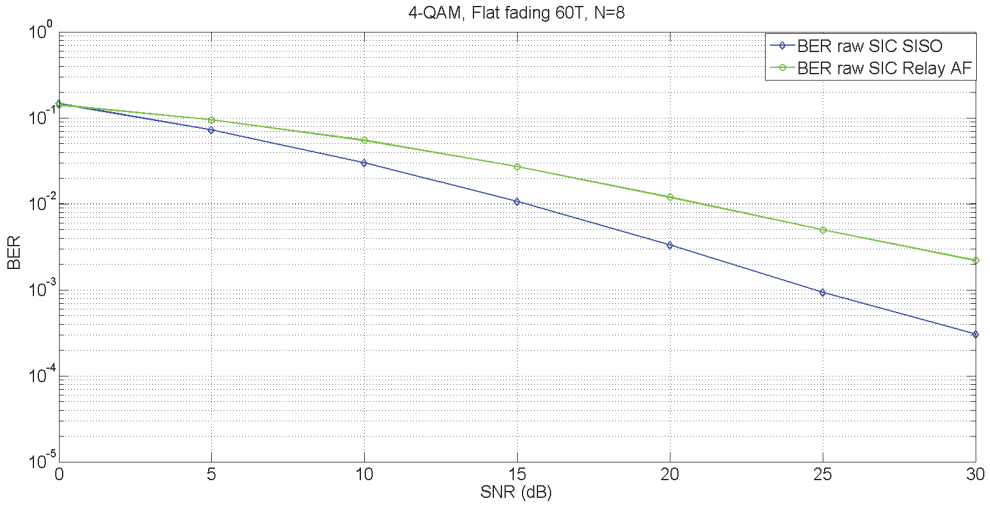

Figure 3-33: BER in function of SNR for the AF relay case for Rayleigh flat fading channel

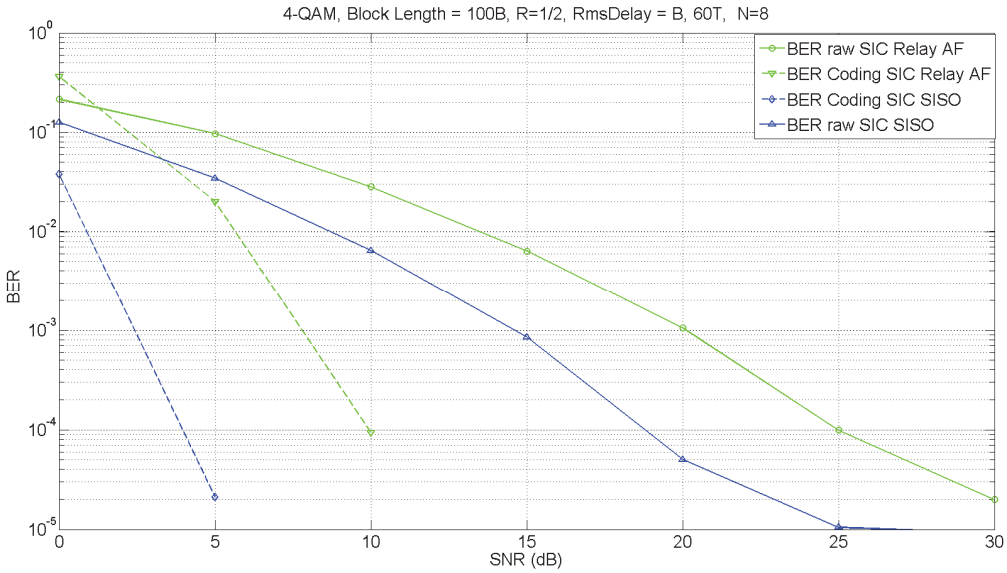

Figure 3-34: BER in function of SNR for the AF relay case for multi-tap channel

While in the flat fading conditions the convolutional code cannot improve performance beyond the un-coded ones, for multi-tap channels the effect of coding is apparent, but still the BER performance is for around 5 dB worse than in the SISO case.

3.3.4 Final remarks

In this section we proposed an AF relay strategies which leverage the real-domain SIC framework for the two-way relaying scheme. A mismatch of several dB with respect to the SISO case can be seen in the performance, but it is expected and it is due to the presence of two noise components, one on the relay side and another on receive-terminal antenna side. For frequency selective channels the effect of coding is apparent and brings a performance improvement in the case of two-way AF relaying too.

The potentials of the real-domain SIC framework in terms of in-phase and quadrature branch diversity and the noise prediction and cancellation, being developed within WP3 and the related deliverable D3.2 [3], will further contribute to the attractiveness of using SIC as a basic element of the basic two-way relaying based networking, even for other relaying strategies like DF.

3.4 AF relaying in highly frequency selective channels

3.4.1 Description and motivation

In this section we investigate the benefits that an AF relay can bring to a point-to-point communications link that employs an FBMC modulation scheme. More specifically, we compare a single-hop system (source to destination) with a two-hop system (source to relay and relay to destination) in terms of spectral efficiency. It is important to remark that we will focus on wireless channels characterized by high frequency selectivity. For this reason, the simple equalizer with one tap per subcarrier is far from being optimal, since it introduces a considerable distortion. In the proposed scheme, the issue is overcome by implementing, at the destination terminal, a parallel, multi-stage equalizer similar to the one introduced by the EMPhAtiC consortium in Section 3 of [1].

At this point, it is worth recalling that an AF relay is a simple device that retransmits an amplified version of the received signal. Its simplicity has two main advantages. First, since almost no signal processing is carried out, an AF relay is a very cheap terminal (or a cheap function in multi-purpose devices) that requires little maintenance and almost no extra power, besides the transmitted one. The second advantage is that an AF relay is transparent to most of the characteristics of the main communications system. Indeed, the AF relay is not required to decode (or not even to demodulate) the received signal. For these reasons, AF relays may be of valuable help in Public Protection and Disaster Relief (PPDR) scenarios, where terminals may be easily lost or difficult to recuperate due to the critical environment conditions and where we may need to extend the coverage of different PMR cellular-based or ad hoc-based systems (see also Figure 3-35).

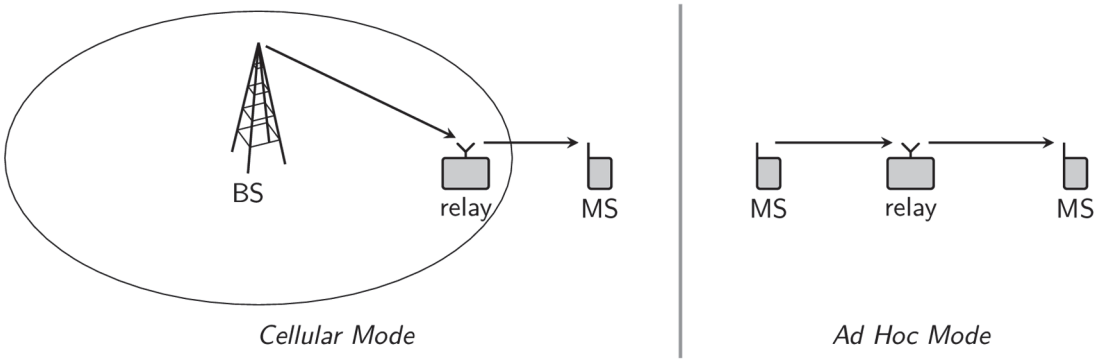

Figure 3-35: Examples of relay application in PMR scenarios.

However, in order to decide whether (or when) AF relaying can be employed to improve coverage extension in PMR/PPDR scenarios, we need to characterize the total noise at the output of the FBMC demodulator at the destination. It is well known, indeed, that the main drawback of AF relaying is the fact that the noise collected by the relay when listening to the channel is amplified and forwarded together with the data signal. At the destination, the relayed noise sums up with the classic additive noise of the relay–destination link, thus

deteriorating the signal quality. Moreover, since we are considering scenarios with frequency selective channels, the noise process at the relay is filtered by the relay–destination channel impulse response. This implies that the receiver must deal with a coloured noise, even when the noise at both the relay and the destination can be modelled as additive white Gaussian processes. In what follows, the quality of the FBMC link with an AF relay is characterized in terms of Signal-to-Noise-plus-Distortion Ratio (SNDR) and, then, this metric is used to compare the relaying scheme with the direct source–destination link.

3.4.1.1 Signal model

Consider a single-antenna, M-subcarrier FBMC system (with M a power of 2). It is well known (see, e.g., [5] and [38]) that the output of the FBMC modulator can be written as

$$\mathbf{x} = \mathrm{vec}([\mathbf{X}_1 \quad \mathbf{0}] + [\mathbf{0} \quad \mathbf{X}_2]),$$

where $\mathrm{vec}(\cdot)$ piles the columns of a matrix and

$$\mathbf{X} = \begin{bmatrix}\mathbf{X}_1 \\ \mathbf{X}_2\end{bmatrix} = \sqrt{2}\left(\mathbf{F}_M \mathbf{\Phi}^* (\mathbf{B} \otimes [1,0] + j\mathbf{C} \otimes [0,1]) \circledast (\mathbf{P} \otimes [1,0])\right)$$

is the matrix collecting the modulated symbols. In the last equation we have also introduced the $M \times M$ Fourier matrix $[\mathbf{F}_M]_{1\le m,n\le M} = M^{-\frac{1}{2}} \exp\left[j\frac{2\pi}{M}(m-1)(n-1)\right]$, the diagonal weight matrix $\mathbf{\Phi} = \mathrm{diag}_{m=1,\dots,M}\left\{e^{-j\pi\frac{M+2}{2M}(m-1)}\right\}$ and the $M \times \kappa$ matrix

$$\mathbf{P} = \begin{bmatrix}\mathbf{P}_1 \\ \mathbf{P}_2\end{bmatrix} = \begin{bmatrix} p_N[1] & \cdots & p_N[M(\kappa-1)+1] \\ \vdots & \ddots & \vdots \\ p_N[M] & \cdots & p_N[M\kappa] \end{bmatrix} \tag{3.4.1}$$

where $p_N[n], n = 1, \dots, N$, is the real-valued prototype pulse of length $N = M\kappa$ and $\kappa \in \mathbb{N}$ is the overlapping factor. Moreover, the operators $\otimes$ and $\circledast$ stand for the Kronecker product and row-wise convolution, respectively, while the $M \times N_s$ matrix $\mathbf{A} = \mathbf{B} + j\mathbf{C}$ gathers the N_s complex multiband symbols to transmit. The elements of $\mathbf{B}$ and $\mathbf{C}$ are modelled as i.i.d. real random variables with zero mean and variance $P_{tx}/2$.

The signal vector $\mathbf{x}$ is received by the relay through the uplink channel $h_u[l], l = 1, \dots, L_u$, together with a circularly symmetric additive white Gaussian noise $\mathbf{n}_u$ of variance σ_u^2. Then, the relay amplifies the signal by a factor $\sqrt{A}, A \in \mathbb{R}^+$, and forwards it to the receiver through the downlink channel $h_d[l], l = 1, \dots, L_d$. At the receiver, new noise samples are added. We assume that the noise $\mathbf{n}_d$ at the receiver is also circularly symmetric, additive, white, Gaussian with variance σ_d^2 and independent of $\mathbf{n}_u$. It is straightforward to prove that, in order for the relay transmitted power to be P_r, one has to fix the amplification factor such that

$$A = \frac{P_r}{2\frac{P_{tx}}{M}\sum_{n=1}^{N} p_N^2[n] \sum_{l=1}^{L_u} |h_u[l]|^2 + \sigma_u^2}. \tag{3.4.2}$$

The receiver implements a parallel K-stage FBMC demodulator/equalizer like the one proposed in [5], which is basically a particular case of the one in Section 3 of [1], with a real-valued prototype pulse $q_N[n]$ of length $N = M\kappa$ as $p_N[n]$. Hereafter, we will assume that the prototype pulses fulfil the reconstruction conditions

$$\left(\mathbf{I}_2 \otimes \left(\mathbf{I}_{M/2} + \mathbf{J}_{M/2}\right)\right) \mathcal{R}(p_N, q_N) = [\mathbf{0}_{M\times(\kappa-1)} \quad \mathbf{1}_M \quad \mathbf{0}_{M\times(\kappa-1)}]$$

and

$$\Big(\mathbf{I}_2 \otimes \big(\mathbf{I}_{M/2} - \mathbf{J}_{M/2}\big)\Big)\, S(p_N, q_N) = \mathbf{0}_{M\times(2\kappa-1)},$$

where

$$\mathcal{R}(p_N, q_N) = \begin{bmatrix}\mathbf{P}_1 \circledast \mathbf{J}_{M/2}\mathbf{Q}_2 \\ \mathbf{P}_2 \circledast \mathbf{J}_{M/2}\mathbf{Q}_1\end{bmatrix}, \quad S(p_N, q_N) = \begin{bmatrix}\mathbf{P}_2 \circledast \mathbf{J}_{M/2}\mathbf{Q}_2 \\ \mathbf{P}_1 \circledast \mathbf{J}_{M/2}\mathbf{Q}_1\end{bmatrix}, \tag{3.4.3}$$

with $\mathbf{Q}$ a matrix built from $q_N[n]$ as $\mathbf{P}$ is built from $p_N[n]$ in (3.4.1), and where $\mathbf{J}_X$ is the $X \times X$ anti-diagonal matrix. Also, $\mathbf{1}_M$ is the column vector of M ones and $\mathbf{0}_{M\times X}$ is the $M \times X$ matrix filled with zeros.

After a careful inspection of the model above, we can think about the signal at the receiver output as consisting of three different components, one due to the data signal $\mathbf{x}$, one due to the AWGN $\mathbf{n}_d$ collected by the receiver and one due to the AWGN $\mathbf{n}_u$ collected by the relay and filtered by the downlink channel $h_d[l]$. Note that, since the system is linear, the first two components correspond to the signal at the output of the receiver if we had transmitted over a direct point-to-point link with channel $h_{eq}[l] = \sqrt{A}(h_u * h_d)[l]$ of length $L_h = L_u + L_d - 1$. This means that, when the transmitter–relay channel is noiseless (i.e., $\sigma_u^2 = 0$), the transmitted symbols at subcarrier m are retrieved with a SNDR given by

$$\mathrm{SNDR}_K(m)|_{\sigma_u^2=0} = \frac{P_{tx}}{P_e^{(K)}(m) + P_{w,d}^{(K)}(m)}, \tag{3.4.4}$$

where, according to [5], $P_e^{(K)}(m)$ is the residual interference power due to a non-perfect equalizer and $P_{w,d}^{(K)}(m)$ is the noise power due to the downlink channel. The expressions for the two terms at the denominator, both depending on the number of demodulation / equalization stages K, are as follows [5]:

$$\begin{aligned} P_e^{(K)}(m) = \frac{2P_{tx}}{M^{2K+1}}\Big(&\mathrm{Re}^2\{\mathbf{K}_K\}_{m,m}\mathrm{tr}\Big[\mathcal{X}_{RR}^{(K)}\mathbf{U}^+ + \mathcal{X}_{SS}^{(K)}\mathbf{U}^-\Big] \\ &+ \mathrm{Im}^2\{\mathbf{K}_K\}_{m,m}\mathrm{tr}\Big[\mathcal{X}_{RR}^{(K)}\mathbf{U}^- + \mathcal{X}_{SS}^{(K)}\mathbf{U}^+\Big]\Big), \end{aligned} \tag{3.4.5}$$

$$P_{w,d}^{(K)}(m) = \frac{2\sigma_d^2}{M}\sum_{l=0}^{K-1}\sum_{r=0}^{K-1}\frac{\mathrm{Re}\{\mathbf{K}_l\mathbf{K}_r^*\}_{m,m}}{M^{l+r}\big|\{\mathbf{\Lambda}_{H^{(0)}}\}_{m,m}\big|^2}\sum_{n=1}^{M}\{\mathbf{r}_{l,r}\}_n, \tag{3.4.6}$$

where we have introduced the following quantities:

- let $\mathbf{x}$ and $\mathbf{y}$ be any two vectors of proper length and build $\mathcal{R}(\mathbf{x},\mathbf{y})$ and $S(\mathbf{x},\mathbf{y})$ as it is done in (3.4.3) for p_N and q_N. Then, $\mathcal{X}_{RR}^{(K)} = \mathcal{R}\Big(p_N, q_N^{(K)}\Big)\mathcal{R}^T\Big(p_N, q_N^{(K)}\Big)$ and $\mathcal{X}_{SS}^{(K)} = S\Big(p_N, q_N^{(K)}\Big)S^T\Big(p_N, q_N^{(K)}\Big)$, with $q_N^{(l)}$ the l-th derivative of the pulse q_N;
- the diagonal matrices $\mathbf{\Lambda}_{H^{(r)}}$ are built from the equivalent channel $h_{eq}[l]$ according to $\big\{\mathbf{\Lambda}_{H^{(r)}}\big\}_{m,m} = \sum_{l=1}^{L_h}(-j(l-1))^r h_{eq}[l]e^{-j\frac{2\pi}{M}(m-1)(l-1)}$;
- the diagonal matrices $\mathbf{K}_l$ are built recursively, starting from $\mathbf{K}_0 = \mathbf{I}_M$, as $\mathbf{K}_l = -\mathbf{\Lambda}_{H^{(0)}}^{-1}\sum_{m=0}^{l-1}\frac{(-j)^{l-m}}{(l-m)!}\mathbf{\Lambda}_{H^{(l-m)}}\mathbf{K}_m$;
- the matrices $\mathbf{U}^{\pm} = \mathbf{I}_2 \otimes \big(\mathbf{I}_{M/2} \pm \mathbf{J}_{M/2}\big)$;
- and the vector $\mathbf{r}_{l,r} = \Big\{\mathcal{R}\Big(\tilde{q}_N^{(l)}, q_N^{(r)}\Big)\Big\}_{:,\kappa}$, that is the κ-th column of $\mathcal{R}\Big(\tilde{q}_N^{(l)}, q_N^{(r)}\Big)$, with $\tilde{q}_N[n] = q_N[N-n+1]$.

To complete the analysis of the relay channel, we still need to characterize the effect of the uplink noise on the received signal quality. Since such a noise is independent from the data signal and from the downlink noise, it is straightforward to see that the SNDR at the m-th subcarrier presents a third term at the denominator, namely

$$\mathrm{SNDR}_K(m) = \frac{P_{tx}}{P_e^{(K)}(m) + P_{w,d}^{(K)}(m) + P_{w,u}^{(K)}(m)}. \tag{3.4.7}$$

The power $P_{w,u}^{(K)}(m)$ of the uplink noise at the output of the equalizer has an expression that is slightly more complex than the one of $P_{w,d}^{(K)}(m)$, since it has to take into account the effect of the downlink channel, which filters and colours the i.i.d. noise samples collected by the relay. More specifically, let $\mathbf{\Theta}_M = \mathrm{diag}_{m=1,\dots,M}\left\{e^{-j\frac{2\pi}{M}(m-1)}\right\}$ and $\mathbf{r}_{l,r}^{s,t}$ be the $(\kappa+1)$-th column of $\mathcal{R}\left(\tilde{q}_N^{(l)}(s), q_N^{(r)}(t)\right)$, with $q_N(s)[n] = q_N[n-s+1]$ a delayed version of $q_N[n]$ and, as before, $q_N^{(l)}(s)$ its l-th derivative, whereas $\tilde{q}_N^{(l)}(s)$ indicates that time has been reversed. Then, the uplink noise power can be written as

$$P_{w,u}^{(K)}(m) = \frac{2A\sigma_u^2}{M}\sum_{l,r=0}^{K-1}\sum_{s,t=1}^{L_d}\frac{\mathrm{Re}\{h_d[s]h_d^*[t]\mathbf{K}_l\mathbf{\Theta}_M^{s-1}(\mathbf{K}_r\mathbf{\Theta}_M^{t-1})^*\}_{m,m}}{M^{l+r}\left|\{\mathbf{\Lambda}_{H^{(0)}}\}_{m,m}\right|^2}\sum_{n=1}^{M}\left\{\mathbf{r}_{l,r}^{s,t}\right\}_n.$$

The proof follows similar steps to those of (3.4.5) and (3.4.6) in [5], thus we report here only the most significant ones. To start with, the contribution of the uplink noise at the output of the equalizer can be written as $\mathbf{W}_u = \mathbf{W}_{u,\mathrm{even}} \otimes [1,0] + \mathbf{W}_{u,\mathrm{odd}} \otimes [0,1]$, where

$$\mathbf{W}_{u,*} = \sqrt{2\mathrm{A}}\sum_{l=0}^{K-1}\sum_{s=1}^{L_d}\frac{h_d[s]}{M^l}\mathbf{\Lambda}_{H^{(0)}}^{-1}\mathbf{K}_l\mathbf{\Theta}_M^{s-1}\mathbf{\Phi}\mathbf{F}_M^H\left(\mathbf{N}_{u,*} \circledast \left(\mathbf{J}_M\mathbf{Q}^{(l)}(s)\right)\right).$$

The $M \times (N_s+\kappa)$ matrices $\mathbf{N}_{u,*}, * \in \{\mathrm{even},\mathrm{odd}\}$, are filled with the elements of $\mathbf{n}_u = \left[\mathbf{n}_{u,0}^T\ \mathbf{n}_{u,1}^T \cdots\ \mathbf{n}_{u,2(N_s+\kappa)}^T\right]^T$ according to

$$\mathbf{N}_{u,\mathrm{even}} = \begin{bmatrix}\mathbf{n}_{u,0} & \mathbf{n}_{u,2} & \cdots & \mathbf{n}_{u,2(N_s+\kappa-1)}\\ \mathbf{n}_{u,1} & \mathbf{n}_{u,3} & \cdots & \mathbf{n}_{u,2(N_s+\kappa)-1}\end{bmatrix}$$

and

$$\mathbf{N}_{u,\mathrm{odd}} = \begin{bmatrix}\mathbf{n}_{u,1} & \mathbf{n}_{u,3} & \cdots & \mathbf{n}_{u,2(N_s+\kappa)-1}\\ \mathbf{n}_{u,2} & \mathbf{n}_{u,4} & \cdots & \mathbf{n}_{u,2(N_s+\kappa)}\end{bmatrix},$$

respectively. Now, naming $\mathbf{w}_{u,*}(r)$ the r-th column of $\mathbf{W}_{u,*}$, the uplink noise vector component corresponding to the r-th multicarrier symbol after destaggering can be written as $\boldsymbol{\omega}_r = \mathrm{Re}\{\mathbf{w}_{u,\mathrm{odd}}(r)\} + j\mathrm{Im}\{\mathbf{w}_{u,\mathrm{even}}(r+1)\}$. After some algebra, the covariance matrix of $\boldsymbol{\omega}_r$ can be shown to be

$$\mathbf{C}_u = A\sigma_u^2\sum_{l,r=0}^{K-1}\sum_{s,t=1}^{L_d}\frac{1}{M^{l+r}}\left[\mathrm{Re}\left\{h_d[s]\mathbf{\Lambda}_{H^{(0)}}^{-1}\mathbf{K}_l\mathbf{\Theta}_M^{s-1}\right\}\quad \mathrm{Im}\left\{h_d[s]\mathbf{\Lambda}_{H^{(0)}}^{-1}\mathbf{K}_l\mathbf{\Theta}_M^{s-1}\right\}\right]$$
$$\times\begin{bmatrix}\mathbf{D}_{l,r}^{s,t} & -j\widetilde{\mathbf{D}}_{l,r}^{s,t}\\ j\widetilde{\mathbf{D}}_{l,r}^{s,t} & \mathbf{D}_{l,r}^{s,t}\end{bmatrix}\begin{bmatrix}\mathrm{Re}\left\{h_d[t]\mathbf{\Lambda}_{H^{(0)}}^{-1}\mathbf{K}_r\mathbf{\Theta}_M^{t-1}\right\}\\ \mathrm{Im}\left\{h_d[t]\mathbf{\Lambda}_{H^{(0)}}^{-1}\mathbf{K}_r\mathbf{\Theta}_M^{t-1}\right\}\end{bmatrix},$$

where

$$\mathbf{D}_{l,r}^{s,t} = \mathbf{\Phi}\mathbf{F}_M^H\left[\mathrm{diag}\left\{\mathbf{U}^+\mathbf{r}_{l,r}^{s,t}\right\} + \mathrm{diag}\left\{\mathbf{U}^-\mathbf{s}_{l,r}^{s,t}\right\}\left(\mathbf{J}_2 \otimes \mathbf{I}_{M/2}\right)\right]\mathbf{F}_M\mathbf{\Phi}^*,$$
$$\widetilde{\mathbf{D}}_{l,r}^{s,t} = \mathbf{\Phi}\mathbf{F}_M^H\left[\mathrm{diag}\left\{\mathbf{U}^-\mathbf{r}_{l,r}^{s,t}\right\} + \mathrm{diag}\left\{\mathbf{U}^+\mathbf{s}_{l,r}^{s,t}\right\}\left(\mathbf{J}_2 \otimes \mathbf{I}_{M/2}\right)\right]\mathbf{F}_M\mathbf{\Phi}^*,$$

with

$$\mathbf{s}_{l,r}^{s,t} = \begin{bmatrix} \left\{S\left(\tilde{q}_N^{(l)}(s), q_N^{(r)}(t)\right)\right\}_{1:M/2,\kappa} \\ \left\{S\left(\tilde{q}_N^{(l)}(s), q_N^{(r)}(t)\right)\right\}_{M/2+1:M,\kappa+1} \end{bmatrix}.$$

The power of the uplink noise component at the m-th subcarrier, that is $P_{w,u}^{(K)}(m)$, is hence the m-th diagonal element of $\mathbf{C}_u$.

3.4.2 Simulation settings

To assess the results presented above, we consider a system that is compliant with the directives of [6] (see Table 3-6 for a summary of the parameters). More specifically, we take $\mathrm{M} = 128$ subcarriers (for simplicity we assume that they are all active) separated by 15 kHz, so that the sampling frequency is 1.920 MHz. The chosen prototype pulse (at both the transmitter and the receiver side) is the one proposed by the PHYDYAS project [7], with overlapping factor $\kappa = 4$, depicted in Figure 3-36.

Frame structure	
Subcarriers number	128 subcarriers
Subcarrier spacing	15 kHz
FBMC filter	OFDM/OQAM PHYDYAS
Overlapping factor	4
Modulation and coding schemes	QPSK (4-QAM)
Propagation	
Path-loss model	$d^{-\alpha}$, where d stands for the distance and $\alpha \in [2,4]$ is the path-loss exponent
Fast fading channel models	ITU Extended Vehicular A (EVA)
Channel estimation	Ideal

Table 3-6: Summary of simulation parameters

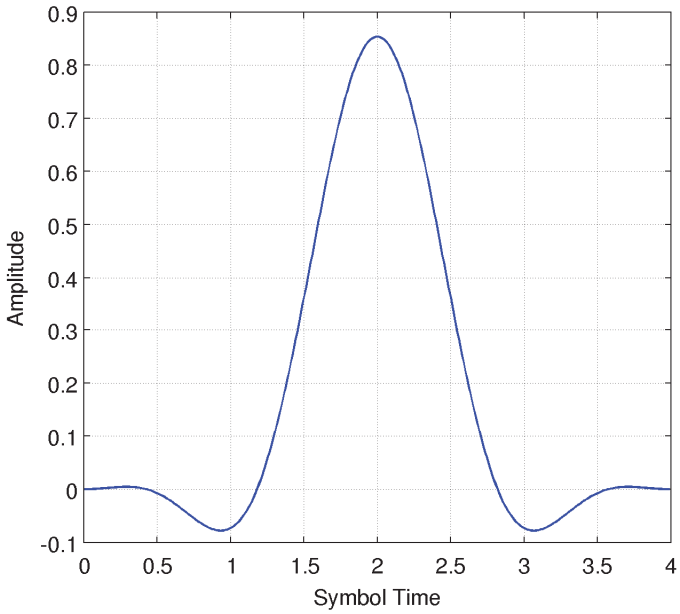

Figure 3-36: Prototype pulse used in all simulations.

The uplink (source to relay) and downlink (relay to destination) channels are generated according to the Extended Vehicular A (EVA) model [8]. In order to have a fair comparison between the AF relay channel and the direct link, we proceed as follows: the direct channel is obtained by taking the convolution of the uplink and downlink channels of the relay and then normalizing the path loss to 1. Moreover, the path losses of the uplink channel and of the downlink channel are given by $d^{-\alpha}$ and $(1-d)^{-\alpha}$, respectively, where $d \in (0,1)$ is the distance from the source to the relay and $\alpha \in [2,4]$ is the path-loss exponent. An example is depicted in Figure 3-37. Also, we assume that the additive white Gaussian noise on both channels has the same variance, namely $\sigma_u^2 = \sigma_d^2 = \sigma^2$.

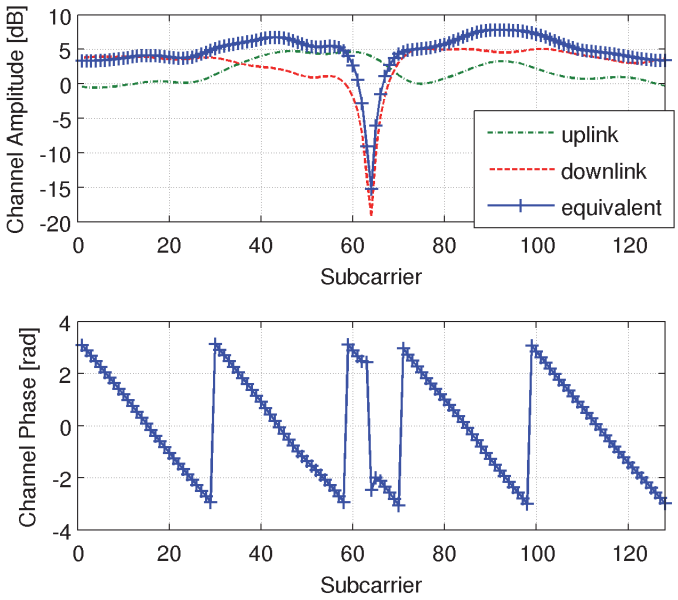

Figure 3-37: Normalized amplitude (unitary path loss) and phase (only for the equivalent channel) of the channels used to compare theoretical and simulated values of SNDR.

Finally, note that we focus on full-duplex relays that can transmit and receive at the same time. For simplicity, we assume an ideal/perfect electromagnetic separation between the receiving and the transmitting radio frequency chains at the relay, thus neglecting all self-interference issues. Naming P_s the total available power in the system, we fix $P_{tx} = P_r = P_s/2$. Conversely, we have $P_{tx} = P_s$ when the direct link with no relay is considered. Note that the same results apply to a half-duplex relay. In that case, however, both the source and the relay transmit during half of the time and, thus, $P_{tx} = P_r = P_s$ while the spectral efficiency of the link for the m-th subcarrier will be given by $I_{HD} = \frac{1}{2}\log(1 + \mathrm{SNDR}_K(m))$, as opposed to $I_{FD} = \log(1 + \mathrm{SNDR}_K(m))$, to account for time duplexing.

3.4.3 Simulation results

To start with, in Figure 3-38 and Figure 3-39, we compare the theoretical results of the previous section with empirical ones, obtained by averaging the measured SNDR of $N_s = 1000$ multicarrier 4-QAM symbols transmitted over the channel represented in Figure 3-37. The SNR, defined as the ratio between the total power P_s and the noise variance σ^2, is set to 20 dB and 40 dB, respectively. First of all, in Figure 3-39, we note that the difference between the empirical results and the theoretical ones increases as we increase the number of equalization stages K. This is due to the fact that the chosen pulse does not fulfil the perfect reconstruction constraints (and the assumptions on its derivatives required by [5]) perfectly and, thus, the expression (3.4.5) of the residual interference power is not exact anymore. This fact can only be noticed at high SNR (e.g., Figure 3-39, 40 dB), where the residual interference after equalization is the most significant source of error. On the other hand, at lower and more practical SNR values (e.g., Figure 3-38, 20 dB), the approximation is tighter, since the noise is the dominating impairment. As a final remark, note that at SNR = 20 dB, there is a noticeable gain of almost 5 dB when going from $K = 1$ to $K = 2$ equalization stages, while adding a third stage brings almost no benefits.

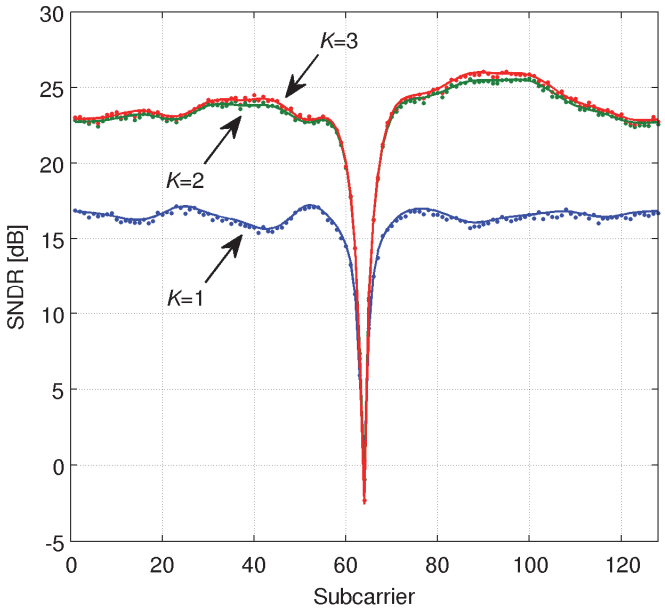

Figure 3-38: Comparison of simulated (dots) and theoretical (lines) values of SNDR at $\mathrm{SNR} = \frac{P_S}{\sigma^2} = 20\ \mathrm{dB}$ and for different numbers of equalization stages.

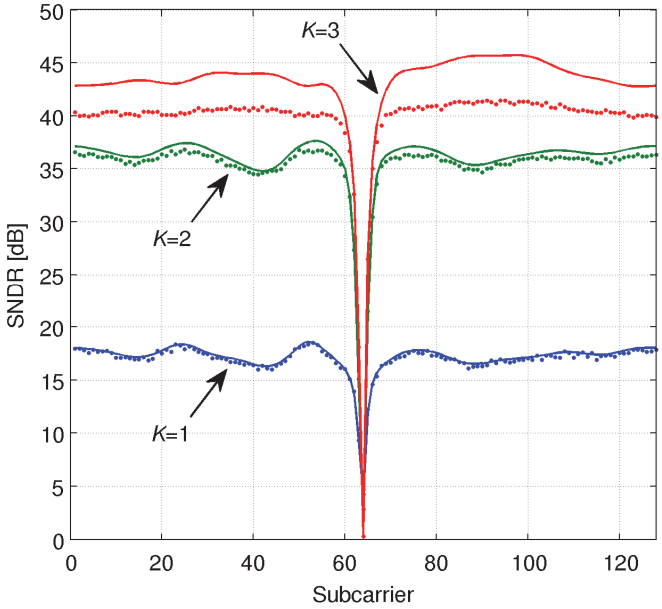

Figure 3-39: Comparison of simulated (dots) and theoretical (lines) values of SNDR at $\text{SNR} = \frac{P_s}{\sigma^2} = 40$ dB and for different numbers of equalization stages.

Having verified that the empirical results fit to the theoretical ones, we now use the latters to compare the AF relay channel to the direct point-to-point channel. More specifically, for a relay placed half way from the source to destination (that is $d = 0.5$), we investigate the mean spectral efficiency over the M subcarriers, namely

$$I = \frac{1}{M}\sum_{m=1}^{M} \log\big(1 + \text{SNDR}_K(m)\big), \tag{3.4.8}$$

where $\text{SNDR}_K(m)$ is given by (3.4.7). The curves in Figure 3-40 and Figure 3-41 are obtained averaging 500 different channel realizations. Apart from the spectral efficiency of the AF relay channel, the figures also report the results of the direct link and of two different flavours of DF relay. More specifically, the spectral efficiency of the direct link is computed as in (3.4.8) but using the SNDR expression for a point-to-point channel that can be found in [5] (basically, the SNDR is given by (3.4.4) with the path loss of the equivalent channel normalized to 1). On the other hand, a DF relay splits the channel into two separate hops and each one of them can be seen as a point-to-point link. The end-to-end spectral efficiency is hence the minimum between the spectral efficiency of the two hops. We can consider two different encoding schemes: the first (the DF-1 curve) scheme encodes each subcarrier stream independently of the others and, then, the spectral efficiency is computed as

$$I = \frac{1}{M}\sum_{m=1}^{M} \log\left(1 + \min\left\{\text{SNDR}_K^{(\text{up})}(m), \text{SNDR}_K^{(\text{down})}(m)\right\}\right).$$

The second scheme (the DF-2 curve), instead, corresponds to the case where all the subcarriers streams are encoded jointly to exploit the diversity offered by the FBMC modulation. The resulting spectral efficiency is

$$I = \frac{1}{M}\min\left\{\sum_{m=1}^{M}\log\left(1+\mathrm{SNDR}_K^{(\mathrm{up})}(m)\right), \sum_{m=1}^{M}\log\left(1+\mathrm{SNDR}_K^{(\mathrm{down})}(m)\right)\right\}.$$

Note that, according to the idea that the relay should be a simple device, the number of equalization stages at the DF relay has been fixed to one, as opposed to $K = 2$ for the equalizer at the destination.

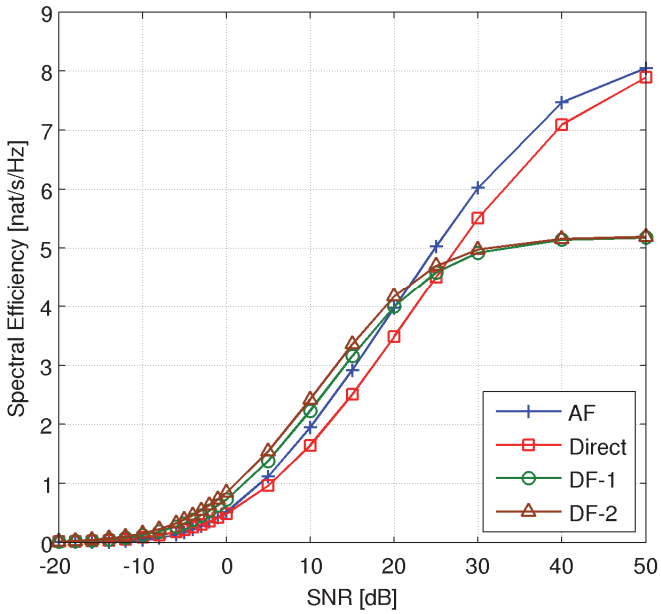

Figure 3-40: Mean per-subcarrier spectral efficiency as function of the SNR for $\alpha = 2.5$ and averaged over 500 channel realizations.

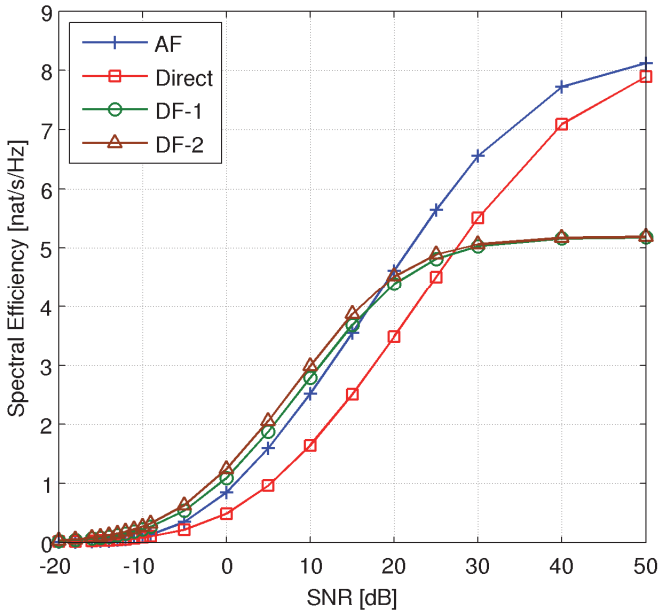

Figure 3-41: Mean per-subcarrier spectral efficiency as function of the SNR for $\alpha = 3.5$ and averaged over 500 channel realizations.

Both Figure 3-40 and Figure 3-41 show that the AF relay improves the spectral efficiency of the link for a wide range of SNR values. Moreover, the gain over the direct link increases with the path-loss exponent. For example, for a spectral efficiency of 4 nat/s/Hz, the gain is around 2 dB for $\alpha = 2.5$ (Figure 3-40) and around 5 dB for $\alpha = 3.5$ (Figure 3-41). A higher gain for larger path-loss exponents was expected, since the channel quality of short links—as compared to a long one—is higher when the path-loss exponent takes large values.

From the two figures one can also realize that the spectral efficiency of both the AF relay channel and the direct link saturate at a common value around 8 nat/s/Hz as the SNR grows large. The reason for this is that the residual interference power $P_e^{(K)}(m)$ in (3.4.5) does not depend on the SNR. Actually, the ratio $P_{tx}/P_e^{(K)}(m)$ only depends on the shape (and not on the amplitude) of the channel. Then, as the noise power tends to zero, the SNDR tends to $P_{tx}/P_e^{(K)}(m)$. In our simulations, this ratio takes the same value for both protocols, since we have built the direct link as a normalized version of the AF relay channel.

As for the DF relay, we see that its spectral efficiency saturates to a much lower value (just above 5 nat/s/Hz) at high SNR. One should recall that the number of equalization stages at the relay has been fixed to one, in order to contain complexity. This is indeed the bottleneck of the DF relay channel, as it can be readily guessed from Figure 3-38 and Figure 3-39. Conversely, for medium values of SNR, the per-subcarrier DF relay (DF-1) gains 1 dB over the AF relay as a result for not forwarding noise, while an extra decibel can be gained if all the subcarriers are jointly coded (DF-2).

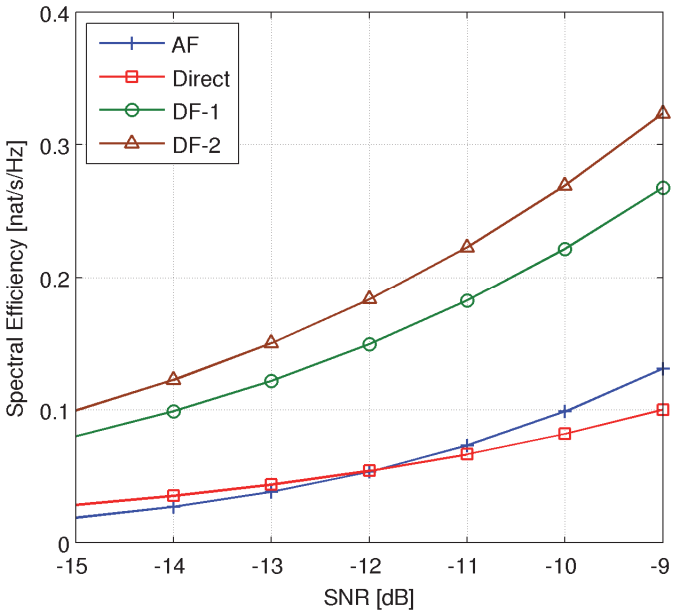

Figure 3-42: Mean per-subcarrier spectral efficiency as function of the SNR for $\alpha = 3.5$ and averaged over 500 channel realizations—zoomed in.

As a final remark, note that the spectral-efficiency curves of the AF relay channel and of the direct link cross at some low SNR value (see, for example, the zoomed in detail of Figure 3-41 in Figure 3-42). This does not happen by chance: it is not difficult to prove that, as the SNR goes to zero, the spectral efficiency of the AF relay channel is given by

$$I_{AF} = \frac{1}{4\eta_{w,d}^{(K)}(m)}\mathrm{SNR}^2 + o(\mathrm{SNR}^2),$$

where $\eta_{w,d}^{(K)}(m) = AP_{w,d}^{(K)}(m)/\sigma^2$, cf. (3.4.6). Conversely, for the direct link, it is

$$I_{DL} = \frac{1}{2\eta_{w,d}^{(K)}(m)}\mathrm{SNR} + o(\mathrm{SNR}),$$

that is, the spectral efficiency of the AF relay channel decays faster than the direct link one as the SNR tends to zero. Note, indeed, that the channel gain[4] appears at the denominator of (3.4.6). When the direct link is considered, the channel gain is one (at least its mean value) and, especially, does not depend on the SNR. Conversely, the equivalent channel of the AF relay scheme is $h_{eq}[l] = \sqrt{A}(h_u * h_d)[l]$ and, then, the channel gain decreases with the SNR, as suggested by (3.4.2), causing the noise power of the downlink channel to increase without bound.

3.4.4 Final remarks

This section has analysed the effect of an AF relay in a point-to-point FBMC link with a parallel multi-stage equalizer at the receiver. More specifically, a theoretical expression for the SNDR has been derived that takes into account the noise forwarded by the relay from the uplink channel to the destination. Simulation results show that reasonable gains can be obtained over a direct point-to-point connection, especially for SNR values in the range 0–30 dB and in lossy environments with a high path-loss exponent. As compared to a simple DF relay (with a classical one-tap equalizer per subcarrier), there are some marginal losses in the range 0–20 dB, while the AF relay becomes a better choice for higher values of SNR.

On the other hand, simulations and a low SNR approximation also revealed that an AF relay is not a good choice when the signal power is feeble. Indeed, the equalizer at the destination is based on channel inversion and the gain of the equivalent AF relay channel is close to zero, since it is proportional to the power transmitted by the relay. For this reason, it is our intention to further investigate into this problem and evaluate the performances of similar schemes employing different equalizers that do not need to invert the channel like, e.g., the MMSE-based equalizer.

3.5 CoF for FBMC: a scheme adaptation and comparison to AF and DF

Cooperative and relay aided communications have attracted a lot of attention due to their ability to provide high data rate, coverage and combat fading in wireless channels. The key idea is to enable users to cooperate, or use relays as intermediate nodes in transmitting their messages to the destination. This offers spatial diversity for applications in which temporal, spectral, and antenna diversity are limited by delay, bandwidth, and terminal size constraints. However, practical implementation of various relaying protocols remains a hard task due to the complexity and the substantial cost of the required coordination between users. Multiple Access Relay Channel (MARC) has emerged as a promising approach offering a compromise between the complexity and the advantages of cooperative systems. In this architecture, the users operate as in the context similar to a multi-access channel (non-cooperative). Thus, for some relaying protocols, users do not need to be aware of the

[4] The elements of the diagonal matrix $\mathbf{\Lambda}_{H^{(0)}}$ are the coefficients of a M-point FFT of the equivalent channel impulse response $h_{eq}[l]$.

existence of the relay. Consequently, all the cost and complexity introduced by exploiting cooperative diversity is placed at the relay and the destination.
In this section, we focus on Compute-and-Forward (CoF) protocol proposed by Nazer and Gastpar [66]. In this scheme, relay nodes decode finite-field linear combinations of transmitters' messages, instead of these latters. However due to the existence of intrinsic interference related to FBMC transmission, relay nodes become unable to compute interference-free linear combinations. Our aim in this work is to overcome this problem by adapting the CoF scheme to FBMC modulation. Moreover, a performance comparison is carried out between CoF and the most commonly used relay schemes: AF and DF, used in a similar MARC setup.

3.5.1 System Model

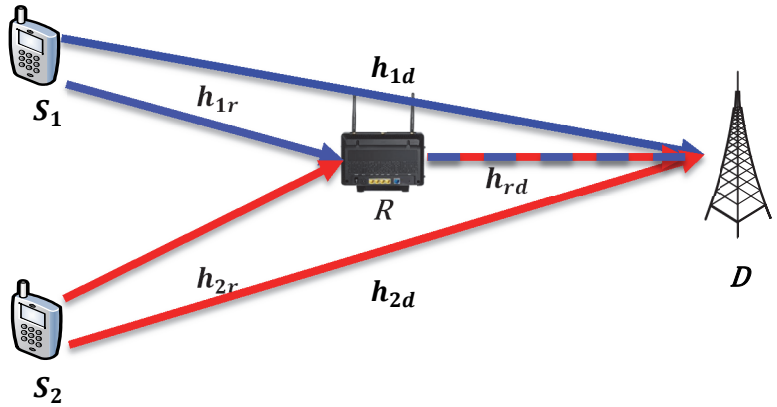

Figure 3-43: Uplink of PMR multi-access relay network

In PMR networks operating in 410-430 MHz or 450-470 MHz bands, implementing MIMO systems is very complicated due to various issues: additional space, weight and wind loading. In order to overcome this problem, multi-access relaying schemes provide a good alternative to conventional MIMO systems. In this section, we consider the uplink of a FBMC based PMR multi-access relay network that consists of two source transmitters $\mathbf{S_1}$ and $\mathbf{S_2}$, a half-duplex relay node **R** and a destination receiver **D**. All nodes are equipped with a single transmit/receive antenna. The key idea of the considered multi-access relaying schemes is that the base station **D** becomes, with the help of the relay, able to decode the signals coming from both source transmitters. However, it is worth mentioning that the following work is not limited to the scenario depicted in Figure 3-43 and can be applied to various scenarios.

The communication between the source transmitters and the destination is achieved with the help of the relay in two time slots. In the first one, both sources transmit their respective signals. Then, **R** implements its relaying protocol on the superposition of received signals and transmits the resulting signal to the destination **D** during the second time slot[5]. Three relaying protocols are considered: CoF which is extended to FBMC in this contribution, and then compared to the other two protocols AF, DF. Each protocol is described further in the following paragraphs.

[5] During the second period, both sources remain silent.

It is wise to mention that, in our model, the relay assigns equal power to help each user. Optimizing the relay's power allocation might further improve performance, but is not considered in this work.

All signals propagate through different multipath channels using a similar propagation model. Let $h_{s.r}$, $h_{s.d}$ and h_{rd} be the impulse responses of the channels of the links: **S**$_{.|\{.=1,2\}}$ →**R**, **S**$_{.|\{.=1,2\}}$ →**D**, and **R** → **D**, respectively. The equivalent sample-spaced impulse response of each channel can be expressed by,

$$h(t) = \sum_{i=0}^{L-1} h_i \delta\left(t - \frac{n_i}{N} T\right) \tag{3.5.1}$$

where, $n_0 < n_1 < \cdots < n_{L-1} < C$ and C is the maximum delay spread of the channel normalized by the sampling period T/N. T and N denote respectively the FBMC symbol duration and the total number of subcarriers in the system. The complex channel path gains h_i are assumed mutually independent where $\mathbb{E}[h_i h_i^*] = \gamma_i$ and $\mathbb{E}[h_i h_j^*] = 0$ when $i \neq j$. We further assume the power is normalized for each channel such that $\sum_{i=0}^{L-1} \gamma_i = 1$. We also assume that the propagation channels are stationary over one FBMC symbol.

3.5.2 Analysis of different Multi-access Relay strategies

In this section, we describe the different protocols used in our multi-access relay network. As mentioned previously, we consider: AF, DF and CoF protocols. Also, each node is equipped with a single antenna except the relay in the DF case which needs two receive antennas to decode the signals of both sources. Furthermore depending on the number of receive antennas at the destination, two cases are analyzed:

a. **Destination with a single receive antenna:** In this case, the existence of the relay is necessary. Otherwise, the destination becomes unable to decode both transmitter messages.
b. **Destination with two receive antennas:** The relay in this case is used to improve the system BER performance since it can be seen as an additional receive antenna.

For the sake of comparison between CoF and other protocols, we analyze in this section respectively, AF, DF and CoF schemes.

3.5.2.1 Multi-access amplify and forward (MAF)

In this protocol, the relay listens to both source transmitters during the first period. Then, it amplifies and forwards the composite signal resulting from the superposition of both received signals to the destination during the second period. It is obvious that in this protocol, the relay needs only a single transmit and receive antenna. Let $s_1(t)$ and $s_2(t)$ be the base-band continuous time model of FBMC transmit signals of **S$_1$** and **S$_2$** respectively. We write then [38],

$$\begin{aligned} s_1(t) &= \sqrt{P} \sum_{n=-\infty}^{+\infty} \sum_{m=0}^{N-1} a_{m,n}^{(1)} f(t - nT/2) e^{j\frac{2\pi}{T}mt} e^{j\varphi_{m,n}} \\ s_2(t) &= \sqrt{P} \sum_{n=-\infty}^{+\infty} \sum_{m=0}^{N-1} a_{m,n}^{(2)} f(t - nT/2) e^{j\frac{2\pi}{T}mt} e^{j\varphi_{m,n}} \end{aligned} \tag{3.5.2}$$

Where, $a_{m,n}^{(.)}$ are the transmitted real-valued PAM symbols with variance $\sigma_a^2 = \frac{1}{2}$ representing both in-phase and quadrature phase components of QAM symbols. Moreover, $f(t)$ is the real-valued pulse response of the prototype filter, P is the source transmit power and $\varphi_{m,n} = \frac{\pi}{2}(m+n) - \pi mn$ is introduced to ensure a phase shift of $\pm\frac{\pi}{2}$ between the adjacent transmitted PAM symbols along time and frequency [38], [59]. We can express the composite signal at the relay receiver with the following sum,

$$y_r(t) = s_1(t) \star h_{s1r}(t) + s_2(t) \star h_{s2r}(t) + n_r(t) \tag{3.5.3}$$

The operator $\star$ stands for the convolution product and $n_r(t)$ is the Additive White Gaussian Noise (AWGN) at the relay receiver with zero mean and variance σ_r^2. In order to calculate the amplification factor, we need to compute the power of $y_r(t)$. Since $s_1(t)$, $s_2(t)$ and $n_r(t)$ are uncorrelated,

$$\begin{aligned}\mathbb{E}[|y_r|^2] &= \mathbb{E}[y_r y_r^*] \\ &= \mathbb{E}\big[\big(s_1(t) \star h_{s1r}(t)\big)\big(s_1(t) \star h_{s1r}(t)\big)^*\big] \\ &\quad + \mathbb{E}\big[\big(s_2(t) \star h_{s2r}(t)\big)\big(s_2(t) \star h_{s2r}(t)\big)^*\big] + \mathbb{E}[n_r(t) n_r^*(t)]\end{aligned} \tag{3.5.4}$$

Furthermore, we can write,

$$\begin{aligned}&\mathbb{E}\big[\big(s_.(t) \star h_{s.r}(t)\big)\big(s_.(t) \star h_{s.r}(t)\big)^*\big] \\ &\quad = \mathbb{E}\left[\sum_{i=0}^{L-1} h_{s.r}(i) s_.\left(t - \frac{n_i}{N}T\right) \sum_{i=0}^{L-1} h_{s.r}^*(i) s_.^*\left(t - \frac{n_i}{N}T\right)\right], \quad .= 1,2\end{aligned} \tag{3.5.5}$$

It is also worth noticing that,

$$\mathbb{E}\left[s_.\left(t - \frac{n_i}{N}T\right) s_.^*\left(t - \frac{n_j}{N}T\right)\right] = \begin{cases} P, & i = j \\ 0, & i \neq j \end{cases} \tag{3.5.6}$$

Consequently, the power of $y_r(t)$ can be written as,

$$\mathbb{E}[|y_r|^2] = \sigma_r^2 + P \sum_{i=0}^{L-1} |h_{s1r}(i)|^2 + |h_{s2r}(i)|^2 \tag{3.5.7}$$

Assuming the knowledge of $\sum_{i=0}^{L-1} |h_{s1r}(i)|^2 + |h_{s2r}(i)|^2$ and σ_r^2 to the relay node, this latter can compute a scalar β_{AF} allowing the normalization of its transmit power:

$$\beta_{AF} = \sqrt{\frac{P}{\mathbb{E}[|y_r|^2]}} = \sqrt{\frac{P}{\sigma_r^2 + P\sum_{i=0}^{L-1} |h_{s1r}(i)|^2 + |h_{s2r}(i)|^2}} \tag{3.5.8}$$

Therefore, we express the signal at the output of the relay transmitter as,

$$s_r(t) = \beta_{AF} y_r(t) = \beta_{AF}(s_1(t) \star h_{s1r}(t) + s_2(t) \star h_{s2r}(t) + n_r(t)) \tag{3.5.9}$$

As mentioned previously, we distinguish two cases at the destination:

c. Destination with a single receive antenna

Let y_{sd} and y_{rd} be, respectively, the received signals from the sources $\mathbf{S}_{.|.=1,2}$ and the relay **R**. Then we write,

$$y_{sd}(t) = s_1(t) \star h_{s1d}(t) + s_2(t) \star h_{s2d}(t) + n_{d1}(t) \tag{3.5.10}$$

Substituting (3.5.1) and (3.5.2) in (3.5.10), we obtain

$$y_{sd}(t) = \sqrt{P}\sum_{.=1}^{2}\sum_{i=0}^{L-1} h_{s.d}(i)\delta\left(t - \frac{n_{i,s.d}}{N}T\right) \star \sum_{m=0}^{N-1}\sum_{n=-\infty}^{+\infty} a_{m,n}^{(.)} f\left(t - \frac{nT}{2}\right) e^{j\frac{2\pi}{T}mt} e^{j\varphi_{m,n}} + n_{d1}(t)$$

$$= \sqrt{P}\sum_{.=1}^{2}\sum_{m=0}^{N-1}\sum_{n=-\infty}^{+\infty} a_{m,n}^{(.)} e^{j\varphi_{m,n}} \sum_{i=0}^{L-1} h_{s.d}(i) f\left(t - \frac{nT}{2} - \frac{n_{i,s.d}}{N}T\right) e^{j\frac{2\pi}{T}m\left(t - \frac{n_{i,s.d}}{N}T\right)} + n_{d1}(t)$$

(3.5.11)

Without loss of generality, let KT be the duration of the prototype filter $f(t)$, where K is an integer greater than or equal to 1 (i.e. $K \geq 1$)[6]. Thus, we can say that the bandwidth occupied by the filter is smaller than the coherence bandwidth of the channel $B_c = 1/(2\tau_{ds})$ [60], [61]. Here, τ_{ds} denotes the maximum channel delay spread. We can also notice that $f(t - nT/2 - \tau)$ may have relatively slow variations when $\tau \in [0, \tau ds]$ [59], [62]. Indeed, compared to the coherence bandwidth B_c, the filter bandwidth is very small, which also means that the time variations of the prototype filter $f(t)$ are necessarily limited. Consequently, (3.5.11) becomes,

$$y_{sd}(t) = \sqrt{P}\sum_{.=1}^{2}\sum_{m=0}^{N-1}\sum_{n=-\infty}^{+\infty} a_{m,n}^{(.)} e^{j\varphi_{m,n}} f\left(t - \frac{nT}{2}\right) e^{j\frac{2\pi}{T}mt} \sum_{i=0}^{L-1} h_{s.d}(i) e^{j\frac{2\pi}{N}mn_{i,s.d}} + n_{d1}(t)$$

$$= \sqrt{P}\sum_{.=1}^{2}\sum_{m=0}^{N-1}\sum_{n=-\infty}^{+\infty} a_{m,n}^{(.)} e^{j\varphi_{m,n}} f\left(t - \frac{nT}{2}\right) e^{j\frac{2\pi}{T}mt} H_{s.d}(m) + n_{d1}(t) \quad (3.5.12)$$

where,

$$H_{s.d}(m) = \sum_{i=0}^{L-1} h_{s.d}(i) e^{j\frac{2\pi}{N}mn_{i,s.d}}$$

is the complex gain at subcarrier m of the channel between sources $\mathbf{S}_{.|.=1,2}$ and the destination. After FBMC demodulation of $y_{sd}(t)$, the m_0-th output of the destination receiver filter on the n_0-th signalling interval (i.e. $t = n_0 T/2$) reads,

$$y_{sd}(m_0, n_0) = \int_{-\infty}^{+\infty} y_{sd}(t) f\left(t - \frac{n_0 T}{2}\right) e^{-j\frac{2\pi}{T}m_0 t} e^{-j\varphi_{m_0,n_0}} dt \quad (3.5.13)$$

$$= \sqrt{P}\sum_{.=1}^{2}\sum_{m=0}^{N-1}\sum_{n=-\infty}^{+\infty} a_{m,n}^{(.)} e^{j(\varphi_{m,n} - \varphi_{m_0,n_0})} H_{s.d}(m) \times \int_{-\infty}^{+\infty} f\left(t - \frac{nT}{2}\right) f\left(t - \frac{n_0 T}{2}\right) e^{j\frac{2\pi}{T}(m-m_0)t} dt + n_{d1}(m_0, n_0)$$

where, $n_{d1}(m_0, n_0) = \int_{-\infty}^{+\infty} n_{d1}(t) f\left(t - \frac{n_0 T}{2}\right) e^{-j\frac{2\pi}{T}m_0 t} dt$. In FBMC, the prototype filter $f(t)$ is designed to be well-localized in time-frequency domain. Hence, one can see that there is a finite set $\Omega_{\Delta m, \Delta n}$ of positions (m, n) in the neighborhood of (m_0, n_0) where the

[6] K is usually called the overlapping factor of the prototype filter.

integral $\int_{-\infty}^{+\infty} f\left(t-\frac{nT}{2}\right) f\left(t-\frac{n_0T}{2}\right) e^{j\frac{2\pi}{T}(m-m_0)t} dt \neq 0$. Accordingly, $y_{sd}(m_0,n_0)$ can be rewritten in the following form,

$$y_{sd}(m_0,n_0) = \sqrt{P}\sum_{.=1}^{2}\left(a_{m_0,n_0}^{(.)} H_{s.d}(m_0) \int_{-\infty}^{+\infty} f^2\left(t-\frac{n_0T}{2}\right) dt \right. \tag{3.5.14}$$
$$+ \sum_{(m,n)\in\Omega_{\Delta m,\Delta n}} a_{m,n}^{(.)} e^{j(\varphi_{m,n}-\varphi_{m_0,n_0})} H_{s.d}(m)$$
$$\left. \times \int_{-\infty}^{+\infty} f\left(t-\frac{nT}{2}\right) f\left(t-\frac{n_0T}{2}\right) e^{j\frac{2\pi}{T}(m-m_0)t} dt \right) + n_{d1}(m_0,n_0)$$

It is worth to recall that the design of the prototype filter $f(t)$ must satisfy the following orthogonality condition,

$$\Re\left[\int_{-\infty}^{+\infty} f\left(t-\frac{nT}{2}\right) f\left(t-\frac{n_0T}{2}\right) e^{j\frac{2\pi}{T}(m-m_0)t} e^{j(\varphi_{m,n}-\varphi_{m_0,n_0})} dt \right] \tag{3.5.15}$$
$$= \delta_{n,n_0}\delta_{m,m_0}$$

Where $\delta_{n,n_0} = \begin{cases} 1, & n = n_0 \\ 0, & n \neq n_0 \end{cases}$ is the Kronecker delta. In other words, since $f(t)$ is real, (3.5.15) can be split into:

$$\int_{-\infty}^{+\infty} f^2\left(t-\frac{nT}{2}\right) dt = 1 \tag{3.5.16}$$

and

$$\sum_{(m,n)\in\Omega_{\Delta m,\Delta n}} a_{m,n}^{(.)} e^{j(\varphi_{m,n}-\varphi_{m_0,n_0})} \int_{-\infty}^{+\infty} f\left(t-\frac{nT}{2}\right) f\left(t-\frac{n_0T}{2}\right) e^{j\frac{2\pi}{T}(m-m_0)t} dt = j u_{m_0,n_0}^{(.)} \tag{3.5.17}$$

with $j u_{m_0,n_0}^{(.)}$ is a purely imaginary term related to the FBMC intrinsic interference. Assuming that $H_{s.d}(m) \simeq H_{s.d}(m_0)$ in the neighborhood $\Omega_{\Delta m,\Delta n}$, we can substitute (3.5.16) and (3.5.17) in (3.5.14) to obtain,

$$y_{sd}(m_0,n_0) = \sqrt{P}\sum_{.=1}^{2} H_{s.d}(m_0)\left(a_{m_0,n_0}^{(.)} + j u_{m_0,n_0}^{(.)}\right) + n_{d1}(m_0,n_0) \tag{3.5.18}$$

The received signal from the relay **R,** $y_{rd}(t)$ is given by,

$$y_{rd}(t) = s_r(t) \star h_{rd}(t) + n_{d2}(t) \tag{3.5.19}$$

Replacing $s_r(t)$ by its expression (3.5.9), y_{rd} becomes,

$$y_{rd}(t) = \beta_{AF}\left(\sum_{.=1}^{2} s_.(t) \star h_{s.r}(t) \star h_{rd}(t) + n_r(t) \star h_{rd}(t) \right) + n_{d2}(t) \tag{3.5.20}$$

Similarly to the changes performed on $y_{sd}(t)$, we can derive the (m_0, n_0)-th output of the destination receiver filter resulting from the FBMC demodulation of y_{rd}. We obtain,

$$y_{rd}(m_0,n_0) = \beta_{AF}\sqrt{P}\sum_{.=1}^{2} H_{rd}(m_0)H_{s.r}(m_0)\left(a^{(.)}_{m_0,n_0} + ju^{(.)}_{m_0,n_0}\right)$$
$$+\beta_{AF}H_{rd}(m_0)n_r(m_0,n_0) + n_{d2}(m_0,n_0) \quad (3.5.21)$$

where, $H_{rd}(m) = \sum_{i=0}^{L-1} h_{s.d}(i)e^{j\frac{2\pi}{N}mn_{i,rd}}$ and $H_{s.d}(m) = \sum_{i=0}^{L-1} h_{s.d}(i)e^{j\frac{2\pi}{N}mn_{i,s.d}}$ are the complex gains at subcarrier m of the channels between (**R**, **D)** and (**S**$_{.|.=1,2}$, **D**) , respectively. Here, the noise terms are given by $n_r(m_0,n_0) = \int_{-\infty}^{-\infty} n_r(t)f\left(t - \frac{n_0T}{2}\right)e^{-j\frac{2\pi}{T}m_0t}dt$ and $n_{d2}(m_0,n_0) = \int_{-\infty}^{-\infty} n_{d2}(t)f\left(t - \frac{n_0T}{2}\right)e^{-j\frac{2\pi}{T}m_0t}dt$.

In order to recover both streams $a^{(1)}_{m,n}$ and $a^{(2)}_{m,n}$, the destination **D** can apply linear equalization on each subcarrier like in FBMC based Spatial Multiplexing (SM) (2×2) MIMO systems [63]. To this end, we can write,

$$\mathbf{y_d}_{\,m_0,n_0} = \mathbf{H_{af}}_{\,m_0}\left(\mathbf{a}_{m_0,n_0} + \mathbf{u}_{m_0,n_0}\right) + \mathbf{n_d}_{m_0,n_0} \quad (3.5.22)$$

where,

- $\mathbf{y_d}_{\,m_0,n_0}$ is the (2×1) demodulated signal vector:
$$\mathbf{y_d}_{\,m_0,n_0} = [y_{sd}(m_0,n_0) \quad y_{rd}(m_0,n_0)]^T ,$$
- $\mathbf{H_{af}}_{\,m_0}$is the (2×2) channel matrix:
$$\mathbf{H_{af}}_{\,m_0} = \begin{bmatrix} H_{s1d}(m_0) & H_{s2d}(m_0) \\ \beta_{AF}H_{rd}(m_0)H_{s1r}(m_0) & \beta_{AF}H_{rd}(m_0)H_{s2r}(m_0) \end{bmatrix} \quad (3.5.23)$$
- $\mathbf{a}_{m_0,n_0}$ is the (2×1) data vector: $\mathbf{a}_{m_0,n_0} = \sqrt{P}\left[a^{(1)}_{m_0,n_0} \quad a^{(2)}_{m_0,n_0}\right]^T$,
- $\mathbf{u}_{m_0,n_0}$ is the (2×1) interference vector: $\mathbf{u}_{m_0,n_0} = \sqrt{P}\left[u^{(1)}_{m_0,n_0} \quad u^{(2)}_{m_0,n_0}\right]^T$
- $\mathbf{n_d}_{m_0,n_0}$ is the (2×1) noise vector:
$$\mathbf{n_d}_{m_0,n_0} = [n_{d1}(m_0,n_0) \quad n_{d2}(m_0,n_0) + \beta_{AF}H_{rd}(m_0)n_r(m_0,n_0)]^T$$

Accordingly, we can compute the equalization matrix $\mathbf{W^H}$ following both Zero Forcing (ZF) and Minimum Mean Square Error (MMSE) criteria as

$$\mathbf{W}^{\mathbf{H}}_{m0,\mathrm{zf}} = \left(\mathbf{H}^{\mathbf{H}}_{\mathbf{af}\,m_0}\mathbf{H_{af}}_{\,m_0}\right)^{-1}\mathbf{H}^{\mathbf{H}}_{\mathbf{af}\,m_0}$$
$$\mathbf{W}_{m0,\mathrm{mmse}} = \left(\mathbf{H_{af}}_{\,m_0}\mathbf{H}^{\mathbf{H}}_{\mathbf{af}\,m_0} + \mathbf{D_{af}}_{\,m_0}\right)^{-1}\mathbf{H_{af}}_{\,m_0} \quad (3.5.24)$$

where, $\mathbf{D_{af}}_{\,m_0}$is a diagonal matrix given by:

$$\mathbf{D_{af}}_{\,m_0} = \begin{bmatrix} \frac{\sigma^2_{nd}}{P} & 0 \\ 0 & \frac{\sigma^2_{nd} + \beta^2_{AF}|H_{rd}(m_0)|^2\sigma^2_{nr}}{P} \end{bmatrix}$$

The recovered data vector $\hat{\mathbf{a}}_{\,m_0,n_0}$ is computed by taking the real part of the equalized signal

$$\hat{\mathbf{a}}_{\,m_0,n_0} = \Re\left[\mathbf{W}^{\mathbf{H}}_{m0,.}\mathbf{y_d}_{\,m_0,n_0}\right]. \quad (3.5.25)$$

d. Destination with two receive antennas

In this case, the destination obtains two versions of both signals y_{sd} and y_{rd}. Let (y_{sd1}, y_{rd1}) and (y_{sd2}, y_{rd2}) be the signals received on antenna 1 and 2, respectively.

$$
\begin{aligned}
y_{sd1}(t) &= \sum_{.=1}^{2} s_{.}(t) \star h_{s.d1}(t) + n_{d1}(t) \\
y_{sd2}(t) &= \sum_{.=1}^{2} s_{.}(t) \star h_{s.d2}(t) + n_{d2}(t) \\
y_{rd1}(t) &= \beta_{AF}\left(\sum_{.=1}^{2} s_{.}(t) \star h_{s.r}(t) \star h_{rd1}(t) + n_r(t) \star h_{rd1}(t)\right) + n_{d3}(t) \\
y_{rd2}(t) &= \beta_{AF}\left(\sum_{.=1}^{2} s_{.}(t) \star h_{s.r}(t) \star h_{rd2}(t) + n_r(t) \star h_{rd2}(t)\right) + n_{d4}(t)
\end{aligned}
\tag{3.5.26}
$$

Doing the same derivation as in the single antenna case, we obtain a system equivalent to a FBMC based spatial multiplexing (4×2)MIMO system. Equation (3.5.22) remains the same but with the following modifications,

- The demodulated signal becomes a (4×1) vector:
$$\mathbf{y_d}_{m_0,n_0} = [y_{sd1}(m_0,n_0) \quad y_{sd2}(m_0,n_0) \quad y_{rd1}(m_0,n_0) \quad y_{rd2}(m_0,n_0)]^T ,$$
- $\mathbf{H_{af}}_{m_0}$ is the (4×2) channel matrix:

$$\mathbf{H_{af}}_{m_0} = \begin{bmatrix} H_{s1d1}(m_0) & H_{s1d2}(m_0) & \beta_{AF}H_{rd1}(m_0)H_{s1r}(m_0) & \beta_{AF}H_{rd2}(m_0)H_{s1r}(m_0) \\ H_{s2d1}(m_0) & H_{s2d2}(m_0) & \beta_{AF}H_{rd1}(m_0)H_{s2r}(m_0) & \beta_{AF}H_{rd2}(m_0)H_{s2r}(m_0) \end{bmatrix}^T \tag{3.5.27}$$

- $\mathbf{n_d}_{m_0,n_0}$ is the (4×1) noise vector:
$$\mathbf{n_d}_{m_0,n_0} = [n_{d1}(m_0,n_0) \quad n_{d2}(m_0,n_0) \quad n'_{d3}(m_0,n_0) \quad n'_{d4}(m_0,n_0)]$$
with
$$n'_{d3}(m_0,n_0) = n_{d3}(m_0,n_0) + \beta_{AF}H_{rd1}(m_0)n_r(m_0,n_0)$$
$$n'_{d4}(m_0,n_0) = n_{d4}(m_0,n_0) + \beta_{AF}H_{rd2}(m_0)n_r(m_0,n_0)$$
- The data vector $\mathbf{a}_{m_0,n_0}$ and the interference one $\mathbf{u}_{m_0,n_0}$ remain the same.

In the same way, ZF and MMSE equalizers can be computed as in (3.5.24). However in this case, it is worth noticing that the autocorrelation matrix of the noise vector becomes,

$$\mathbb{E}\left[\mathbf{n_d}_{m_0}\mathbf{n_d}^{\mathbf{H}}_{m_0}\right] = \begin{bmatrix} \sigma_d^2\mathbf{I_2} & \mathbf{0_{2\times 2}} \\ \mathbf{0_{2\times 2}} & \mathbf{R} \end{bmatrix} \tag{3.5.28}$$

where

$$\mathbf{R} = \begin{bmatrix} \sigma_d^2 + \beta_{AF}^2|H_{rd1}(m_0)|^2\sigma_r^2 & \beta_{AF}H_{rd1}(m_0)H_{rd2}^*(m_0)\sigma_r^2 \\ \beta_{AF}H_{rd1}(m_0)H_{rd2}^*(m_0)\sigma_r^2 & \sigma_d^2 + \beta_{AF}^2|H_{rd2}(m_0)|^2\sigma_r^2 \end{bmatrix}$$

3.5.2.2 Multi-access decode and forward (MDF)

We consider in this case, an FBMC based static Multi-access Decode and Forward (MDF). In this relaying scheme, the relay listens during the first time slot, and jointly decodes the signals from both source transmitters. This protocol is called “static” because the relay always tries to decode the received signal even for low SNR, which may propagate the errors and lead to bad performance in that case. During the second time slot, the relay transmits the superposition of the FBMC modulation of the decoded signals. The

transmission of the new modulated signals can be performed using a common transmit antenna or each source signal is transmitted using an individual antenna. It is worth noting that decoding at the relay requires two receive antennas.

In this section, H_{sirj} and H_{sidj} stand for the FFT transforms of the channels between: (**S**$_{i|i=1,2,}$j-th **R** Rx antenna) and (**S**$_{i|i=1,2,}$j-th **D** Rx antenna[7]), respectively. Also, $y_{srj}(m_0, n_0)$, $y_{sdj}(m_0, n_0)$ and $y_{ridj}(m_0, n_0)$ denote, respectively, the demodulated signals of the following links: (both sources, j-th **R** Rx antenna), (both sources, j-th **D** Rx antenna[7]) and (i-th **R** Tx Antenna[8], j-th **D** Rx antenna[7]). Now, the processing at the relay receiver is the same as an FBMC SM (2×2) MIMO one. Hence, after FBMC demodulation, we have

$$\mathbf{y_r}_{\,m_0,n_0} = \mathbf{H_{sr}}_{\,m_0}\left(\mathbf{a}_{m_0,n_0} + \mathbf{u}_{m_0,n_0}\right) + \mathbf{n_r}_{m_0,n_0} \tag{3.5.29}$$

Where,

- $\mathbf{y_r}_{\,m_0,n_0}$ is the (2×1) demodulated signal vector at the relay:
$$\mathbf{y_r}_{\,m_0,n_0} = [y_{sr1}(m_0, n_0) \quad y_{sr2}(m_0, n_0)]^T ,$$
- $\mathbf{H_{sr}}_{\,m_0}$is the (2×2) channel matrix:
$$\mathbf{H_{sr}}_{\,m_0} = \begin{bmatrix} H_{s1r1}(m_0) & H_{s2r1}(m_0) \\ H_{s1r2}(m_0) & H_{s1r2}(m_0) \end{bmatrix} \tag{3.5.30}$$
- $\mathbf{n}_{m_0,n_0}$ is the (2×1) noise vector:
$$\mathbf{n_r}_{m_0,n_0} = [n_{r1}(m_0, n_0) \quad n_{r2}(m_0, n_0)]^T$$
- The data vector $\mathbf{a}_{m_0,n_0}$and the interference one $\mathbf{u}_{m_0,n_0}$remain the same.

After ZF or MMSE equalization, the recovered data vector $\tilde{\mathbf{a}}_{\,m_0,n_0}$ is computed by taking the real part of the equalized signal

$$\tilde{\mathbf{a}}_{\,m_0,n_0} = \Re\left[\mathbf{W}^{\mathbf{H}}_{m0,.}\mathbf{y_r}_{\,m_0,n_0}\right]. \tag{3.5.31}$$

In order to normalize the transmit power at the relay (i.e. it is equal to P), the recovered data vector $\tilde{\mathbf{a}}_{\,m_0,n_0}$ is divided by $\sqrt{2}$.

As aforementioned, in the second time slot, the relay transmits the FBMC modulation of the normalized vector $\tilde{\mathbf{a}}_{\,m_0,n_0}$ by:

- Sending the sum of both streams $\sqrt{P/2}\left(\tilde{a}^{(1)}_{m_0,n_0} + \tilde{a}^{(2)}_{m_0,n_0}\right)$ on a single common antenna
- Or sending each stream $\sqrt{P/2}\,\tilde{a}^{(.)}_{m_0,n_0}$ on an individual antenna.

Similarly to MAF case, we distinguish two cases depending on the number of receive antennas at the destination.

a. Destination with a single receive antenna

Assuming a perfect data recovery at the relay ($\tilde{\mathbf{a}}_{\,m_0,n_0} = \mathbf{a}_{\,m_0,n_0}$), the destination **D** obtains after demodulation of the received signals from the direct link and the relayed one,

$$\mathbf{y_d}_{\,m_0,n_0} = \mathbf{H_{df}}_{\,m_0}\left(\mathbf{a}_{m_0,n_0} + \mathbf{u}_{m_0,n_0}\right) + \mathbf{n_d}_{m_0,n_0} \tag{3.5.32}$$

where, the channel matrix $\mathbf{H_{df}}_{\,m_0}$ is given by (3.5.33) in case of a single Tx relay antenna and by (3.5.34) in case of two Tx relay antennas,

[7] The index j is omitted when **D** has a single Rx antenna.

[8] Here, the index i is omitted when **R** is equipped with a single Tx antenna.

$$\mathbf{H}_{\mathbf{df}\,m_0} = \begin{bmatrix} H_{s1d}(m_0) & H_{s2d}(m_0) \\ H_{rd}(m_0)/\sqrt{2} & H_{rd}(m_0)/\sqrt{2} \end{bmatrix} \quad (3.5.33)$$

$$\mathbf{H}_{\mathbf{df}\,m_0} = \begin{bmatrix} H_{s1d}(m_0) & H_{s2d}(m_0) \\ H_{r1d}(m_0)/\sqrt{2} & H_{r2d}(m_0)/\sqrt{2} \end{bmatrix} \quad (3.5.34)$$

The autocorrelation matrix of the noise vector in this case is given by, $\mathbb{E}\left[\mathbf{n}_{\mathbf{d}_{m_0}}\mathbf{n}_{\mathbf{d}_{m_0}}^{\mathbf{H}}\right] = \sigma_d^2\mathbf{I_2}$

b. **Destination with two receive antennas**

As in MAF protocol, the destination receiver performs a processing similar to FBMC based spatial multiplexing (4×2) MIMO one. It is worth to highlight that this is valid under the assumption that we have a perfect data recovery at the relay Rx. Thus, after FBMC demodulation, we obtain a (4×1) vector,

$$\mathbf{y}_{\mathbf{d}\,m_0,n_0} = \mathbf{H}_{\mathbf{df}\,m_0}\left(\mathbf{a}_{m_0,n_0} + \mathbf{u}_{m_0,n_0}\right) + \mathbf{n}_{\mathbf{d}_{m_0,n_0}}$$

with,

$$\mathbf{H}_{\mathbf{d}\,m_0} = \begin{bmatrix} H_{s1d1}(m_0) & H_{s1d2}(m_0) & H_{rd1}(m_0) & H_{rd2}(m_0) \\ H_{s2d1}(m_0) & H_{s2d2}(m_0) & H_{rd1}(m_0) & H_{rd2}(m_0) \end{bmatrix}^T \quad (3.5.35)$$

in the case of a single **R** Tx antenna, and

$$\mathbf{H}_{\mathbf{d}\,m_0} = \begin{bmatrix} H_{s1d1}(m_0) & H_{s1d2}(m_0) & H_{r1d1}(m_0) & H_{r1d2}(m_0) \\ H_{s2d1}(m_0) & H_{s2d2}(m_0) & H_{r2d1}(m_0) & H_{r2d2}(m_0) \end{bmatrix}^T \quad (3.5.36)$$

when we have 2 Tx antennas at **R**. The autocorrelation matrix of the noise vector in this case is given by, $\mathbb{E}\left[\mathbf{n}_{\mathbf{d}_{m_0}}\mathbf{n}_{\mathbf{d}_{m_0}}^{\mathbf{H}}\right] = \sigma_d^2\mathbf{I_4}$

3.5.2.3 Multi-access compute and forward (MCoF)

The idea of this protocol comes from linear network coding, where each intermediate node sends out a function of the packets that it receives [64], [65]. Nazer and Gastpar were the first who proposed a scheme called “Compute-and-forward” (CoF) in which intermediate nodes decode finite-field linear combinations of transmitters’ messages, instead of these latters [66]. In this configuration, a receiver is able to recover the original messages using a sufficient amount of linear combinations of these messages. It should be mentioned that the coefficients of these combinations must be integer-valued. The authors in [67], have proposed CoF as a relaying protocol for multi-access relay networks with the optimization of the integer coefficients in order to maximize the achievable symmetric rate. It is worth noticing that in these references, the channel gains are assumed to be real-valued.

To the best of our knowledge, the usability of CoF protocol with multicarrier techniques has not yet been addressed in the literature. Our aim in this work is to investigate the possibility of using CoF protocol in a FBMC based multi-access relay network.

In a such protocol, the relay should compute a linear combination relating both components of the input data vector $\mathbf{a}_{m_0,n_0}$. As given by (3.5.3), the composite signal received at the relay is:

$$y_r(t) = s_1(t) \star h_{s1r}(t) + s_2(t) \star h_{s2r}(t) + n_r(t)$$

In order to compute this linear combination, an FBMC demodulation should be performed on $y_r(t)$. Accordingly, we obtain,

$$y_{sr}(m_0,n_0)=\sqrt{P}\sum_{.=1}^{2}H_{s.r}(m_0)\left(a^{(.)}_{m_0,n_0}+ju^{(.)}_{m_0,n_0}\right)+n_r(m_0,n_0) \quad (3.5.37)$$

Since the sources are not situated at the same position, the complex channel gains $H_{s1r}(m_0)$ and $H_{s2r}(m_0)$ are necessarily uncorrelated. Therefore, the relay is unable to eliminate the intrinsic interference terms $jH_{s1r}(m_0)u^{(1)}_{m_0,n_0}$ and $jH_{s2r}(m_0)u^{(2)}_{m_0,n_0}$, since they are not aligned (i.e. both terms have different phase angles). Such a problem will make impossible the computation of a linear combination relating both data streams. In order to overcome this problem, we propose a precoding of both input data signals allowing the alignment of the intrinsic interference terms at the relay receiver. Such a precoding consists in multiplying the input data $a^{(1)}_{m_0,n_0}$ and $a^{(2)}_{m_0,n_0}$ by $H^*_{s1r}(m_0)/|H_{s1r}(m_0)|$ (i.e. $e^{-j\varphi_{H_{s1r}(m_0)}}$) and $H^*_{s2r}(m_0)/|H_{s2r}(m_0)|$ (i.e. $e^{-j\varphi_{H_{s2r}(m_0)}}$), respectively. Consequently, the new input data becomes,

$$\mathbf{b}_{m_0,n_0}=\sqrt{P}\left[b^{(1)}_{m_0,n_0}\quad b^{(2)}_{m_0,n_0}\right]^T=\sqrt{P}\left[\frac{H^*_{s1r}(m_0)}{|H_{s1r}(m_0)|}a^{(1)}_{m_0,n_0}\quad \frac{H^*_{s2r}(m_0)}{|H_{s2r}(m_0)|}a^{(2)}_{m_0,n_0}\right]^T$$

The FBMC transmit signals of **S_1** and **S_2** become,

$$\begin{aligned}s_1(t)&=\sqrt{P}\sum_{n=-\infty}^{+\infty}\sum_{m=0}^{N-1}b^{(1)}_{m,n}f(t-nT/2)e^{j\frac{2\pi}{T}mt}e^{j\varphi_{m,n}}\\ s_2(t)&=\sqrt{P}\sum_{n=-\infty}^{+\infty}\sum_{m=0}^{N-1}b^{(2)}_{m,n}f(t-nT/2)e^{j\frac{2\pi}{T}mt}e^{j\varphi_{m,n}}\end{aligned} \quad (3.5.38)$$

It is worth noticing that new input data are no longer real-valued. Therefore, in order to preserve the real orthogonality condition of FBMC systems given in (3.5.15), the proposed precoding or the new complex input data must lead to intrinsic interference terms[9] $ju'^{(1)}_{m_0,n_0}$ and $ju'^{(2)}_{m_0,n_0}$ orthogonal to $b^{(1)}_{m,n}$ and $b^{(2)}_{m,n}$, respectively. In other words,

$$\varphi_{b^{(i)}_{m,n}}=\varphi_{u'^{(i)}_{m_0,n_0}},i=1,2 \quad (3.5.39)$$

Similarly to (3.5.17), we can write,

$$\begin{aligned}ju'^{(.)}_{m_0,n_0}&=\sum_{(m,n)\in\Omega_{\Delta m,\Delta n}}b^{(.)}_{m,n}e^{j(\varphi_{m,n}-\varphi_{m_0,n_0})}\int_{-\infty}^{+\infty}f\left(t-\frac{nT}{2}\right)f\left(t-\frac{n_0T}{2}\right)e^{j\frac{2\pi}{T}(m-m_0)t}dt\\ &=\sum_{(m,n)\in\Omega_{\Delta m,\Delta n}}\frac{H^*_{s.r}(m)}{|H_{s.r}(m)|}a^{(.)}_{m,n}e^{j(\varphi_{m,n}-\varphi_{m_0,n_0})}\int_{-\infty}^{+\infty}f\left(t-\frac{nT}{2}\right)f\left(t-\frac{n_0T}{2}\right)e^{j\frac{2\pi}{T}(m-m_0)t}dt\end{aligned} \quad (3.5.40)$$

$$\Rightarrow\frac{H^*_{s.r}(m)}{|H_{s.r}(m)|}=\frac{H^*_{s.r}(m_0)}{|H_{s.r}(m_0)|},m\in\Omega_{\Delta m,\Delta n} \quad (3.5.41)$$

In fact, the good frequency localization of the prototype filter implies that a small number of adjacent subcarriers are contributing in the total intrinsic interference term[10]. In such a

[9] Obviously, the interference terms disappear after respective FBMC demodulation of $s_1(t)$ and $s_2(t)$.

[10] This assumption is reasonable. In fact in PHYDYAS prototype filter, only the immediate adjacent subcarrier one both sides is interacting with the one of interest. In IOTA filter, we have two subcarriers on each sides.

case, the condition given in (3.5.41) can be satisfied in weakly and mildly frequency selective channels. From (3.5.17), (3.5.40) and (3.5.41) , we get,

$$u'^{(i)}_{m_0,n_0} = \frac{H^*_{sir}(m_0)}{|H_{sir}(m_0)|} u^{(i)}_{m_0,n_0}, \qquad i = 1,2 \tag{3.5.42}$$

Thus, the demodulated signal at the relay receiver becomes,

$$\begin{aligned} y_{sr}(m_0,n_0) &= \sqrt{P}\sum_{.=1}^{2} H_{s.r}(m_0)\left(b^{(.)}_{m,n} + ju'^{(.)}_{m_0,n_0}\right) + n_r(m_0,n_0) \\ &= \sqrt{P}\sum_{.=1}^{2} H_{s.r}(m_0)\left(\frac{H^*_{s.r}(m_0)}{|H_{s.r}(m_0)|} a^{(.)}_{m,n} + j\frac{H^*_{s.r}(m_0)}{|H_{s.r}(m_0)|} u^{(.)}_{m_0,n_0}\right) + n_r(m_0,n_0) \\ &= \sqrt{P}\sum_{.=1}^{2} |H_{s.r}(m_0)|\left(a^{(.)}_{m,n} + ju^{(.)}_{m_0,n_0}\right) + n_r(m_0,n_0) \end{aligned} \tag{3.5.43}$$

Consequently, the intrinsic interference terms can be completely eliminated by taking the real part of the resulting demodulated signal,

$$y'_{sr}(m_0,n_0) = \Re[y_{sr}(m_0,n_0)] = \sqrt{P}\sum_{.=1}^{2} |H_{s.r}(m)| a^{(.)}_{m,n} + n'_r(m_0,n_0) \tag{3.5.44}$$

where, $n'_r(m_0,n_0) = \Re[n_r(m_0,n_0)]$ with a variance $\sigma'^2_r = \sigma^2_r/2$. Finally, the linear combination $\hat{y}_{sr}(m_0,n_0)$ can be computed as follows,

$$\hat{y}_{sr}(m_0,n_0) = \sqrt{P}\sum_{.=1}^{2} |H_{s.r}(m)| \hat{a}^{(.)}_{m,n} = \operatorname{argmin} \left\| y'_{sr}(m_0,n_0) - \sqrt{P}\sum_{.=1}^{2} |H_{s.r}(m)| a^{(.)}_{m,n} \right\|^2 \tag{3.5.45}$$

In order to normalize the transmit power at the relay, the linear combination $\hat{y}_{sr}(m_0,n_0)$ needs to be multiplied by some factor $\beta_{CoF}(m_0)$, given by

$$\beta_{CoF}(m_0) = \sqrt{\frac{P}{\mathbb{E}[|\hat{y}_{sr}(m_0,n_0)|^2]}} = \sqrt{\frac{1}{\sum_{.=1}^{2}|H_{s.r}(m_0)|^2}} \tag{3.5.46}$$

The relay sends the FBMC modulation of the normalized version of linear combinations $\beta_{CoF}(m_0,n_0)\hat{y}_{sr}(m_0,n_0)$.

As in MAF and MDF, we consider two cases at the destination.

a. Destination with a single receive antenna

Similarly to MAF, the destination in this case performs a processing analogous to FBMC SM (2×2) MIMO receiver. Hence, we can write,

$$\mathbf{y_d}_{m_0,n_0} = \mathbf{H_{CoF}}_{m_0}\left(\mathbf{a}_{m_0,n_0} + \mathbf{u}_{m_0,n_0}\right) + \mathbf{n_d}_{m_0,n_0} \tag{3.5.47}$$

where, the channel matrix $\mathbf{H_{CoF}}_{m_0}$ is given by

$$\mathbf{H}_{\mathbf{CoF}\,m_0} = \begin{bmatrix} \frac{H_{s1r}^*(m_0)}{|H_{s1r}(m_0)|} H_{s1d}(m_0) & \frac{H_{s2r}^*(m_0)}{|H_{s2r}(m_0)|} H_{s2d}(m_0) \\ \beta_{CoF}(m_0)|H_{s1r}(m_0)|H_{rd}(m_0) & \beta_{CoF}(m_0)|H_{s2r}(m_0)|H_{rd}(m_0) \end{bmatrix} \quad (3.5.48)$$

and the autocorrelation matrix of the noise vector in this case is given by,

$$\mathbb{E}\left[\mathbf{n}_{\mathbf{d}\,m_0}\mathbf{n}_{\mathbf{d}\,m_0}^{\mathbf{H}}\right] = \sigma_d^2\mathbf{I_2}.$$

b. Destination with two receive antennas

In this case, the demodulated signal $\mathbf{y}_{\mathbf{d}\,m_0,n_0}$ is a (4×1) vector. The channel matrix becomes,[11]

$$\mathbf{H}_{\mathbf{CoF}\,m_0} = \begin{bmatrix} \frac{H_{s1r}^*}{|H_{s1r}|} H_{s1d1} & \frac{H_{s1r}^*}{|H_{s1r}|} H_{s1d2} & \beta_{CoF}|H_{s1r}|H_{rd1} & \beta_{CoF}|H_{s1r}|H_{rd2} \\ \frac{H_{s2r}^*}{|H_{s2r}|} H_{s2d1} & \frac{H_{s2r}^*}{|H_{s2r}|} H_{s2d2} & \beta_{CoF}|H_{s2r}|H_{rd1} & \beta_{CoF}|H_{s2r}|H_{rd2} \end{bmatrix}^T \quad (3.5.49)$$

Moreover, the autocorrelation matrix of the noise vector in this case is given by,

$$\mathbb{E}\left[\mathbf{n}_{\mathbf{d}\,m_0}\mathbf{n}_{\mathbf{d}\,m_0}^{\mathbf{H}}\right] = \sigma_d^2\mathbf{I_4}.$$

3.5.3 Diversity gain analysis

In this section, we investigate the diversity gains of the different protocols previously described. Due to the similarity between MAF and MCoF, the diversity gain provided by both schemes will be the same. Therefore, the diversity analysis will be split into two parts: the analysis of the MAF/MCoF case, and the analysis of the MDF case.

3.5.3.1 MAF/MCoF diversity gain

The relay in both schemes is equivalent to an additional receive antenna at the destination. Accordingly, the whole system is equivalent to an SM (2×2) MIMO in the case of a destination with a single receive antenna and an SM (3×2) MIMO, when the destination is equipped with two receive antennas. It is well known that, linear receivers in SM MIMO system with N_t Tx antennas and N_r Rx ones achieve a diversity gain of $N_r - N_t + 1$ [68]. This implies that MAF/MCoF schemes provide diversity gains of 1 and 2 in the cases of a destination with a single and two Rx antennas, respectively. It should be noted that these gains are valid only when the magnitudes of the channel matrix components are independent Rayleigh random variables. However, in our case, we can see that the magnitudes of the channel gains related to the indirect link via the relay are the product of two Rayleigh random variables [see equations (3.5.23), (3.5.27), (3.5.48) and (3.5.49)]. Consequently, the expected diversity gains given in the previous paragraph may be different from the actual gains due to the fact that the indirect link channel gains are not Rayleigh random variables.

[11] Due to the lack of space, we have omitted the subcarrier index.

3.5.3.2 MDF diversity gain

In contrast to the previous schemes, the diversity of the MDF protocol described in section 3.5.2.2 is limited to 1 even in the case of two receive antennas at the destination. In the case of a single Rx destination antenna, the system is equivalent to an SM (2×2) MIMO [see equation (3.5.33), (3.5.34)] which provides a diversity gain of 1. In the case of 2 Rx antennas at **D**, the channel matrix of the corresponding system given in (3.5.35) and (3.5.36) is similar to an SM (4×2) MIMO which should provide a diversity gain of 3. However, it should be noted that this scheme is static, meaning that, the relay always decodes the data of both sources, and the destination considers both signals from the direct link and the indirect one to recover the source streams. In such a case, the BER of the whole system will be limited by the BER of the bad link (source-relay link or relay-destination one) which can be seen as a SM (2×2) MIMO. Therefore, we obtain a diversity gain of 1.

A potential improvement can be achieved using a hybrid AF/DF protocol [69]. In this latter, the relay re-encodes and transmits the source data only if it successfully decodes the received signal. Otherwise, it amplifies and forwards the received signal as in the MAF protocol. A dynamic DF can be also considered as a potential protocol to improve our system performance. In this protocol, the relay compares the received SNR to a threshold one in order to forward or not the received signal [70]. Similarly, a selective processing at the destination may enhance the performance. It is called selective because the destination can choose, based on a given criterion (e.g. SNR) a subset of signals among all received ones.

3.5.4 Complexity analysis

The following table presents the different requirements of each protocol in term of:

- Knowledge of the Channel State Information at the Receiver (CSIR), at the transmitter (CSIT) or both.
- The minimum number of receive antenna required at the relay and/or the destination to make possible the transmission. Obviously, each receive antenna is related to an FBMC receiver except the relay in the MAF case.
- The diversity gain achieved by each protocol.

Protocol	MAF	MDF	MCoF
CSIT (**S**)	x	x	(**S,R**)
CSIR (**R**)	(**S,R**)	(**S,R**)	(**S,R**)
CSIT (**R**)	x	x	x
CSIR (**D**)	(**S,R**) (**S,D**) (**R,D**)	(**S,R**) (**S,D**)	(**S,R**) (**S,D**) (**R,D**)
Rx at **R**	1	2	1
Diversity (1Rx at **D**)	$\simeq 1$	1	$\simeq 1$
Diversity (2Rx at **D**)	2	1	2

Table 3-7: Complexity analysis of MAF, MDF and MCoF protocols

The cross mark (x) means no requirement. It should be mentioned that each source in MCoF needs only the knowledge of its corresponding Channel State Information (CSI) with the relay.

3.5.5 Interest of proposed schemes in PMR scenario

The implication of two antennas at PMR base station operating in frequency bands 410-430 MHz and 450-470 MHz, will give rise to various issues such as: additional cost and also

additional space, weight and wind loading on radio masts [71]. This report concludes that the need of two independent antenna systems (2 Tx × 2 Rx) at base station sites is unacceptable for a TEDS (Tetra Enhanced Data Service) network using 410-430 MHz or 450-470 MHz bands.

We can see that the proposed multi-access relay schemes present an alternative solution to the problem of implementing a MIMO system in PMR base stations. In fact, with the help of the relay node, MAF and MCoF protocols with a single transmit/receive antenna at each node, are equivalent to an SM (2×2) MIMO system. Moreover, it should be mentioned that these protocols are also interesting in the ad-hoc mode where the implementation of MIMO in nodes becomes much more complicated due the reduced space and the mobility of these nodes.

Unfortunately, the MDF scheme is not suitable since the relay needs at least 2 Rx antennas in order to decode the source's messages.

It is worth pointing out that despite MAF and MCoF benefits, the main challenge in both schemes is the knowledge of CSI of the different links.

3.5.6 Simulation settings

In order to analyze the performances of the proposed multi-access relay schemes: MAF, MDF and MCoF, simulations of FBMC based PMR signals (emission and reception) have been performed using parameters given in [72] and presented in

Parameter description	**Parameter value**
Frame structure	
Bandwidth	1.4 MHz,
Sample frequency	1.92 MHz
Subcarriers number	128 subcarriers, 72 useful
Frame length in time	10 ms
Subcarrier spacing	15 kHz
FBMC filter	OFDM/OQAM PHYDYAS [73]
FBMC symbol duration	66.67 µs
Overlapping factor	4
Modulation and coding schemes	QPSK
Transmitter/Receiver	
BS number of antenna	From 1 to 4
HH number of antenna	1
MS/RS number of antenna	1 or 2
Transmission scheme	SISO, MIMO (2x1, 2x2, up to 4x2).
HH antenna model	Isotropic

Propagation	
Carrier frequency	422.5 MHz (Downlink), 412.5 MHz (Uplink)
Fast fading channel models	ITU PedA
Channel estimation	Ideal

Table 3-8 Simulation parameters

Moreover, the channel state information (CSI) is assumed to be perfectly known as described in Table 3-7. We note that the following results are compared to the optimal cases considering a noiseless relay receiver. For simplicity sake, the noise variance at the relay receiver and the destination one are supposed to be the same ($\sigma_d^2 = \sigma_r^2$).

3.5.7 Simulation results

In Figure 3-44 we investigate performance of the three proposed protocols: MAF, MDF and MCoF with a single receive antenna at the destination. The respective BERs of the different protocols are plotted against the SNR. Similarly to the theoretical analysis, two linear detections are considered: ZF and MMSE. Comparing the different curves related to ZF equalization, one can see that the three strategies provide almost the same performance. As previously expected, the diversity gain in MAF and MCoF is slightly less than one. Such a result can be explained by the fact that the channel gains related to the indirect link follow the product of two Rayleigh random variables. Besides, we can observe a slight gain of MCoF compared to the rest of schemes. Furthermore, an improvement of almost 2 dB is achieved by MMSE compared to ZF equalizer.

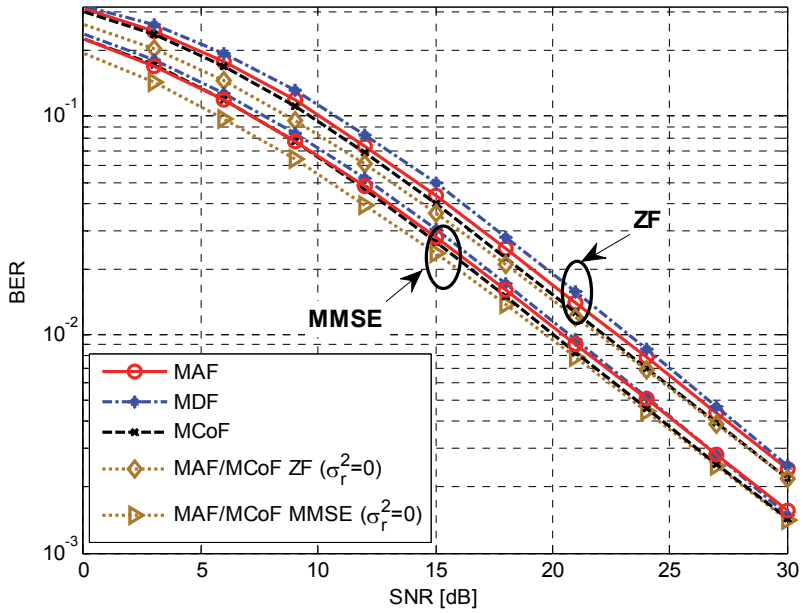

Figure 3-44: MAF, MDF and MCoF performances, 1Rx at D

In order to evaluate the impact of the noise at the relay, we have compared the different schemes to the optimal case ($\sigma_r^2 = 0$). We can see that this latter outperforms the others particularly in low SNR regime. In high SNR, the MCoF performance reaches the optimal

one. This is due to the fact that the estimation of the linear combination of both source's messages is detrimentally affected by the noise at the relay receiver.

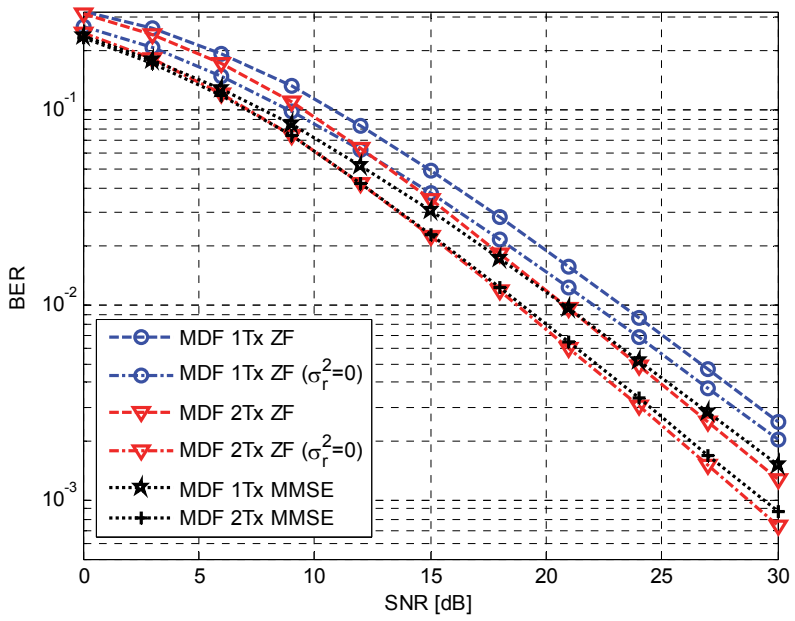

Figure 3-45: MDF performance in 1 D Rx ant.: 1 relay Tx ant. vs. 2 relay Tx ant

Since the relay in MDF case decodes both source data streams, it can send after re-encoding each stream on an individual transmit antenna. Figure 3-45 investigates the performance improvement provided by the utilization of a relay equipped with two transmit antennas compared to the previous one with a single one. This improvement can be explained by the fact that the channel gains of the indirect link in the two transmit antennas case [equation (3.5.34)] are uncorrelated, offering additional degree of freedom compared to the single transmit antenna one [equation (3.5.33)] in which both streams experience the same channel gain.

Moreover, we have also compared the MDF performance to its corresponding optimal case which is similar to an SM (2×2) MIMO system.

The BERs of the three protocols have been plotted against the SNR in the case of a destination with two receive antennas in Figure 3-46. In addition to the ZF/MMSE comparison, the obtained results are compared to the optimal case where we consider a noiseless relay receiver.

As expected in the theoretical analysis, both MAF and MCoF schemes achieve a diversity gain of 2. It is worth pointing out the difference between both schemes with respect to the gains provided by MMSE. In MCoF, the MMSE equalization does not improve the performance with respect to ZF one. In fact, the destination in MCoF underestimates the effective noise variance since it assumes that the linear combination has been perfectly computed at the relay. On the other hand, the MAF destination takes into consideration both noises $\mathrm{n_r}$ and $\mathrm{n_t}$. The good estimation of the autocorrelation of the noise vector makes the MMSE equalization more efficient in MAF case (In this case, we assume the knowledge of the relay noise variance to the destination receiver). In addition, a constant gap between

the optimal performance and MAF/MCoF ones can be mentioned, which is due to the absence of the noise at the relay receiver.

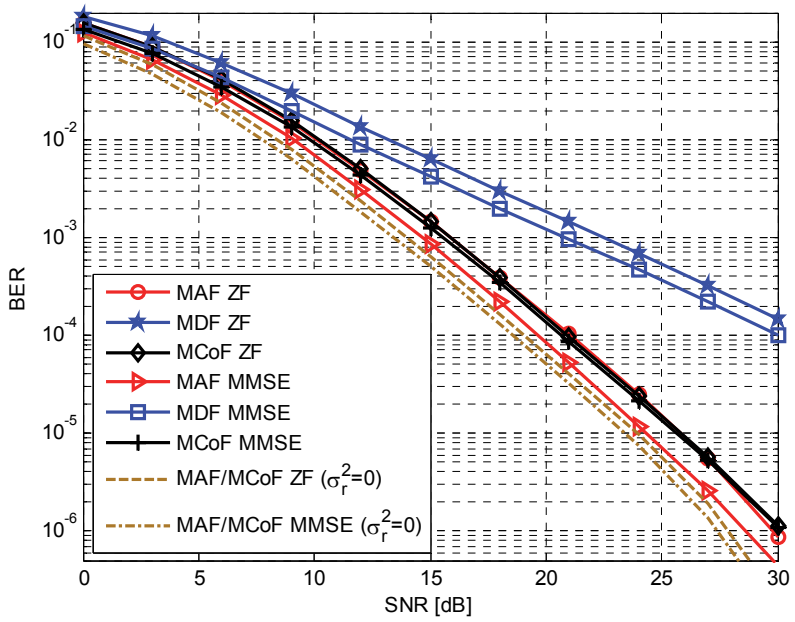

Figure 3-46: MAF, MDF and MCoF performances, 2Rx at **D**

Furthermore, we can see that MDF performance is limited to a diversity gain of 1. Such a behavior is due to the fact that the whole system performance is already limited by the performance of decoding at the relay. We recall that the proposed scheme is static, in other words, the relay decodes the sources' messages without any control on the quality of the link between the source transmitters and the relay receiver.

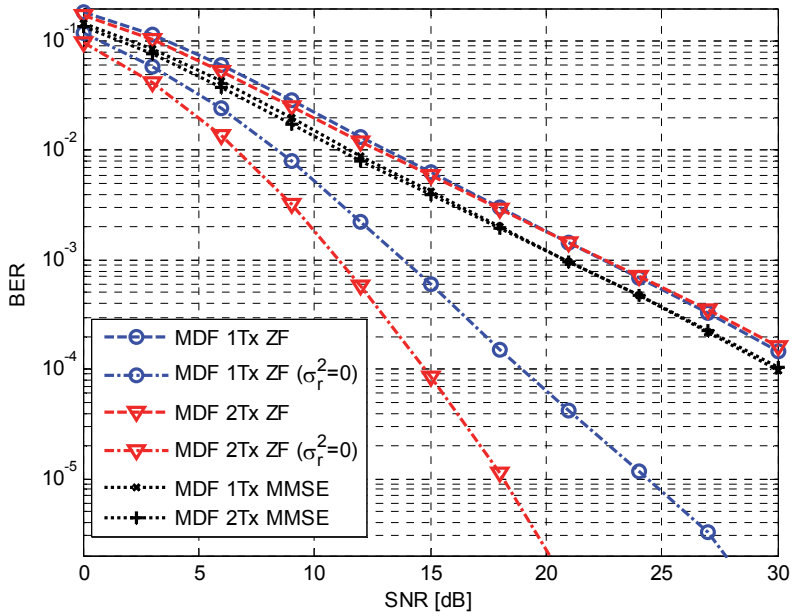

Figure 3-47: MDF performance in 2 **D** Rx ant.: 1 relay Tx ant. vs. 2 relay Tx ant

Figure 3-47 depicts the BERs of the MDF protocol when the relay is equipped with a single and two transmit antennas. Thanks to the additional degree of freedom provided by the second transmit antenna, we have a constant gain of the two transmit antennas case versus the single transmit antenna one. Besides, we have also evaluated the optimal performance that can be achieved by MDF when the noise at the relay is zero. A diversity gain of 3 is observed in the case of two transmit antennas at the relay. Such a gain is due to the fact that the whole system is an SM (4×2) MIMO one as shown in (3.5.36) (i.e. $\mathrm{d} = 4 - 2 + 1$). However, the diversity gain decreases to 2 in the case of a single transmit antenna at the relay due to the correlation between the gains related to the indirect link as shown in (3.5.35). Finally, the obtained results confirm the limitation of the MDF performance caused by the performance of the source-relay link impacted by the noise.

3.5.8 Final remarks

In this section, we have investigated the usability of the CoF protocol in FBMC based MARC network. In order to generate an interference-free linear combination at the relay, we have proposed a complex precoding strategy of the data at the input of the FBMC transmitters. This precoding allows aligning the intrinsic interferences caused by source transmitters. Moreover, a comparison study has been carried out between MAF, MDF and MCoF protocols in term of complexity, performance and suitability to the PMR case. In contrast to MDF protocol, the obtained results have shown that MAF and MCoF are more appropriate to PMR communications. However, the main challenge of both protocols remains the need of a complete CSI knowledge of all links to the destination.

4 Conclusion

This deliverable presented the first part of the work performed in WP7 and in particular under T7.1 and T7.2 of the EMPhAtiC project. It deals with relaying applied to FBMC, OFDM and SC-FDMA waveforms and specifically on range extension using cooperative MIMO as well as the design and evaluation of relay strategies. The work ranges from theoretical investigation of the performance of the two relaying scheme via the characterization of the achievable rate region of a two-way DF relaying strategy, to more applied work like practical channel estimation schemes for two-way relaying.

Section 2.1 reports work performed under the umbrella of T7.1 “Range extension by using cooperative MIMO”. A coordinated beamforming scheme for multi-hop relaying is presented for FBMC/OQAM systems with application to relaying in DMO for next generation PMR systems. The proposal focuses on MIMO schemes with joint design of the precoding and decoding matrix at each hop. Compared to multi-hop relaying in CP-OFDM with ZF precoding, for 1 or 2 relays the proposed technique has better performance for low SNRs levels, in which the intrinsic interference of the FBMC scheme can be neglected. By increasing the number of relays for fixed source-to-receiver distance, the receiver SNR of each hop is increased dramatically, and therefore, a much lower BER performance is obtained. However, when multiple relay nodes are used, the FBMC system performance is limited by residual intrinsic interference. When more than 2 relays are used CP-OFDM starts again to be an interesting solution in this scenario.

Section 3 reports work performed under the umbrella of T7.2 “Design of relaying strategies”. The first three sections under section 3 are dedicated to two-way relaying. The remaing two sections are dedicated to AF/DF relaying in FBMC and to a more complex setting where relaying is also combined to multiple access.

In section 3.1 a two-way relaying protocol for SC-FDMA based in DF strategy is introduced. DF can be applied in a variety of PMR scenarios both cell-based and ad hoc. However, for the work presented, a hypothesis of time synchronization of the received signals was assumed, which is simpler to achieve in a cell-based scenario. Then the focus is on channel estimation in the multiple access phase, since it is one of the fundamental functionalities which can set limitations to the technique. The standard LS channel estimation algorithm was compared to another ML algorithm. The latter is able to improve the estimate quality, especially for frequency selective channels, whose delay spread is lower than the CP length. A third algorithm estimating at the same time the channel and the noise was tested but it is not retained due to its inferior performance. Extensive simulations were done (not all shown in this deliverable) in order to have a characterization of the behaviour of the LS and ML algorithms over multi-tap channels with a degree of frequency selectivity going from mild to severe. Simulation results helped to tune the algorithm parameters according to the number of channels to be estimated but without the knowledge of the channel fading statistics. The parameters are optimized in the case of medium frequency selectivity with a CP of 16.67 μs (covering the delay spread of most of PMR channel models), which introduces performance degradation in certain cases. Even if the LS estimation algorithm has similar or slightly better performance than the ML one in channel with low frequency selectivity, the ML algorithm seems to be the best choice when the estimation algorithm must face channels with changing frequency selectivity. The conclusion is that there is no blocking point to the implementation of the two-way relaying technique as far as channel

estimation is concerned and the number of users is less or equal to 4. Increasing the number of users above 4 without substantial performance degradation is not possible by using the current reference signal structure which is inherited by LTE, and based on cyclically shifted CAZAC sequences.

In section 3.2, we study the achievable rate region of FBMC based 3-node two-way DF relaying system, where each node has a single antenna. This work helps understanding the fundamental limits of the two-way DF relaying techniques that can find useful applications in the PMR context both in cell-based and ad hoc scenarios. The rate region problem, which yields a power allocation problem in our case, is a fundamental problem (or a basis) for DF based relaying systems. What distinguishes FBMC from OFDM is the presence of inter-carrier and inter-symbol interference in frequency selective channels. This fact makes the rate region problem non-convex and in general NP-hard. Nevertheless an efficient polynomial-time solution is developed. Moreover, the work done enables further extensions to the multi-antenna case or to PMR systems with specific constraints, e.g., out of band interference constraints. The FBMC achievable rate region was compared to the one of OFDM and compares favourably to it. However, the FBMC two-way DF relaying strategies wins over the OFDM one over the whole range of SNR of interest (i.e. below 30 dB) only if multi-tap equalizers or pre-equalizers are used at the terminals. Hence, the gain of FBMC solution is paid by an increase of computational complexity with respect to its OFDM counterpart and by the need of channel state information at the terminals for doing a proper pre-equalization.

Section 3.3 presents an AF two-way relaying protocol for FBMC, in which the receiver terminals apply a successive interference cancellation algorithm. Initial performance is presented. The AF method suffers from degradation with respect to the SISO reference, which constitutes a lower bound, but it is nevertheless able to exploit the frequency diversity of the channel to improve its performance with respect to the flat fading channel.

AF relays are simple and economic devices that can be deployed in both cellular and ad hoc scenarios of PMR systems. Section 3.4 analyses the effect of an AF relay on a point-to-point link where FBMC/OQAM modulation is employed together with a parallel multistage demodulator/equalizer to transmit over a highly frequency selective channel. More specifically, for a receiver with K demodulation/equalization stages, it is shown that the signal quality at the m-th subcarrier can be expressed in terms of signal-to-noise-plus-distortion ratio (SNDR), which takes into account the effects of (a) an imperfect equalization, (b) the noise of the source–relay channel and (c) the noise of the relay–destination channel. The SNDR is then used to compute the spectral efficiency of the relay link, which is compared to the spectral efficiency of the direct link. The AF relay shows some gain over the direct link, especially at medium SNR and for environments with high path loss. Conversely, at low SNR, the spectral efficiency of the relay scheme tends to zero faster than the direct link one. This is due to the fact that the magnitude of the AF relay channel tends to zero as we reduce the relay transmit power, making channel inversion an indeterminate operation. For this reason, equalizers based on operations other than channel inversion are under investigation.

Finally, in section 3.5, an adaptation of the CoF protocol to FBMC based MARC network is established. This strategy can be applied in a PMR cell-based scenario, in which the PMR users are helped in the UL transmission by a relay. Hence relaying is combined with a multiple access phase. A complex precoding strategy of the data at the input of the FBMC

transmitters is proposed to generate an interference-free linear combination at the relay. The key idea of this precoding is to align the intrinsic interferences caused by source transmitters. Of course, precoding needs channel state information to work. The requirements in terms of channel state information have clearly been identified in our work. Furthermore, MAF, MDF and MCoF protocols have been compared in terms of complexity, performance and suitability to the PMR case. In contrast to MDF protocol, MAF and MCoF are demonstrated to be more appropriate to PMR communications. However, the main challenge of both protocols remains the need of a complete CSI knowledge of all links to the destination.

5 References

[1] "MIMO Transmission and Reception Design Schemes," Deliverable D4.1, ICT EMPhAtiC, August 2013.

[2] "Training design and algorithms for channel estimation," Deliverable D3.1, ICT EMPhAtiC, november 2013.

[3] "Adaptive equalization and Successive Self-Interference Cancellation (SIC) methods," Deliverable D3.2, ICT EMPhAtiC, February 2014.

[4] "Multimode non-uniform filterbank," Deliverable D2.2, ICT EMPhAtiC, February 2014.

[5] Xavier Mestre, Marc Majoral, Stephan Pfletschinger, "Am Asymptotic Approach to Parallel Equalization of Filter Bank Based Multicarrier Signals," *IEEE Trans. Signal Process.*, vol. 61, no. 14, pp. 3592–3606, Jul. 2013.

[6] "Definition and Specification of Requirements for the Physical Layer Implementation and Channel Model," Milestone MS4, ICT EMPhAtiC, 2013.

[7] "Prototype Filter and Structure Optimization," Deliverable D5.1, ICT PHYDYAS, 2009.

[8] 3rd Generation Partnership Project, "LTE; Evolved Universal Terrestrial Radio Access (e-UTRA); Base Station (BS) Radio Transmission and Reception," Technical Report TS 36.104 v11.4.0 release 11, 3GPP, 2013.

[9] A. Ancora, C. Bona and D.T.M. Slock, "Down-Sampled Impulse Response Least-Squares Channel Estimation for LTE OFDMA", Proc. IEEE International Conference on Acoustics, Speech and SignalProcessing (ICASSP2007), Hawaii, USA, 2007.

[10] Artist4G D2.2, "Advanced receiver signal processing techniques: evaluation and characterization", v. 1, November 21st 2011.

[11] J. D. C. Chu, "Polyphase Codes with Good Periodic Correlation Properties" IEEE Trans. on Information Theory, Vol. 18 pp. 531-532 July 1972.

[12] M. Chen and A. Yener, "Multiuser two-way relaying for interference limited systems", the IEEE International Conference on Communications, ICC'08, 2008.

[13] Luc Deneire, Patrick Vandenameele, Liesbet van der Perre, Bert Gyselinckx, and Marc Engels, "A low complexity ML channel estimator for OFDM", IEEE Trans. Commun., vol. 51, no. 2, pp. 931-939, Feb. 2003.

[14] H. Eghbali, S. A. Hejazi, S. Muhaidat, N. Al-Dhahir, "Multiuser Two-way relaying with power control for SC-FDE systems", 2013 IEEE24th International Symposium on Personal, Indoor and Mobile Radio Communications (PIMRC 2013), pp: 961-965, London, United Kingdom, September 8-11, 2013.

[15] O. Edfors, M. Sandell, J.-J. van de Beek, S. K. Wilson and P. O. Borjesson, "OFDM channel estimation by singular value decomposition," IEEE Trans. Commun., vol. 46, no. 7, pp. 931-939, Jul. 1998.

[16] C. Esli, A. Wittneben, "Multiuser MIMO two-way relaying for cellular communications", IEEE 19th International Symposium on Personal, Indoor and Mobile Radio Communications, (PIMRC 2008), Cannes, France, 15-18 Sept. 2008.

[17] C. Esli, A. Wittneben, "One- and Two-Way Decode-and-Forward Relaying for Wireless Multiuser MIMO Networks", IEEE Global Telecommunications Conference, 2008.

[18] R. Frank, S. Zadoff and R. Heimiller, "Phase Shift Pulse Codes With Good Period Correlation Properties", IEEE Trans. on Information Theory, Vol. 8 pp 381-382 October 1962.

[19] I. Hammerstrom, M. Kuhn, C. Esli, J. Zhao, A. Wittneben, and G. Bauch, “MIMO two-way relaying with transmit CSI at the relay,” in Proc. IEEE SPAWC, June 2007.

[20] X. Hou and H. Kayama, "Demodulation Reference Signal Design and Channel Estimation for LTE-Advanced Uplink", Advances in Vehicular Networking Technologies, Dr Miguel Almeida (Ed.), InTech, 2011.

[21] Shih-Chan Huang, Jia-Chin Lin, Kao-Peng Chou, "Novel Channel Estimation Techniques on SC-FDMA Uplink Transmission", 2010 IEEE 71st Vehicular Technology Conference (VTC 2010-Spring), 16-19 May 2010.

[22] H. Hamdoun, P. Loskot, T. O'Farrell, J. He, "Practical Network Coding for Two Way Relay Channels in LTE Networks", IEEE 73rd Vehicular Technology Conference (VTC Spring 2011), 15-18 May 2011.

[23] Xue Jianbin, Li Songbai, "An SC-FDMA Channel Estimation Algorithm Research Based on Pilot Signals", 2nd Int. Symposium on Computer, Communication, Control and Automation (ISCCCA-13), pp: 179-182, Shijiazhuang, China, February 22-24, 2013.

[24] S. Kay, Fundamentals of Statistical Signal Processing: Estimation Theory ,Vol I. New Jersey: Prentice-Hall, 1993.

[25] T. Koike-Akino, P. Popovski, and V. Tarokh, "Optimized Constellations for Two-Way Wireless Relaying with Physical Network Coding", IEEE Journal on Selected Areas in Communications (JSAC), Special Issue on Network Coding for Wireless Communication Networks, Vol. 27, No. 5, pp. 773-787, June 2009.

[26] H. Liu, P. Popovski, E. de Carvalho, and Y. Zhao, "Sum-Rate Optimization in a Two-Way Relay Network with Buffering", IEEE Communications Letters, vol. 17, no. 1, pp. 95-97, January 2013.

[27] H. G. Myung, “Introduction to Single Carrier FDMA”, 15th European Signal Processing Conference (EUSIPCO) 2007, Poznan, Poland, September 2007.

[28] H. G. Myung, D. G. Goodman, Single Carrier FDMA: a new air interface for Long Term Evolution, Wiley, 2008.

[29] X. Ma, L. Yang, G. B. Giannakis, "Optimal Training for MIMO Frequency-Selective Fading Channels", IEEE Trans. on Wireless Communications, vol. 4, no. 2, pp. 453-466, March 2005.

[30] B. Nazer, M. Gastpar, "Reliable Physical Layer Network Coding", Proceedings of the IEEE, vol. 99, no. 3, pp. 438-460, March 2011.

[31] S. Omar, A. Ancora, D.T.M. Slock, "Performance analysis of general pilot-aided linear channel estimation in LTE OFDMA systems with application to simplified MMSE schemes", IEEE 19th International Symposium on Personal, Indoor and Mobile Radio Communications (PIMRC 2008), 15-18 Sept. 2008.

[32] M. Pischella and D. Le Ruyet, "Optimal Power Allocation for the Two-Way Relay Channel with Data Rate Fairness", IEEE Commun. Letters, vol. 15, no. 9, pp. 959-961, September 2011.

[33] B. M. Popovic, “Generalized Chirp-Like Polyphase Sequences with Optimum Correlation Properties”, IEEE Trans. on Information Theory, Vol. 18 pp. 533-536, November 1991.

[34] S. Sesia, I. Toufik and M. Baker, LTE - Long Term Evolution: From Theory to Practice, Second Edition, 2011, John Wiley & Sons.

[35] 3GPP TS 36.211 v10.5.0, “E-UTRA; Physical Channels and Modulation”, June 2012.

[36] K. Takeda, Y. Kishiyama, M. Tanno, T. Nakamura, "Investigation of Two-Dimensional Orthogonal Sequence Mapping to Multi-Layer Reference Signal for LTE-Advanced Downlink", IEEE 72nd Vehicular Technology Conference Fall (VTC 2010-Fall), 2010.

[37] E. Yılmaz and R. Knopp, "Hash-and-Forward Relaying for Two-Way Relay Channel", IEEE International Symposium on Information Theory (ISIT 2011), Saint-Petersburg, Russia, July 2011.

[38] P. Siohan, C. Siclet, and N. Lacaille, “Analysis and design of OFDM/OQAM systems based on filterbank theory,” IEEE Transactions on Signal Processing, vol. 50, no. 5, pp. 1170 – 1183, May 2002.

[39] M. G. Bellanger, “FBMC physical layer: a primer,” June 2010.

[40] R. Zakaria, D. Le Ruyet, and M. Bellanger, “Maximum Likelihood Detection in spatial multiplexing with FBMC,” in Proc. 2010 European Wireless, June 2010.

[41] Y. Cheng and M. Haardt, “Widely Linear Processing in MIMO FBMC/OQAM Systems,” in Proc. ISWCS 2013, Aug. 2013.

[42] M. Caus and A. I. Perez-Neira, “Multi-stream transmission in MIMO-FBMC systems,” in Proc. ICASSP 2013, May 2013.

[43] M. Caus and A. I. Perez-Neira, “Comparison of linear and widely linear processing in MIMO-FBMC systems,” in Proc. ISWCS 2013, Aug. 2013.

[44] Y. Cheng, S. Li, J. Zhang, F. Roemer, B. Song, M. Haardt, Y. Zhou, and M. Dong, “An Efficient and Flexible Transmission Strategy for the Multi-carrier Multi-user MIMO Downlink,” IEEE Transactions on Vehicular Technology, 2013, accepted for publication.

[45] B. Song, F. Roemer, and M. Haardt, “Flexible coordinated beamforming (FlexCoBF) for the downlink of multi-user MIMO systems in single and clustered multiple cells,” Elsevier Signal Processing, vol. 93, pp. 2462 – 2473, Sept. 2013.

[46] Q. H. Spencer, A. L. Swindlehurst, and M. Haardt, “Zero-forcing methods for downlink spatial multiplexing in multiuser MIMO channels,” IEEE Trans. Signal Process., vol. 52, no. 2, pp. 461–471, Feb. 2004.

[47] FP7-ICT Project PHYDYAS Physical Layer for Dynamic Spectrum Access and Cognitive Radio. http://www.ictphydyas.org.

[48] D. S. Waldhauser, L. G. Baltar, and J. A. Nossek, “MMSE Subcarrier Equalization for Filter Bank based Multicarrier Systems,” in Proc. IEEE 9th Workshop on Signal Processing Advances in Wireless Communications, pp. 525 – 529, Jul. 2008.

[49] D. S. Waldhauser, L. G. Baltar, and J. A. Nossek, “Adaptive Decision Feedback Equalization for Filter Bank based Multicarrier Systems,” in Proc. IEEE International Symposium on Circuits and Systems, pp. 2794 – 2797, May 2009.

[50] A. Ikhlef and J. Louveaux, “Per subchannel equalization for MIMO FBMC/OQAM systems,” in Proc. PACRIM 2009, Aug. 2009.

[51] C. Rao and B. Hassibi, “Diversity-multiplexing gain trade-off of a MIMO system with relays," in Proc. IEEE Inf. Theory Workshop, July 2007.

[52] S. Yang and J.-C. Belfiore, “Distributed (space-time) codes for the MIMO multihop channel via partitions for the channel,” in Proc. IEEE Inf. Theory Workshop, July 2007.

[53] F. Khan, “Capacity and Range Analysis of Multi-Hop Relay Wireless Networks," in Proc. IEEE Vehicular Technology Conference, 2006. VTC-2006 Fall. pp.1,5, 25-28 Sept. 2006.

[54] ITU-R Recommendation M.1225, “Guidelines for evaluation of radio transmission technologies for IMT-2000,” 1997.

[55] Y. Cheng, P. Li, and M. Haardt, “Coordinated beamforming in MIMO FBMC/OQAM systems,” accepted by ICASSP 2014.

[56] F. He, Y. Sun, X. Chen, L. Xiao, and S. Zhou, “Optimal power allocation for two-way decode-and-forward OFDM relay networks,” in IEEE International Conference on Communications (ICC), Dec. 2012.

[57] M. Caus and A. Perez-Neira, “Transmit-receiver designs for highly frequency selective channels in MIMO FBMC systems,” in IEEE Trans. Signal Processing, Dec. 2012.

[58] A. Khabbazibasmenj, F. Roemer, S. A. Vorobyov, and M. Haardt, “Polynomial-time DC (POTDC) for sum-rate maximization in two-way AF MIMO relaying: polynomial time solutions to a class of DC programming problems,” in IEEE Trans. Signal Processing, Oct. 2012.

[59] C. Lélé, "OFDM/OQAM : Méthodes d’Estimation de Canal, et Combinaison avec l’Accès Multiple CDMA ou les Systèmes Multi-Antennes," Ph.D. thesis, 2008.

[60] A. Goldsmith, Wireless Communications, New York: Cambridge University Press, 2005.

[61] D. Tse, P. Viswanath, Fundamentals of Wireless Communications, New York: Cambridge University Press, 2004.

[62] H. Lin, P. Siohan, P. Tanguy and J.-P. Javaudin, "An Analysis of the EIC Method for OFDM/OQAM Systems," Journal of Communications, vol. 4, no. 1, p. 52–60, Feb 2009.

[63] M. El Tabach, J.-P. Javaudin, M. Helard, "Spatial Data Multiplexing Over OFDM/OQAM Modulations," in IEEE International Conference on Communications, ICC'07, 2007.

[64] L. R. Ford and D. R. Fulkerson, "Maximal flow through a network," Can. J. Math, vol. 8, pp. 399-404, 1956.

[65] P. Elias, D. R. Feinstein, and C. E. Shannon, "A note on the maximal flow through a network," IRE Trans. Inf. Theory, vol. 72, pp. 117–119, Dec. 1956.

[66] B. Nazer, M. Gastpar, "Compute-and-forward: Harnessing interference through structured codes," IEEE Trans. Inf. Theory, vol. 57, p. 6463–6486, 2011.

[67] M. El Soussi, A. Zaidi, L. Vandendorpe, "Compute-and-Forward on a Multiaccess Relay Channel: Coding and Symmetric-Rate Optimization," accepted to IEEE Trans. wireless Commun., 2013.

[68] J.H. Winters, J. Salz, R.D. Gitlin, "The impact of antenna diversity on the capacity of wireless communication systems," IEEE Transactions on Communications, vol.42, no.234, pp.1740 - 1751, Feb/Mar/Apr 1994, vol. 42, no. 234, pp. 1740-1751, 1994.

[69] M.R. Souryal, B. R. Vojcic, "Performance of Amplify-and-Forward and Decode-and-Forward Relaying in Rayleigh Fading with Turbo Codes," in IEEE International Conference on Acoustics, Speech and Signal Processing, 2006. ICASSP 2006, 2006.

[70] D. Chen, J. N. Laneman, "The Diversity-Multiplexing Tradeoff for the Multiaccess Relay Channel," in 40th Annual Conference on Information Sciences and Systems, 2006.

[71] ETSI TR 102 513, "Terrestrial Trunked Radio (TETRA); Feasibility Study into the Implications of Operating Public Safety Sector (PSS) TEDS using the proposed "Tuning Range" concept in the 410 MHz to 430 MHz and 450 MHz to 470 MHz frequency bands," ETSI, 2006.

[72] V. Ringset; T. A. Myrvoll; N. Bartzoudis; O. Font-Bach, "Definition and specification of requirements for the physical layer implementation and channel model," EMPhAtiC internal document, 2013.

[73] M.G. Bellanger, "Specification and design of a prototype filter for filter bank based multicarrier transmission," in IEEE International Conference on in Acoustics, Speech, and Signal Processing, 2001.

[74] A. Vahlin and N. Holte, “Specification and design of a prototype filter for filter bank based multicarrier transmission,” IEEE Tr. On Communications, Vol. 44, No. 1, pp. 10-14, Jan 1996.

Glossary and Definitions

Acronym	Meaning
AF	Amplify-and-Forward
AFB	Analysis FilterBank
AWGN	Additive White Gaussian Noise
BC	BroadCast
BER	Bit Error Rate
BS	Base Station
CAZAC	Constant Amplitude Zero Auto-Correlation
CBF	Coordinated BeamFoming
CDMA	Code Division Multiple Access
CH	Cluster Head
CoF	Compute-and-Forward
CP	Cyclic Prefix
CP-OFDM	Cyclic Prefix-Orthogonal Frequency Division Multiplexing
CRS	Common Reference Signals
CSI	Channel State Information
CSIR	Channel State Information at the Receiver
CSIT	Channel State Information at the Transmitter
DC	Difference of Convex functions
DF	Decode-and-Forward
DFT	Discrete Fourier Transform
DL	DownLink
DMO	Direct Mode Operation
DNF	DeNoise-and-Forward
EPA	Extended Pedestrian-A [channel]
ETU	Extended Typical Urban [channel]
FBMC	Filter-Bank Multi Carrier
FF	Filter-and-Forward
FFT	Fast Fourier Transform
HHT	Hand Held Terminals
HT1	Hilly Terrain 1 [channel]
ICI	Inter-Carrier Interference
IDFT	Inverse Discrete Fourier Transform
IFFT	Inverse Fast Fourier Transform
ISI	Inter-Symbol Interference

ITU	International Telecommunication Union
LS	Least Squares
LTE	Long Term Evolution
LTE-A	Long Term Evolution-Advanced
MA	Multiple Access Relay Channel
MAC	Medium Access Control
MAF	Multi-access Amplify-and-Forward
MARC	Multiple Access Relay Channel
MCoF	Multi-access Compute-and-Forward
MDF	Multi-access Decode-and-Forward
MIMO	Multiple Input Multiple Output
ML	Maximum Likelihood
MMSE	Minimum Mean Square Error
MS	Mobile Station
MSE	Mean Square Error
MU	Multi User
MUI	Multi User Interference
NP	Non-Polynomial [time]
NTMSE	Normalized Truncated Mean Squared Error
OCC	Orthogonal Cover Code
OFDM	Orthogonal Frequency Division Multiplexing
OQAM	Offset Quadrature Amplitude Modulation
PAM	Pulse Amplitude Modulation
Ped-A	Pedestrian-A [channel model]
PHY	PHYsical [Layer]
PMR	Private Mobile Radio
POTDC	POlynomial-Time DC
PPDR	Public Protection and Disaster Relief
QAM	Quadrature Amplitude Modulation
QPSK	Quadrature Phase Shift Keying
RB	Resource Block
RS	Reference Signals
SC-FDE	Single-Carrier Frequency Domain Equalization
SC-FDMA	Single-Carrier Frequency Division Multiple Access
SDMA	Space Division Multiple Access
SIC	Successive Interference Cancellation
SISO	Single Input Single Output

SLNR	Signal to Leakage plus Noise Ratio
SM	Spatial Multiplexing
SNDR	Signal-to-Noise-plus-Distortion Ratio
SNR	Signal to Noise Ratio
SVD	Singular Value Decomposition
TB	Transport Block
TDMA	Time Division Multiple Access
TETRA	TErrestrial Trunked RAdio
TMO	Trunked Mode Operation
UE	User Equipment
UL	UpLink
Veh-A	Vehicular-A [channel model]
WLAN	Wireless Local Area Network
ZF	Zero Forcing